RARE EARTH DOPED SODIUM ALUMINIUM SILICATE FOR OPTICAL COOLING APPLICATION

by

KYALO NGESU KITEME

Submitted in accordance with the requirements

for the degree of

MASTER OF SCIENCE

in the subject

PHYSICS

at the

UNIVERSITY OF SOUTH AFRICA

SUPERVISOR: Prof. M. S. Dhlamini

CO-SUPERVISOR: Prof. A. E. Botha

(February 2021)

Declaration

Name: Kyalo Ngesu Kiteme

Student Number: 48091561

Degree: MASTER OF SCIENCE (PHYSICS)

Dissertation title: **RARE EARTH DOPED SODIUM ALUMINIUM SILICATE FOR OPTICAL COOLING APPLICATION**

I declare that the above dissertation is my own work and that all the sources that I have used orquoted have been indicated and acknowledged by means of the complete references.

I further declare that I submitted the dissertation to originality checking software and it falls within the accepted requirement for originality. I further declare that, I have not previously submitted this work, or part of it, for examination at UNISA for another qualificationor at any other higher education institution.

SIGNATURE: DATE: 18/02/2021

Acknowledgement

This work is a collection of many ideas gathered from all those who did suggest, correct, and even gave help in the advanced physics laboratory at University of South Africa, as we gathered data and other relevant information. I cannot possibly acknowledge them all individually but would like to sight some whose contribution was of great importance towards the completion of this dissertation.

I acknowledge the timely advice, suggestions and scientific discussions I have had with my two supervisor Prof. M. S. Dhlamini and co-supervisor Prof A. E. Botha. Their guidance and continuous monitoring of this work is highly appreciated.

I thank Professor T. Kroon of the Physics Department at the University of the Free State for his help in making sure our samples were analyzed on time, for hosting me and leadingme in performing my research experiments, and for his contribution in suggesting solutions to questions that arose in key areas of the project.

I also thank fellow students and staff members Dr L. E. Mathevula, Luleka Menzi, Collen Manaka, Mduduzi Mbongo, Victor Molefe, Oliver Mnisi, Dumisani Mlotswa, Dr David Omoefe, Seithati Qotso and Dr G. L. Kabongo, including all the others that I cannot name individually. In fact, I would like to thank the entire Physics department staff at the University of South Africa from colleagues, supporting staff, their input is highly recognized.

In general, I would like to thank the University of South Africa for having accepted and nurtured me 7 years ago when I joined the honors degree class in Physics, its support in supervisors, laboratory equipment up to and including a bursary; I am highly indebted for such a generous package.

I also acknowledge the National Research Foundation (NRF) scholarship that made it possible for me to study.

Lastly, I wish to thank the two ladies in my life who gave me study time and moral support while I worked on this dissertation; namely, my wife Rebecca Kyalo and daughter Leah Waeni.

And to all those not mentioned explicitly by name, thank you

Dedication

To my wife Rebecca Kyalo and daughter Leah Waeni.

Epigram

"QUOTECAPITES, TOTS SENSUS", Terence: Roman (170-160 BC).

Translation: The more the people the more the opinion.

Key Words

- Laser optical cooling
- Sodium aluminium silicate
- Zeolite
- Nanoparticles and nanomaterials
- Activator
- Sensitizer
- Absorption
- Transmittance
- Down-conversion
- Up-conversion
- Thermalization

Acronyms and Abbreviations

- NRF- National Research Foundation
- UNISA - University of South Africa
- UFS- University of the Free State
- FWHM- Full width at half maximum
- XRDP- X-ray diffraction powder
- ICDD -The International Centre for Diffraction Data
- JCPDS-Joint Committee on Powder Diffraction Standards
- HR-SEM -High Resolution Scanning Electron Microscope
- Laser- light amplification by stimulated emission of radiation
- EDS- Energy Dispersion X-ray Spectroscopy
- XPS- X-ray Photo Electron Spectroscopy
- UV VIS- Ultraviolet -Visible Spectroscopy
- PL- Photoluminescence spectroscopy

Page left intentionally blank.

Abstract

In the present research we successfully synthesized $NaAlSiO_2$ crystals and doped (co-doped) them with various concentrations of Er^{3+}, and Yb^{3+} ions via a hydrothermal method to unveil their up-conversion absorption bands in the visible region under 980 nm tuned laser pumping. The hydrothermal process was preceded by a hydro-gel preparationstep and finally by an incipient wetness impregnation for successful doping.

X-ray diffraction analysis revealed that crystallite size ranged between 14.5 nm to 37.4 nm. Moreover, elemental analyses performed on the prepared samples via scanning electron microscope (SEM) equipped with Energy Dispersive X-ray Spectrometer (EDS) unraveled even distribution of both ions. In addition, FTIR analysis demonstrated the presence of absorbed OH group in the host materials which were removed via optimized annealing of the sample. To elucidate absorption behavior of the as-synthesized host material, UV-Vis-NIR spectroscopy was used and resulted in absorption bands at 487 nm, 521 nm, 540 nm, 651 nm and 971 nm, respectively. On the other hand, emission properties were investigated by means of Photoluminescence (PL) spectroscopy. PL analysis revealed emission lines in the visible range of spectrum at 521 nm, 540 nm and 651 nm. Optimizing annealing temperature proved critical in enhancing up-conversion emission, Power dependence analysis showed increased emission with increasing pumping power.
Finally, temperature dependency tests showed the crystals to be promising materials for up-conversion laser optical cooling application at temperature ranging from 50 to 400 °C.

Table of Contents

List of Tables

List of Figures

Chapter 1

Introduction

Background

Over the past four decades modern condensed matter physics has witnessed revolutionary advances in dozens of cutting-edge techniques including laser cooling. Laser optical cooling (refrigeration cooling) is a process that physically takes place when a mono-chromatically tuned laser beam is refracted through a m aterial, the interaction of laser light and the atoms/ions in the material results in a 'thermalization' process whose net effect is cooling of the material. Moreover, laser optical cooling is easily extendable to molecules and allows multiple absorption and spontaneous emission that involve approximately 10^4 photons [1].

It is important to note that laser optical cooling is totally different to what is commonly referred to as Doppler cooling where gas atoms are cooled by use of laser in a process of atomtrapping [2].

Generally, optical cooling process is subject to up-conversion mechanism in which low energy photons are absorbed by a rare earth doped material. Consecutively, the material will then undergo a thermalization process resulting in the emission of high energy photons.

History of Laser Optical Cooling

Refrigeration cooling at molecular level or Laser optical cooling as a result of interaction of light with matter was predicted as early as 1960 when the first laser was built by Theodore H. Maiman [3].

In 1852 Sir Stokes G. G. Published his work that resulted into stokes law. Stokes' law states that the emitted energy (photons) after refraction of light through a photonic material is always less than the incident beam (energy) and associated loss resulted into heating up of the material [4].

In 1929, Pringsheim had suggested a theory in explaining the phenomenon of laser optical cooling also referred to as refrigerative cooling, it was thought then that he contradicted the second law of thermodynamics [5]. However, in 1946 Landau [6] suggested a classical thermo-dynamical explanation to the phenomenon of laser optical cooling. In his report, he further demonstrated that net cooling was possible by a method that was later called anti- stokes cooling theory, where losses by means of monochromatism, and coherence of the laser photons outstripped gains in internal energy.

In 1968, Kushida and his colleagues attempted cooling a neodymium doped yttrium aluminium transparent material, by pumping it with 1064 nm laser line, they noticed only a reduction in heating [7]. A decade later, Djeu and Whitney succeeded in cooling a low-pressure CO_2 gas using anti-stokes fluorescence by a drop of 1 K [8].

It was not until 1995 that experimental laser optical cooling at a laboratory level was achieved by a group led by Epstein at Los-Alamos laboratory (New Mexico) [9]. During the experiment, they were able to demonstrate cooling of -0.5 K in a crystal by us e of laser.However, in the last two decades a sizeable number of experimental physicists and materialscientists has put work into laser cooling, where nanomaterial have been cooled to lowerand lower temperatures using the laser optical cooling technique.

It is worthwhile mentioning that this has made realization of laser optical cooling of certain material whose cooling ability is highly favored and have possible application in medicine, industry, and research. To date, the record for lowest achieved temperature in a laboratory set up is 119 Kelvin, recorded by the team at the Los-Alamos research laboratory in August 2016

[10]. More importantly, it is established that current mechanical refrigerating heat pump system were developed in the 1800s and have served mankind for over 170 y ears [11]. In addition, they are bulky, noisy, use too much energy, accompanied by a lot of vibrations, and are not suited for use as coolants at inter atomic levels. Interestingly, development in Science and Engineering have created new methods and applications for materials use, among them refrigeration of pinpoint spots in electronic circuits and cooling biomedical cells [12]. Finally, optical laser coolers are compact, non-vibration and very useful in cooling at atomic and molecular level, specifically on a spot cooling at micro-scale application.

The Research Problem

Equipment that is kept in remote areas (e.g. cell phone towers, satellite stations, and floating climate gathering balloons) require cooling that is done by convectional cooling air-conditioners. Such air-conditioners are great energy consumers and require regular maintenance. Moreover, it is thus paramount we search for, experiment, and build better cooling systems in particular for extreme uses in remote sites (satellites) and at micro-scale application or on the point cooling in medicine and microbiology application. Emerging technologies such as cryogenic electronics have evolved from giant circuitry to low energy micro-circuitry that requires alternative cooling mechanism away from dust blowing fan coolers be produced.

Moreover, research activities that have been conducted by scientists at the Los-Alamos laboratory have shown promising results in the creation of compact laser optical cooling materials [13]. Laser optical coolers promise very compact, non-vibration, low energy consumption, and long-life cooling systems as an alternative to current systems however, Researchers face several challenges in this critical field. First, it is difficult to upscale the synthesis of highly pure crystal; secondly it is difficult to successfully choose a material that suits laser optical coolers in a field that is just attracting interest no later than the last two decades [14]. This study synthesized, characterized and investigated $NaAlSiO_2$ crystals for possible up-conversion characteristics and a practical application.

Research Objective

General objective

In this work, we aim to synthesize pure crystals of Sodium aluminium silicate ($NaAlSiO_2$), this will be followed by investigating the $NaAlSiO_2$ to unveil its structural, micro structural and chemical composition.

Specific objectives

We will further, dope it with Er^{3+}, and c o-dope with Er^{3+} /Yb^{3+} ions and investigate its photoluminescence and its photonic behavior under laser excitation at 980 nm pumping. Finally, we will look for one possible up-converting application and establish its practical application.

Dissertation layout

Chapter 1; an overview and history of laser optical cooling, the research problem, and objective are presented.

Chapter 2; this chapter provides fundamental theory of laser optical cooling.

Chapter 3; Discusses the experimental methods and equipment setup used in the current study.

Chapter 4; Discusses the synthesis of the host materials including the results obtained via analytical characterization techniques such as XRD, SEM, EDS and FTIR.

Chapter 5; Comprises detailed discussion of optical properties of the doped and co-doped host material, including PL, power and temperature dependence photoluminescence measurements.
Chapter 6; Presents the conclusion/summary of the work.

References

[1]   Hansch, T. W., and Schawlow, A. L. 'Cooling of gases with laser radiation'. Opt. commun.13, (1975). pp. 68-69.

[2]   Galina Nemova. *Laser cooling; fundamental properties and application*. 978-981-4745-05-5 (ebook). USA: Pan Stanford publishing (2017).

[3]   Massimo G. 'More light on information historical'. *IEEE Industrial Electronics Magazine* 9.4, (2015). pp. 58-61.

[4]   StokesG G. 'On the change of refrangilibility of light. *philos. Trans. R.Soc. Lond.* 142, (1852). pp. 463-563.

[5]   Thiende JJ, Distel J., Greenfields. R., and Epstein R. I. 'Cooling to 208K by optical Refrigeration'. *Appl. Phy. lett.* 86 (2005). p.154107.

[6]   Landau L. 'On the thermodynamics of photo luminescence'. *J. of Phy.* (1946). 10 pp. 503-506.

[7]   Kushida T., and Geusic J.E. 'Optical refrigeration in Nd-doped. yttrium-aluminium garnet'. *Phys. Rev. lett*. (1968). 21, pp. 1172-1175.

[8]   Djeu N., and Whitney W.T. 'Laser cooling by spontaneous anti-stoke scattering'. *phys.Rev. lett.*(1981). 46,pp. 236-239.

[9]   Epstein R I., Buchwald M.I. Edwards B.C., Gosnell T.R., and Mungane C.E. 'Observation of laser-induced fluorescent cooling of a solid'. *Nature* 377, (1995). pp. 500-503.

[10]   Melgaard S. D., Denis V. Seletskiy, Alberto Di Lieto, and Mauro Tonelli. (2013). 'Optical refrigeration to 119 K below National Institute of standards and technology cryogenic temperature'. *Opt. Lett*. 38, pp. 1588-1590.

[11]   George L Chapel. *Gorrie's fridge*. Apalachiola,FL, 32329, USA. (2000).

[12]   Akiyama Yoshitake, Masato Shinose, Hiroki Watanabe, Shigeru Yamada, and Yasunari Kandabet. 'Cryoprotectant-free cryopreservation of mammalian cells by super flash freezing'. *National Academy of Sciences* 116.16, (2019) pp. 7738-

7743. doi: 10.1073/pnas.1808645116.

[13]   Seletskiy D. V., Markus P. Hehlen, Richard I. Epstein, and Mansoor Sheik-Bahae. 'Cryogenic optical refrigeration'. *Adv. Opt. Photonics*

4, (2012) pp. 78-104.

[14]   SeletskiyD. V., Richard Epstein, and Mansoor Sheik-Bahae. 'Laser cooling in solids: Advances and prospects'. R*ep. Prog. Phys*. 79, (2016). p. 096401.

Chapter 2

2.1 Theoretical background

Introduction

A Boltzmann statistical approach is applied to generate the equations of up-conversion and thus laser optical cooling processes equations and its analytical description is also discussed in detail, photon excitation at the atomic level is analyzed to give conditions necessary for up-conversion emission to take place in rare earth doped materials.

We further look at factors affecting the choice of our host material and its activation doping rare Earth elements. In addition, sodium aluminium silicate chemical characteristics are discussed. Finally, decay lifetime and its implication in the up- conversion processes are covered as we look at a possible up-conversion application.

Cooling by laser

The fundamental mechanism in cooling by laser is based on the multiplicity of intermolecular which describes the physical cooling of a crystal when pumped with a tuned laser beam, known as laser optical cooling as it involves light interaction within a crystal i.e. photon-phonon-electron at atomic levels [1, 2].

When a long-wavelength monochromatic beam of wavelength ($\sim$ 980nm) is directed onto specifically well-designed material, a process of thermalization takes place within the crystal resulting in a change in phonon energy as photons are absorbed and emitted from the crystal. The emitted photons have shorter wavelengths i.e. higher energies.
Analytically, the efficiency of such a system can be expressed as the difference in emitted energy to the absorbed energy [3].

$$oE = \text{absorbed Energy - emitted Energy} \tag{2.1}$$

$$aE = \frac{h\nu_e - h\nu_i}{h\nu_i} = \quad \boxed{} - 1 \tag{2.2}$$

where h= planks constant, ν_i is the initial frequency of the absorbed photons and ν_e is the frequency of the emitted photon.   7

Assuming that ve > vi then the value oE is negative, implying loss of energy from the system.

A net loss of energy from the system/crystal leads to anti-stokes cooling (laser optical cooling) taking place.

To understand how laser optical cooling develops in a system we look at a four-level model [4], the four level models are a consequence of interaction of electric charges of nearest neighboring ions in a host material. The stacks effect partially lifts each manifold into a degeneracy of (2j + 1) fold or (2j + 1)/2 levels, where j is total angular momentumof the system. Importantly the most efficiently used dopant in up-conversion experimentation is the Yb^{3+} ions as it has an advantage of possessing two simple states,it's ground state $^2F_{5/2}$, and an exited state $^2F_{5/2}$. Basically, the $^2F_{7/2}$ ground state has four steps named E1, E2, E3, and E4, the exited states has three steps namely E5, E6, and E7 thus in total seven degenerate energy steps. In representing the diagram of a degenerate structure, the steps are arranged in ladder form with a wider gap between the E4 and the E5 steps as this represents the main transition between the ground state and the excited state, this gap is the band gap and any excitation between this two levels may result in laser optical cooling when a lower wavelength beam than the absorbed beam is emitted.

It is worth noting that the ladder steps are also referred to as stark levels in many literatures.

Figure 2.1(a) shows the Yb^{3+}seven step degeneracy energy structure which are presented in a 4-step energy 4-step energy level structure in order to explain as to how laser optical cooling takes place in a Yb^{3+}. However, Figure 2.1(b) shows two energy level systems, the ground state has a width of oE_g and the excited state with oE_e.
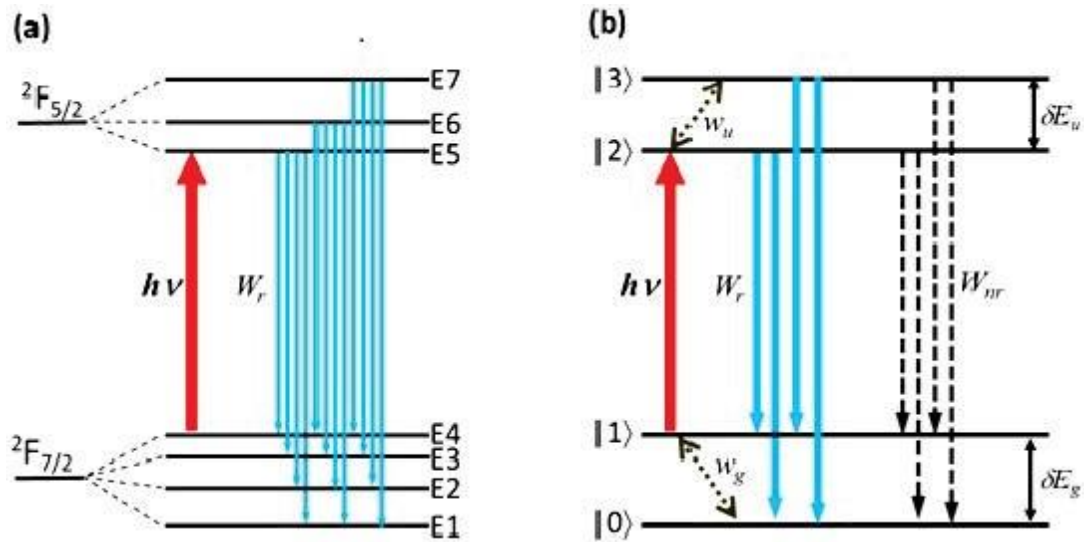
Figure 2.1: (a) Yb3$^+$ 7 steps degenerate energy structures showing the ground state and the excited states horizontal bars with all possible 12 transitions (arrows) that occur when thermalization occurs usually fluorescence is observed as the excited phonons transition back to ground state. (b) The simplified four level degenerate structure with two level ground states and two level excited states [4].

Once a monochromatic laser beam of energy hv is absorbed, excitation of phonon within the crystal takes place between step -I1 > and step I2 >, where the energy $hv_i = E_2 - E_1$ is absorbed, the 4f electrons in the Yb^{3+} interact with the electron-phonon interchanging thermalization, leading to attainment of an equilibrium in a fraction of a second after the excitation process, the system returns to equilibrium with ejection of a photon of energy hv$_e$ whose frequency ve is higher than the absorbed photons energy's frequency vi, thus the system losses energy in either a radiative process or a non-radiative process, the process is called relaxation. The process is thermodynamically expressed in a Boltzmann equilibrium distribution equations where

N_1, N_2, N_3, N_4 a e the phonon population density.

$$\frac{dN_1}{6} = -a_{12} \left(N_1 - \frac{g_2 N_2}{g_1}\right)_{h_u} + R (N_2 + N_3) - w_g (N_1 - \frac{}{g_2}N_0)e^{-\frac{E_g}{k_b T}} \qquad (2.3)$$

$$\frac{6N_2}{6} = -a_{12}\left(N_1 - \frac{g_2 N_2}{g_1}\right)\frac{I}{h_u} - RN_2 + w_e(N_3 - \frac{g_3}{g_2}(N_2)e^{-\frac{E_e}{k_b T}} \qquad (2.4)$$

$$\frac{6N_3}{6} = -RN_3 - w_e(N_3 - \frac{g_3}{g_2}(N_2)e^{-\frac{E_e}{k_b T}} \qquad (2.5)$$

$$N_t = N_0 + N_1 + N_2 + N_3 + N_4 \qquad (2.6)$$

where R is the total decay rate of the excited state, 012 the cross section of absorption associated with the energy transition from ground step I1 > into the excited step I2 >, I is the incidence laser beam, gi represents the factor of degeneracy, m(i) represent the interaction between the electrons and phonon.

It is worth noting that the total decay rate can be written as the $R = 2m (rad) + 2m (nonrad)$ and $k_b T$ is the Boltzmann distribution.

The difference between the initial absorbed energy and the emitted energy, the net power (P_{net}) is given by;

$$p_e = -a_{12}\left(N_1 - \frac{g_2 N_2}{g}\right)I - w(\text{rad})[\;_2(E_{21} + E_{20}) + \;_3(E_{31} + E_{30})] + I \qquad (2.7)$$

$$6E_i = -a_{12}\left(N_1 - \frac{g_2 N_2}{g_1}\right)I \qquad (2.8)$$

The absorbed energy in the transition (Ij1> - Ij2 >) can be expressed as in equation (2.8) and the emission equation for the state (Ij2 > -Ij3 >) can be expressed as

$$m(\text{rad}) \ [N_2(E_{21} + E_{20}) + N_3(E_{31} + E_{30})] \tag{2.9}$$

There are obviously other loses due to impurities and crystalline defects that we chose to represent with the terms $a_b I$.

To solve the above equations (eqns 2.3, 2.4, and 2.5) we equate the differential to zero as,

$$\frac{\partial[N_o, N_1, N_2, N_3]}{\partial t} = 0 \tag{2.10}$$

with

$$a = \frac{a_0}{1 + I/I_s} \tag{2.11}$$

Where

$$\alpha_0 = \varpi_{12} N_{\emptyset\emptyset} \frac{e^{\frac{-\delta E_{gg}}{K_{bb} T}}}{1 + e^{\frac{-\delta E_{gg}}{K_{bb} T}}} \tag{2.12}$$

and

$$I_s = \frac{h\varpi_{12} R}{\sigma_{12} Z g_{ee}} \tag{2.13}$$

$$Z g_e = 1 + \frac{e^{\frac{-\delta E_{gg}}{K_{bb} T}}}{1 + e^{\frac{-\delta E_{gg}}{K_{bb} T}}} [1 + e^{\frac{-\delta E_{gg}}{K_{bb} T}}] \tag{2.14}$$

$$\approx 1 + e^{\frac{-\delta E_{gg}}{K_{bb} T}} \tag{2.15}$$

The net power may be expressed as

$$P_{net} = \alpha \alpha I I \left(1 - \eta q \frac{h \nu \nu_{ee}}{h \nu \nu_{ii}} \right) + \underset{b}{\alpha} I \tag{2.16}$$

of course $\eta q = (1 + \omega nrad/\omega rad)-1$ is the quantum efficiency of the system. The mean energy in a four-step system is thus

$$\nu \nu_{ee} = h\nu_{ii} + \frac{\delta \partial \partial_{gg}}{2} + \frac{\delta \partial \partial_e}{1 + \left(1 + \frac{R}{\omega \omega_{ee}}\right) e^{\frac{-\delta E_{gg}}{K_{bb} T}}} \tag{2.17}$$

12

There are three possible scenarios as the limit $\delta E_g \rightarrow +\infty, -\infty$, and 0.

We are more concerned with laser optical cooling or refrigerative cooling that will happen when $k_bT \ll \delta E_g$ i.e. at low temperature δE_g must be very narrow if cooling has to

take place, from eqn. (2.17) m_e is much less than the recombination rate (R), $m_e < R$ otherwise radiative decay will occur before recombination thus no up-conversion emission would take place [5].

$$\eta = P_{net}/P_{abs.} = \eta_q \eta_{abs} h\nu e/h\nu \qquad (2.18)$$

The total absorbed power is expressed as Pabs = (a + ab) thus the efficiency of the system 11, is

where 11_q is the external quantum efficiency of the system while $11_{abs.}$ oE ;: 0 or very small. We see that as the above conditions are fulfilled ai --- ae, ; this shift in wavelength is referred to as the red shift. When the red shift occurs then loss in cooling occurs as stokes fluorescence takes place, the system undergoes quenching and thus no cooling can occur, this process is accompanied by r e re-absorption and phonon that generates reduced net cooling, to minimize these losses we require that 11 ;: 1 and ve < vi.

We have shown through a Boltzmann equilibrium distribution for laser optical cooling or up-conversion to occur, we have to have the following conditions fulfilled;

oEg ~0, $k_b T < oEg$, me < R, 11 ;: 1, and ve << vi

In words, the change in energy must be narrow, the recombination rate must be slower than the interaction between the electrons and the phonon, the quantum efficiency of the energy of the emitted photons must be higher than that of the absorbed beam and the efficiency of the system must approach unit.

It is already known that rare earth (lanthanide) ions emit and absorb laser in a narrow frequency range, the emission and absorption frequencies are independent of the host material or rather insensitive to the host. The lifetime of the thermalization process is always between μs and ms [6].

All rare earth (lanthanide) ions have an outer electronic structure of the form $5s^2 5p^6 6s^2$, this structure has shells filled up with electrons. The shielded 4f inner shells determine the optical properties of rare earth ions and are responsible for the up-conversion process.

14

The Choice of Host and Dopant

In their work in studying laser induced lensing in solid state optical refrigerators J.R. Silva and others [7] found out that aluminium silicate zeolites were a promising laser optical cooling materials, they too found out that doping with rare earth's improved the qualities of up-conversion (laser optical cooling) in the material, these occurs only when thematerial is dominated by anti-Stokes's luminescence centres. Further work by H Bowman and colleagues [8] revealed that doped calcium aluminium silicate was a possible laser optical cooling material, see table below.

Table 2.1, lists possible optically cooled host when doped with Yb^{3+} ions, among them $Ca_2Al_2SiO_7$ (arrowed).

For laser optical cooling to take place it is required that the material of choice have high quantum luminescence efficiency ;: 1, low intrinsic absorption, low non-radiative luminescence, and low phonon energy.

The aluminium silicate of calcium has been covered and thus we chose the next nearest alkaline aluminium silicate, as chemistry dictate that similar elements (e.g. alkaline earth metals) have almost the same physical, chemical and photonic characterization, thus we chose sodium aluminium silicate compound for synthesis, characterization and up-conversion investigation.

Table 2.1: Table of laser optical cooling materials.[8]

Host	λ_f	λ_{cp}	λ_{cl} nm (polarization)	np %	r ms	J_{min}	J_{max} kW/cm²	Z_1/Z_2 x 295 K	$F_{\infty 1}$	F_{eff} $10^{7\,22}$ cm²	F_{pie}	Ref
$KY(WO_4)_2$	992	1002 (a)	1041 (b)	20	0.60	1.6	55	123	1.50	41	36	11–13
$KGd(WO_4)_2$	993	1001 (a)	1042 (b)	17	0.60	13	43	123	1.33	36	37	11–13
$Lu_3Al_5O_{12}$	1002	1033	1048	67	0.92	26	303	0.89	0.49	5.1	0.83	14
$Sr_5(VO_4)_3F$	1041	1047 (m) , 1117 (m)		8	0.59	0.14	16	1	0.45	5.8	9.2	15–16
$Ca_5(PO_4)_3F$	1033	1046 (m)	1123 (m)	14	1.10	0.14	29	1	0.35	3.8	4.6	17
$Y_3Al_5O_{12}$	1007	1031	1049	56	0.95	15	133	0.88	0.32	4.3	1.1	18
$BaCaBO_3F$	1020	1035 (m)	1084 (b)	22	1.17	1.7	20	1	0.19	2.1	1.9	19
Y_2SiO_5	1001	1007 (c)	1036 (c)	18	1.04	11	18	1	0.15	2.8	5.5	20
BaY_2F_8	995	1015 (c)	1030 (c)	58	2.04	51	97	1	0.14	2.3	1.8	20
Sc_2O_3	1022	1042	1095	27	0.80	23	34	1	0.13	1.25	1.0	22
KY_3F_{10}	992	1003	1014	49	1.87	63	64	1	0.12	2.0	3.0	20
$YAl_3(BO_3)_4$	999	1008 (b)	1037 (b)	22	0.68	21	13	119	0.114	2.1	12	21
$LiYF_4$	996	1004 (m)	1017 (m)	41	2.21	34	19	0.90	0.108	2.0	6.0	20
$Ca_2Al_2SiO_7$	1012	1028 (b)	1081 (b)	22	0.82	4.7	16	117	0.077	1.02	3.0	23
$ZBLANP$	995	1005	1024	36	1.70	38	46	107	0.070	1.32	2.4	6
$Ca_4GdO(BO_3)_3$	1011	1032 (c)	1083 (c)	30	2.50	2.5	35	118	0.068	0.84	0.54	24
Rb_2NaYF_4	996	1011	1068	20	10.8	1.8	17	1	0.020	0.25	0.34	20
$YCaO(BO_3)_3$	1035	1047 (c)	1084 (c)	25	2.28	8.9	15	0.96	0.013	0.21	0.63	25

We are interested in its visible region up-conversion emissions (laser optical cooling characteristics) when doped with Er^{3+}, and Yb^{3+} and any combination in single doping that give maximum luminescence in up-conversion. The alkaline earth (sodium) aluminium silicate was our choice of host.

The choice of the host material and the dopant are critical in our case in determining the shift in the absorption and emission curves as stated by Dwivedi.

In their work Dwivedi Y. and others, suggested the use of Eu^{3+} and Tb^{3+} as suitable wide shift in up-conversion from a 980nm pumped laser beam but Bowman and others suggested a Er^{3+}/Yb^{3+} d o p e d matrix [9].

Bowman further emphasized of a crystalline host due to their high cross section ascompared to amorphous glass. However Xi-xian Luo and his colleagues showed that a Yb^{3+}/Ho^{3+} doped matrix exhibited NIR, red, green, blue and even ultraviolet-blue emission bands under 980 nm pumping and an excellent up-conversion luminescence[10]. Most work done on up-conversion uses Yb^{3+} as the main sensitizing agent.

In their work Ventrone F. and colleagues [11] found that the co-doped pair of Er^{3+} and Yb^{3+} had a highly enhanced up-conversion emission in the visible region after pumping with laser at 980 nm as compared to other pairs. They linked the increase in concentration of the Yb^{3+} to the relative increase in emission at the green region compared to the red region.

Sodium aluminium Silicate (NaAlSiO$_2$)

Sodium aluminium silicate is a member of the Zeolite group of compounds whose high ability to absorb water gave them their name from the Greek words Zeo (boiling) and lithos (a stone) when in 1756 a Swedish mineralogist A. Fredrick Cronstedt heated some stibnite and a large amount of steam was produced [12].

Generally, Zeolites are porous compounds formed by hydr ated aluminium silicate of group I and II alkaline earth metals. The main frame works in this compound are the$[AlO4]^{5-}$and the $[SiO4]^{4-}$[13].The formula for a Zeolite unit cell is given by

$$M^{x}(AlO_2)_x(SiO_2)_y]wH_2O \qquad\qquad (2.19)$$
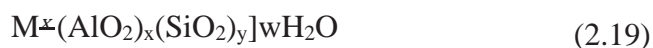
where M is the metallic alkaline cation, *n* is the valence of the cations, w is the number of water molecules, x and y are the number of tetrahedrons for each unit cell. The ratio of y/x is between 10 – 100 for silicate Zeolites. Zeolites can be classified according to the structure of the cages formed within a lattice from those with low Al/Si :S 2 ratio to those with higher ratios 2 – 5 as intermediates and high silica Zeolites those with ratios > 5. shown in table 2.2. Synthesized zeolites are named as " A, X, L, and Zsm and omega [15].

Table 2.2: Grades of Zeolites [14].

Zeolite grades	Si/Al ratio	Common zeolite names/frame works
Low silica	< 2	Analcime (ANA), Na-X(FAU)
Medium silica	2~5	Chabazite (CHA), Faujisite (FAU)
High silica	>5	ZSM-5(MFI), Zeolite-β(BEA

Properties of NaAlSiO$_2$

To understand the properties of NaAlSiO$_2$,the crystalline phase transformations that occur in the synthesis of the zeolite materials has to be looked into.NaAlSiO$_2$is formed through the process of polymorphic transformation whose structure can be classified as, hexagonal, and cubic depending on the reaction thermo-chemistry[16].

 The by-product of the reaction is determined by the composition of the reactants and the environmental condition available. The composition of Na$_2$O, Al$_2$O$_3$, and SiO$_2$ is varied with the ratio Na$_2$O/Al$_2$O$_3$ that favors the formation of three structure; when the ratio of Na$_2$O/Al$_2$O$_3$ is greater than 1 a cubic structure is the stable phase, a rich Al^{3+} reaction will have the ratio of Na$_2$O/Al$_2$O$_3 <$ 1, this will have Si^{4+} replace the Al^{3+} cation favoring the formation of the hexagonal polymorphic structure of SiO$_2$.

When the ratio of Na/Al =1 an amorphous form of the formulae $Na_2O.Al_2O_3.2SiO_2$ is formed. The chemical and thermal dynamical properties are determined by their Si-Al ordering and the Al^{3+} ions charge compensation that affects the structural behavior.

The crystallization of pure Na based $NaAlSiO_2$ is initiated by formation of a metastable form carnegieite phase that is transformed into a hexagonal structure with increase in reaction time and temperature.[17]

In a stoichiometric reaction, the by product in the synthesis of $NaAlSiO_2$ formed are othorhombic, the hexagonal structure and the cubic phases, formed at low, medium and high reaction temperature respectively. Temperature wise we may write at low temperature the orthorhombic phase is the product, at medium temperatures a hexagonal structure is produced, and at high temperature a cubic structure is the product, however, in a non-stoichiometric reaction several multiples of orthorhombic cubic tetragonal and hexagonal phases are produced. [18, 19, 20, 21, 22]

Where the concentration of Na is equimolar to that of Al, the reaction is rich in Si ions. The by roduct is referred as nepheline and has a general formulae $Na_{(1-x)}, Al_{(1-x)}, Si_{(1+x)}O_4$. While when the reaction is Al ion-rich in composition we refer to it as a carnegieite with a general formulae $Na_{(2-y)}, Al_{(2-y)}, Si_yO_4$.[22],

When the ratio of Na/Al=1 the amorphous structure formed corresponds to Na_2O, Al_2O_3, SiO_2 and its structure resembles that of pure SiO_2. The Si-Al ordering and charge compensation of Al^{3+} ions govern the chemical and thermodynamic properties of the $NaAlSiO_2$ [23].

In this study the non-stoichiometric reaction route is taken, thus the ratio of Na/Al $;:1$ as we work at low temperatures ($;:100\ ^{o}C$) and thus we expect a by-product of the amorphous Na_2O, Al_2O_3, SiO_2 with multiple structures of orthorhombic, cubic, tetragonal and hexagonal phases.

Mechanism   of   Photoluminescence

Luminescence occurs when a solid material phosphor emits electromagnetic (EM) radiation in the region between Ultra violet and infra-red radiation [24]. There are several types of luminescence as listed in the table 2.3 below,

Table 2.3: Types of Luminescence.

Type	Excitation source
Photoluminescence, Cathodoluminescence,	Light Electrons X-rays,
Radioluminescence, Thermoluminescence ,	Heating,
Electroluminescence, Triboluminescence ,	Electric field or current ,
Sonoluminescence,	Mechanical energy, sound waves in liquids,
Chemiluminescence, and bioluminescence,	Chemical reactions

In , this work, we will deal with luminescence experienced in the visible region of the EM(from 380 nm to 720 n m) i.e. photoluminescence(PL). Photo luminescence materials are nano-phosphors of inorganic origin doped with very low percentage levels of impurities of rare earth compounds. The maximum photoluminescence absorption
-emission levels may have to be determined as to avoid dope quenching that occurs when high percentage concentration of the dopant exceeds the saturation level above which excitation emission are suppressed. Photoluminescence occurs when absorption of phonon energy into the host material leads to excited photons being ejected from the nano-phosphor [25]. Rare earth ions that do absorb phonon energy and thus emit photon energy are known as activators. This is the basic method of   photoluminescence but there are other methods under which luminescence occurs, e.g., when a weak absorbing do-pant (activator) becomes a sensitizer by passing its phonon energy to a neighboring activator that then emits   a luminescence photon [26]. There are two classes of photo-luminescence,

Phosphorescence and fluorescence are classed according to the life time of their thermalization process. Thermalization process is the term used to encompass the process of photon absorption into a doped host, conversion into phonon, excitation and thenthe emission of a new frequency photon, coupled with relaxation to ground state [27]. Phosphorescence occurs, when a material remits an absorbed photons in a continuous stream long after the excitation source has been withdrawn, it could be for μs or even hours (long after glow emission). Importantly, fluorescence is a process that stops emissions immediately the excitation source is withdrawn.

Photoluminescence (PL) is a process in which an electron is excited to higher energy level upon photon absorption. There are two types of photoluminescence namely intrinsic photoluminescence and extrinsic photo luminescence. Intrinsic photo luminescence occurs in pure materials that contain no impurities. Extrinsic photo luminescence occurs in materials that have impurities introduced intentionally usually rare earth metals in a process called doping.

In this work we shall deal with extrinsic photoluminescence and will refer to it as photoluminescence [28, 29].

Up-conversion Process

The optical process where long wavelength photons get converted into short wavelength photons after being transmitted through a doped nanomaterial [30] is called up- conversion. Experimentally, most photo luminescence materials e.g. quantum dots, dyed molecules emit light under down conversion process that emits longer wavelength light under short wavelength pumping. Moreover, high up-converting materials e.g. fluorides have the following desirable properties and are excellent hosts for up-conversion research, high refractive index, high transparency, and low photon energy [31]. It is worth noting that these properties favor non-radiative decay or high quantum efficiency that enhances up-conversion. It is materials with these photonic characteristic that are suitable for laser optical cooling [32].

In the context of the present study, we are in need of high quality, high efficient up- conversion rare earth doped nanomaterials for application in laser optical cooling in physical and biological field, infra-red sensors, microelectronic coolers, remote sensing, in vivo and in vitro bio- imaging [33]. In addition, up-converting laser optical coolers may find great use in manufacturing of temperature sensors, compact solid state coolers, infra-red counters and detectors, bio-imaging, cancer surface sensing.

Theoretically most rare earth ions can undergo up conversion by pumping at low energy 980nm from near infra-red (NIR) to visible region, but only few are efficient enough to show high intensity up- conversion emissions e.g. Yb^{3+}/Er^{3+} or Yb^{3+}/Tm^{3+} co-doped nanomaterials. Generally, there are at least three basic mechanism of up-conversion that dominate most up-conversion processes that interest our research. They are known as excited state absorption (ESA), photon avalanche (PA), and energy transfer up-conversion (ETU). The up-conversion efficiency diagrams indicate the efficiency of the three up conversion processes with efficiencies 10^{-3}, 10^{-5}, 10^{-15} for ETU, ESA and PA respectively figure. 2.2.
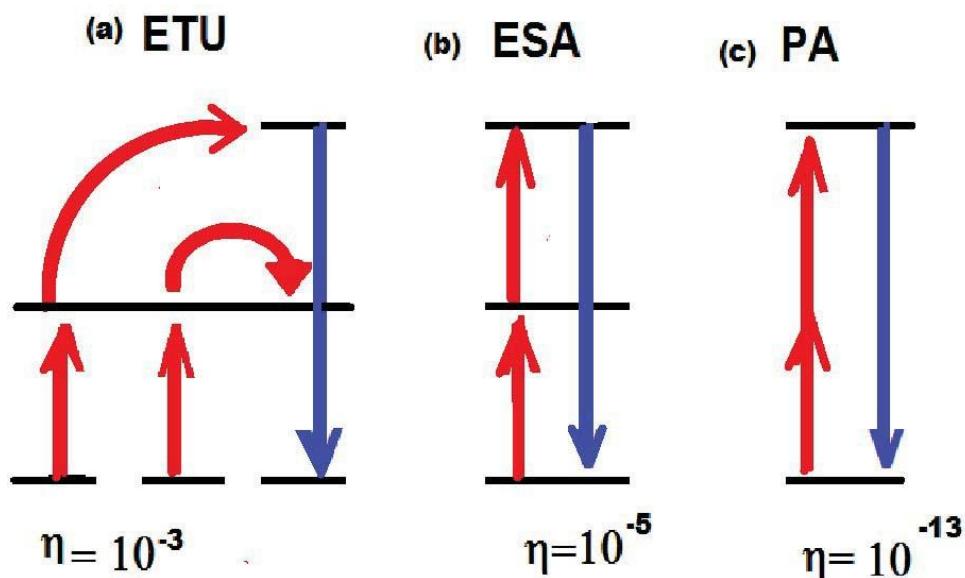
Figure 2.2: Up conversion efficiency diagrams for ETU, ESA and PA [34].

We see that the most efficient process of up conversion is the ETU and it involves two dopants or what we call co-doping in nanomaterial physics.

Excited state absorption

Ions with single ion centres e.g. Er^{3+}, Ho^{3+}, Tm^{3+}, and $Nd^{3+}$are highly favored in multi- step excitation up-conversion emission, They absorb photons from ground state
that jump into an intermediate stage and finally populate the excited state that leads to relaxation in radiative or non-radiative process, when non radiative relaxation takes place up-conversion takes place as the ions relax at ground state with emission of higher energy photons. Figure 2.3 describes the ESA process in a schematic form, we have mt > m1, mo. E_0, E_1, and E_2 represent the ground state, intermediate state and the excited state respectively.
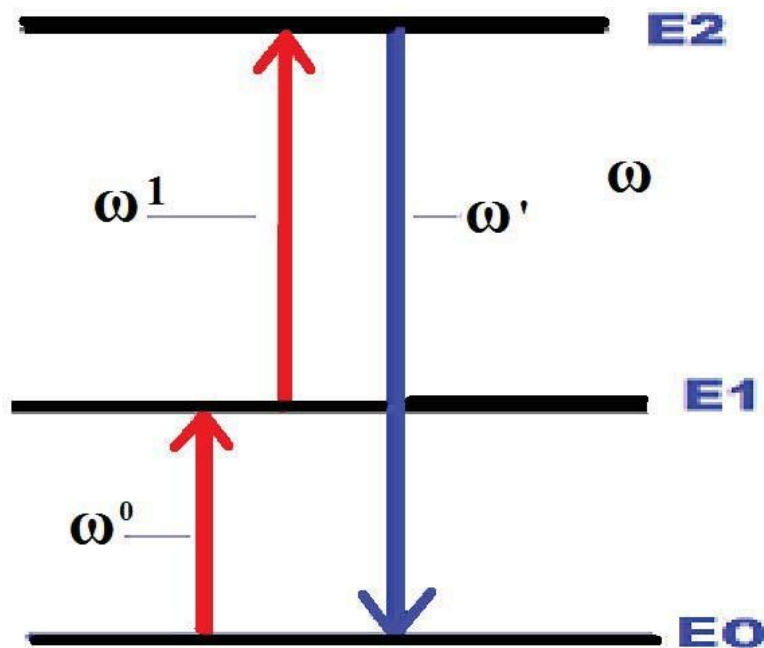
Figure 2.3: Excited state absorption (ESA) up-conversion mechanism [35].

When one ion or electron in Eo state absorbs a photon, it first gets elevated to the intermediate state E_1, then after a subsequent absorption of a second photon it is pumped into the excited state E_2, but due to instability in that state it relaxes back to ground state with emission of a higher energy photon [36].

21

Photon Avalanche

Photon Avalanche (PA) is a complex process that has three distinct nonlinear qualities that takes the form of an energy transfer emission step system with energies E_0; E_1; E_2 and E representing levels from ground state through intermediate state to excited state respectively, figure 2.4.
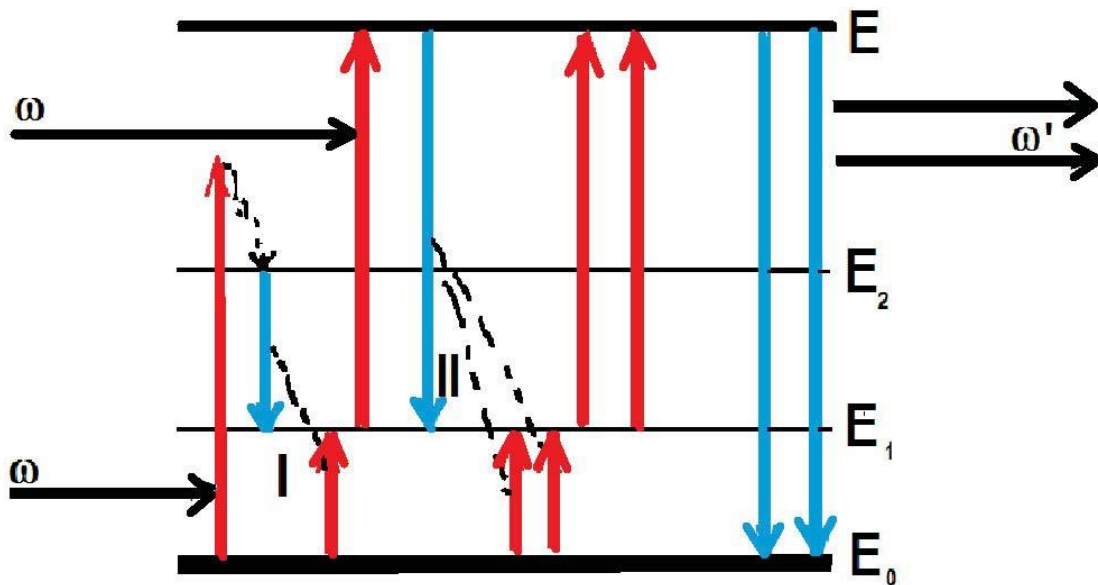
Figure 2.4: Schematic diagram for Photon avalanche up-conversion mechanism [36].

An electron or ion is excited once it absorbs a photon m and jumps into the higher intermediate states E_1 or E_2. As it is not stable the absorption transitions to a level a little higher than the E_2 but cross relaxes back into state E_2, Energy transfer follows between states E_2 and E_0 leading to two electrons being formed in the state E_1, One electron absorbs the photon of excitation and is ejected into state E. Interaction with E_0 electrons step II occurs as three E_1 electrons are absorbed. This photon excitation is in resonance with the transition E_1 to E_2, the process is repeated severally drastically increasing the number of electrons excited at E state, due to laws of equilibrium the electrons relax to state E_0 emitting low wavelength photons that have higher energy than the absorbed photons.

Energy Transfer Up-conversion

Energy transfer up-conversion (ETU) is the most efficient up-conversion method known to date[9].This process involves two do-pants and a host, one do-pant is called the activator while the other is called a sensitizer. We can say one do-pant acts like a catalyst to the other enhancing up-conversion emissions much more than when each other do-pants are tested for up-conversion individually.

Activators have weak electron-phonon coupling in the f-f transition band. Most of these rare earth activators have a single 4f energy levels e.g. Yb^{3+}; La^{3+}; Ce^{3+} [37]. In addition, dopant contact in a host is limited by cross-relaxation and quenching effect, thus the most efficient co-doping process is introduced by adding a sensitizer that has sufficient absorption cross section in the near infra read region(NIR).Furthermore, best used sensitizers are Er^{3+} and Yb^{3+}. The Yb^{3+} possess a simple energy level scheme with one ground state and one excited state in the 4f level at $^{2}F_{5/2}$ these states match very well with Er3+s', $^{4}I_{5/2}$;$^{4}I_{7/2}$;$^{4}I_{1/2}$ allowing energy transfer in the ions seamlessly. See figure 2.5.

Overall, Yb^{3+} is co-doped into the host lattice at high concentrations of 10 -20%, the activator is doped at less than 2% to minimize cross relaxation[38].The above statementby Richard B. S. [38] will later influence our choice of concentration of the dopant andthe co-dopant.
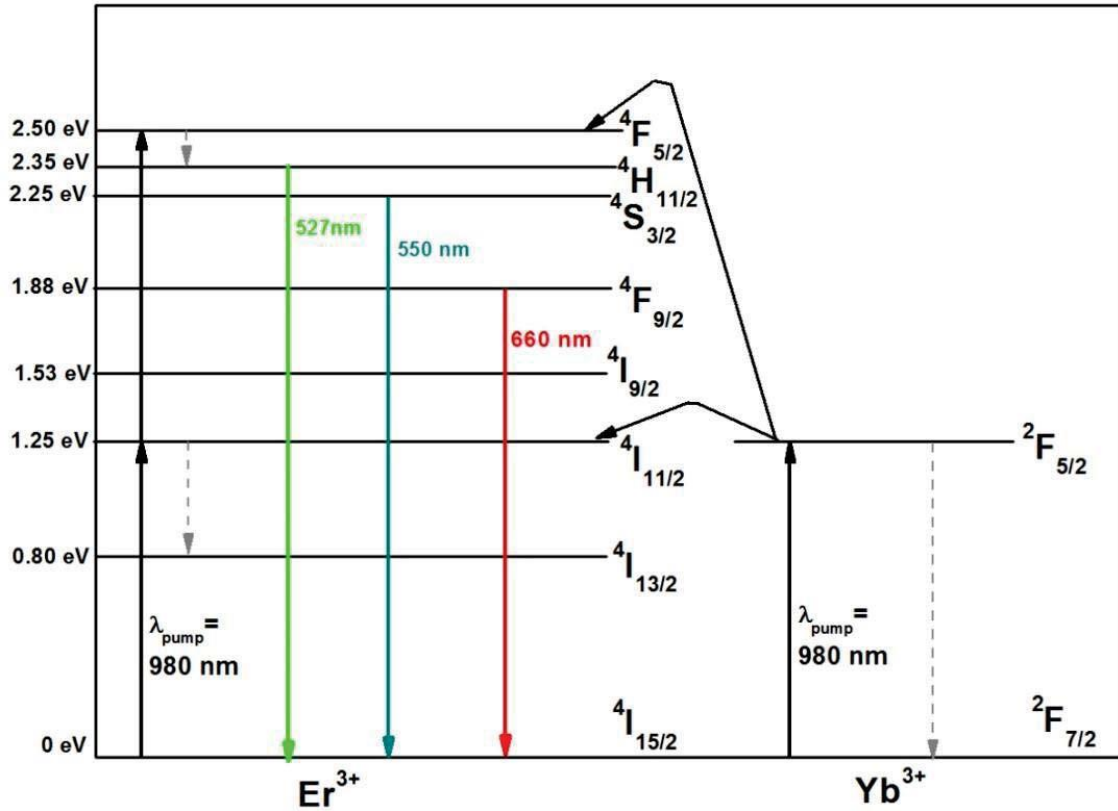
Figure 2.5: Schematic diagram for a free structured Er^{3+} ion. Up arrows assign transitions in up-conversion under excitation at 1500nm, Down arrows are emission after up conversion process with emission given [39].

Decay life time

As we have seen the Yb^{3+} /Er^{3+} up-conversion co-doped system emits high intensity photo-luminescence through absorption of two high wavelength 980nm low energy (< *2m W*) photons, giving three sharp emissions in the visible region, with two in the green region and one in the red region at exactly 520 nm; 540 n m and 656 nm [40].These emissions leave sharp broad peaks with little background noise and long decay times in the region of micro second (*μs*) to the millisecond(*ms.*) [41,42].

Convectional fluorescence materials have lifetimes in the order of nano seconds; this

include quantum dots and organic dyes [43] such life times are too short to give us any meaningful information on identification of luminescence interferences from photons that get scattered during the up-conversion process. However, rare earth doped nanomaterials give lifetimes in the order of micro second (*μsec*) to the millisecond (*msec.*).Up-conversion photoluminescence in doped nanomaterials can be used to realize frequency conversion, high resistance to optical pulsing, and intense peaks, with high photo stability, all qualities we may use in practical application [44].

Study of the decay curves is one method in enhancing knowledge of up-conversion quantum yield, this helps in reaching full potential for practical applications in science, medicine and industry of up-conversion nanomaterials [45].The Yb^{3+}/Er^{3+} co-doped nanomaterials show up-conversion processes that is dominated by excitation state absorption(ESA) and energy transfer up-conversion(ETU) processes[46, 47]. A ground state $^4I_{15/2}$ Er^{3+}ion is exited to state $^4I_{11/2}$ by either ground state absorption of one 980 nm photon or through energy transfer (ETU) from an exited Yb^{3+} ion. The process is summerized in Eq. 2.20

$$^4I_{15/2}(Er) \ + \ ^2F_{5/2}(Yb) \ \text{---} \ ^4I_{11/2}(Er) + \ ^2F_{7/2}(Yb) \tag{2.20}$$
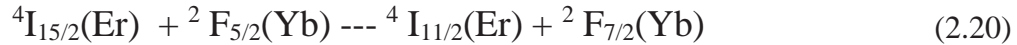
The Er^{3+}ions in $^4I_{11/2}$ are immediately excited to $^4I_{7/2}$ level of the Er^{3+}ions after absorbing another Yb^{3+} ion.

The Er^{3+}ions decays non- adiatively to the photo luminescent states$^2H_{11/2}$ and $^4H_{9/2}$ or else the Er^{3+} ions at the $^4I_{11/2}$ could undergo non radiative decay to $^4I_{13/2}$ level and then get further excited to $^4F_{9/2}$ after absorbing a second 980nm photon[48]. The decay life time of a nano-materials is a spontaneous process when photo-luminescence is released but with reducing intensity as time increases [49] ; longer decay life time indicates slow decay time and long after glows, the exponential decay equation can be expressed as

$$I(t) = I_1 \, e^{-t/rD} + I_2 \, e^{-t/rR} \tag{2.21}$$

where; $I(t)$= photo luminescence intensity at the time t corresponding to the on and off of the pulse laser, r_D =decay life time of the up-conversion process, r_R = rise time influenced by the

life time of the emission state and the ETU rate. It is from this equation that we will calculate our decay lifetime from curve fitting of our co-doped sodium aluminium silicate nanomaterial's exponential decay curves.

References

[1]   Seletskiy D V, Markus P. Hehlen, Richard P. E& Mansoor Sheik-Bahae. 'Cryogenic optical refrigeration'. *Adv. Opt. Photonics* 4.(2012)pp. 78-104.

[2]   Kastler A.'Some suggestions concerning the production and detection by optical means of inequalities in the populations of levels of spatial quantization in atoms. Application to the Stern and Gerlach and magnetic resonance experiments'. *J. Phys.Radium* 11, (1950). ' p. 11.

[3]   Epstein R. P., and Mansoor Shiek-Bahael. 'Observation of laser-induced fluorescent cooling of a solid'.*Nature 377*, (1995).pp. 500-503.

[4]   Seletskiy D V, and Richard Epstein. 'Laser cooling in solids: advances and prospects'. *Rep. Prog. Phys.* 79 (2016) , p. 096401.

[5]   Emin D, and Sheik Bahae M. 'Laser cooling via excitation of localised electrons'. *phys. Rev.* 76.B, (2007). p. 024301.

[6]   Galina Nemova, .ed. *Laser cooling; fundamental properties and application*. 978-981-4745-05-5(ebook). USA: Pan Stanford publishing (2017).

[7]   Silva JR, Andrade LHC, Lima LC, and Hehlen MP 'Laser induced lensing in solid state optical refrigerators',*App.phy.lette*.102 (2013)., pp. 1419101-4.

[8]   Bowman Hand Carl Mungan. 'New materials for Optical cooling',*appl.phys.*71.B, (2000). pp. 807-811.

[9]   Dwivedi Y. 'Advances in rare earth spectroscopy and application', *J.nanosci and Nano technol* 14.2, (2014). pp. 1578-96.

[10]   Luo X, Ying Tian, and Yao Fu. 'Up-conversion luminescence of holmium and ytterbium co-doped yttrium oxysul de phosphor', *mat. lett.* 61.17, (2007). pp. 3696-3700. doi: https://doi.org/10.1016/j.matlet.2006.12.021

[11]   Ventrone F., and John Christopher Boyer. 'Significance of Y b^{3+} concentration on the up conversion mechanism in co dope Y$_2$O$_3$: Er^{3+} Y b^{3+}nanocrystal'.*J. appl. Phy.* 96, (2004). pp. 661-667.

[12]   Edwin M. G. and Nickel M. 'Beginning of greatness in Swedish chemistry II Axel Fredrick Crostedt'. *Transactions of Cansas Academy of Science* 72.4,(1969). pp.476-485.

[13]   Petrov I., and Michalev T. 'Synthesis of zeolite'. A. Review. J. of Russian Scientific works 51, (2012). pp. 30-35.

[14]   Christopher Amrhein, Gholam H. Haghnia, Tai Soon Kim, Paul A. Mosher, Ryan C. Gagajena, TedrosAmanios, and Laura de la Torre. 'A review on s ynthesis, characterization and industrial application of fly ash Zeolites'. *J.Mater.Edu.* 33.1-2, (2011). pp.65-130.

[15]   Walter M.Meier. *Atlas of Zeolites*. Netherlands (2007).

[16]   Volter K., and Bohm H. '*Crystal* structure of hexagonal trinepheline; Anew syntheticNaAlSiO4 modification'. *American Mineralogist* 83, (1998).pp.631-637.

[17]   Thompson JG, and Withers, Ray L. 'A reinvestigation of low-carnegiete by XRD,NMR, and TEM'. *J solid state chem*. 104, (1993). pp. 59-73.

[18]   Thompson, John G.Withers, Ray L. and Richard M.An XRD and electron diffraction study of cristobalite related phases in the NaAlO2-NaAlSiO4 system. *J.solidstate chem.*131, (1997).pp.24-37.

[19]   Thompson JG. & Traill, Richard M. Cristobate related phases in the NaAlO2 - NaAlSiO4 system two tetragonal and two Orthorhombic structures. *Struc.Sci.*54 (1998), pp.531-547.

[20]   Wither RL. 'Cristobate related phases in the NaAlO2 -NaAlSiO4 system A commensumately modulated cubic structure'. *Struc. Sci.*54 (1998), pp.547-557.

[21]   Dimitrijevic R., and Dondur V. 'Structural characterization of pure Na-nephelines synthesized by zeolite conversion route'.*J.phys.chem.solids.*65, (2004). pp. 1623-1633.

[22]   MarkovicS.,and Dondur V. 'FTIR spectroscopy of frame work allumino silicate structural carnagieite and pure sodium nepheline'. *J.Mol.struc*. 654, (2003). pp. 223-234.

[23]   Seifert F A., and Mysen B O. 'Three dimensional network structure of quenched melts (glass) in the systems SiO2-NaAlO2, SiO2-CaAl2O4 and SiO2-MgAl2O4'. *Am. mineral* 67 (1982), pp. 696-717.

[24]   Ozawa w.,ed. *Cathode luminescence and phot oluminescence; theory and ap - plication*. Baco Raton, FL, USA: CRC press (2007)..

[25]   NikitenkoVA.,andTereshchenko IA.Photo- and thermo-luminescence excitation spectra of zinc oxide single crystals. *Journal of Applied Spectroscopy* 30.5, (1979).pp. 599-602.

[26]   Zhang F. *Photon up-conversion nano materials*. Ed. by S pringe. First. Springe heidelburg, New york: Springer(2015).

[27]   Briggs M. *Synthesis, characterization and l uminescence of Z nS : M n2+ nan o phosphor*. MA thesis. University of the Free state, South Africa: University of Free State (2009).

[28]   Dhlamini M.S. *Luminescent properties of synthesized PbS nanoparticle phos-phors*". PhD thesis. University of the Free State, South Africa (2008).

[29]   Kabongo GL. *Luminescence investigation of zinc oxide nanoparticles doped with rare earth ions*. MSc thesis. Unisa, Physics Department. (2013).

[30]   Chen J, and Zhao J. 'Up-conversion n anomaterials:Synthesis mechanism and application in sensing'. *Sensors* 12, (2012). pp. 2414-2435.

[31]   Egger P., and Wang K. 'A new near infra red to ultra violet up-conversion material'. *J. of Adv. mater.* 8, (1996).pp. 668-672.

[32]   Markus P. H., and Mansoor Sheik-Bahae. 'Materials for Optical cryocoolers'. *J. of Matt. Chem.*1 ,(2013). pp. 7471-7478.

[33]   Liu Q., and SunY.Sub. '10 nm, hexagonal lanthanide doped Sodium lutetium fluoride up-conversion nano crystals for sensitive bio imaging in vivo'. *J. Am. Chem. Soc.*133 , (2011). pp. 17122-17125.

[34]   Strumpel C. *Application of Erbium doped up converters to silica solar cells*. PhD Thesis. Germany: University of Konstanz. (2007).

[35]   Auzel F. 'Up-conversion anti stoke process with f and d ion in solid's.

Chem. Rev. 104, (2004). pp. 139-143.

[36]   Wang G., and Batentschuk M. 'Rare earth ion doped up-conversion materials for photo voltaic application'. *Adv. Mater.* 23, (2011). pp. 2675-2680.

[37]   Strumpel C, and Mc Cann. 'Modifying the solar spectrum to enhance silica solar cell efficiency'. *Soll. Energy Mat. and Soll. Cells* 91, (2007). pp. 238-249.

[38]   Shalav A., Richards B. S.,and GreenM. A. 'Luminescence layers for enhanced silica solar cell performance down conversion'. *Soll. Energy Mat. and Soll. Cells* 90, (2006). pp. 1189-1207.

[39]   Johannsen S R ."*Up-conversion of near infra red light through Er doped Tio2 and the e ffect of plasmonics and c o-doping with y tterbium*". Ph D Thesis. University of Aarhus (2015)..

[40]   Heng Qin, Danyang Wu, JunaSathian, XiangyuXie, Mary Ryan, and Fang Xie . 'Tuning the up-conversion photo luminescence lifetime of Sodium ytriumfloride co-doped with Ytterbium with Erbium and triple doped with Lathanide Gadolinium'. *Nature* 8, (2018). pp. 12683-12691.

[41]   Zhou B., and Bingyang S. 'Controlling up -conversion nano crystals for energy application'. *Nature tech*. 10, (2015). pp. 924-929.

[42]   Liu X., and Renren D. 'Probing the nature of up-conversion nanocrystals, Instrumentation matters'. *Chem. Soc. Reviews* 44, (2015). pp. 1479-1508.

[43]   Resch-Genger U., and Markus G. 'Quantum dots versus organic dyes as fluorescence labels'. *Nature Methods* 5, (2008). pp. 763-775.

[44]   Wang F., and Liu X. 'Multi color tuning of lanthanide doped nano particles by single wavelength excitation'. *Accounts of Chem. Research* 47 (2014)., pp. 1378-1385.

[45]   Li Z., and Yong Z. 'Multicolor Core/Shell-Structured Up-conversion Fluorescent Nano particles'. *Adv. Matt*. 20, (2008). pp. 4765-4769.

[46]   Lu D., and Mao C. 'Experimental demonstration of plasmon enhanced energy transfer rate in NaYF4:Yb3+, Er3+ up-conversion nanoparticles'. *Nano letters* 14, (2014). pp. 101-106.

[47]   Lu D. , and Mao C. 'Plasmon enhancement of luminescence up-conversion'. *Chem. Soc. Reviews* 44, (2015). pp. 2940-2962.

[48]   Ding M., and Chen D. 'Simultaneous morphology manipulation and up-conversion luminescence enhancement of beta-NaYF4:Yb3+/Er3+ microcrystals by simply tuning the KF dosage'. *Scientific Reports* 5, (2015). pp. 12745-12759.

[49]   Wei T., and Ying T.Mid-infrared fluorescence, energy transfer process and rate equation analysis in Er3+ doped germanate glass'. *Scientific Report* 4, (2014).' p. 6060

Chapter 3

Experimental Methods

Introduction

The synthesis approach used in the present research project is the hydrothermal process. The hydrothermal method was successfully used to synthesize pure $NaAlSiO_2$ samples that were further used as a h ost material. Moreover, the incipient wetness method was employed to dope and co-dope the host $NaAlSiO_2$ with Er^{3+} and Yb^{3+} ions. Furthermore, the adopted synthesis procedure was critical to realizing a high level of purity in the as-synthesized un-doped, doped, and co-doped $NaAlSiO_2$ host material, respectively. More importantly, several analytical non-destructive methods were used to perform the characterization of both samples. Finally, in the next sections, we provide a detailed description of the hydrothermal method and also characterization techniques that comprise X-ray diffraction (XRD), Scanning Electron Microscopy (SEM), Energy Dispersive X-ray Spectroscopy (EDS), Fourier Transform Infra-Red (FTIR) spectroscopy, Ultraviolet-Visible-Near Infra-Red (UV/Vis/NIR) Spectroscopy, Photoluminescence Spectroscopy (PL) and Thermal Dependence Spectroscopy (TD).

Synthesis of Sodium aluminium silicate crystals

Hydrothermal synthesis and doping process

The hydrothermal synthesis is a technique that takes place in aqueous conditions at high temperatures, and favors crystallization. This encourages the formation of different phases as the synthesis parameters change [1].

 In their work Kosanovic and co-w.orkers [2] stated that the hydrothermal
process enhanced nucleation of micro-structure. Besides, D. Georgiev and colleagues [3] suggested a solution to gel mixture that generated granules of irregular shapes. On the other hand, in their work Manuel M and colleagues [4] suggested that a seeding method be used where initial crystals formed were seeded to increase crystal sizes, this process was adopted and later abandoned after we realized it did not influence the up-conversion in the rare-earth-doped sodium aluminium silicate crystals.

To optimize the synthesis processes we looked at work done by Hums and others, [5] where the composition of the initial reactants, careful choice of reactants, temperature, and allowing enough reaction time were discussed. To obtain narrow particle size distribution we required a homogeneous distribution of the viable nuclei. All the above-mentioned researchers used varied methods of hydrothermal in their synthesis of aluminium silicate crystals, we thus adopted the hydrothermal path. In their work on doping techniques, J. E. Townsend [6] said good doping techniques should provide excellent do-pant uniformity in distribution and be sufficiently versatile to allow co-doping with different ions. The incipient wetness impregnation doping method was adopted due to the structure of our sodium aluminium silicate of having pores and a tetrahedral structure . Incipient wetness doping method is simple and has no material wastage
 [7].

Reagents and equipment required for this experiment are ;

    NaOH pellets (97% sigma Aldrich) 200g, de-ionized water(plenty), silicon dioxide (SiO_2 99% sigma Aldrich) 200g, sodium aluminate ($NaAlO_2$ 99% sigma Aldrich) 500g, several Teflon containers, (sizes 100 ml and 200 ml two of each) an oven (150 ^{o}C),

centrifuge, and a furnace (1200 ºC) [8,9,10,11,12].

Experimental Process

4.0 grams of sodium hydroxide (NaOH) pellets were dissolved into 20 ml of de-ionized water stirred until fully dissolved. Then 6.0 grams of silicon dioxide (SiO_2) powder were added into the solution and stirred for 1 hour while being heated gradually to below boiling point of water (~94 ºC) in a hydro-gel process. The process is discontinued when clear hourglass liquid is observed. The clear solution formed sodium silicate

(Na_2SiO_3) is cooled to room temperature. 6.0 gr ams of sodium aluminate ($NaAlO_2$) is dissolved into 20 ml of de-ionized water and stirred until completely dissolved. Care is taken to maintain the ratio Si/Al at 1.

The contents of sodium silicate are poured into the sodium aluminate, Fig. 3.1, a jelly like substance is immediately formed. The mixture is transferred into a oven set at 90 ºC for as long as the reaction is desired. Samples are withdrawn from the chamber at 2 hr, 4 hr, 24 hrs, and 2 weeks, they are labeled as A1, A2, B1, and B2 respectively.
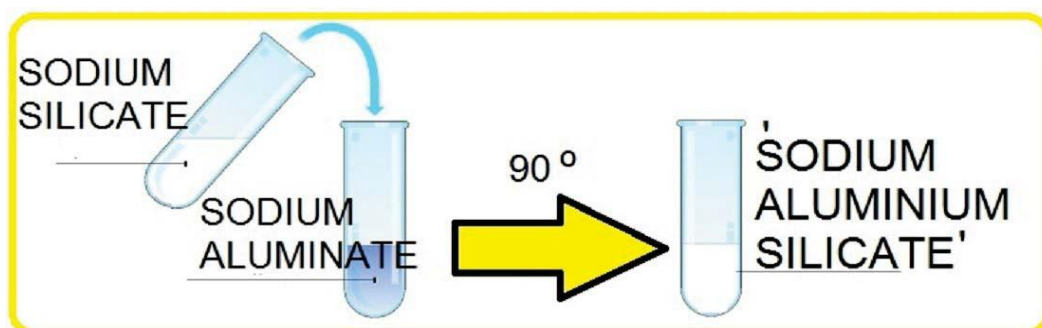
Figure 3.1: Mixing order diagram for mixing Sodium silicate into Sodium aluminate an important step.

Each time a sample is withdrawn a dilution process is started that lowers the pH of the solution from 14 to between pH 7 and pH 8 (this is to stop the reaction and to neutralize the product for storage), the contents are added to an amount of de-ionized water stirred and the mixture decanted in a centrifuge.

The centrifuge is done for 10-minutes intervals at 4000 rpm, separating the water from the solid each time the centrifuge terminates, decantation is done. The centrifuge-decantation process is repeated until the pH of the dissolved solution is at the desired value between pH 7-8. After decantation., the solid is dried in an oven at 110 $^\circ$C to remove the excess water and stored in labeled airtight containers.

The samples were ready for structural analysis figure. 3.2. The doping of Er^{3+} was doneat different concentrations by di ssolving $Er(NO_3)_3$: H_2O (99% Sigma Aldrich) at a concentration of 1, 2, 3, 4 mol %. Co-doping was done with Er^{3+}, Yb^{3+} ions from $Er(NO_3)_3$: H_2O and $Yb(NO_3)_3$: $6H_2O$ at 20 mol % were dissolved into a solution of weighed $NaAlSiO_2$ under ultrasonic treatment for 2 hours and dried at 90 $^\circ$C for 12 hours followed by calcination at 400 $^\circ$C one batch and the other 1000 $^\circ$C.

Figure 3.2 Flow chart of basic processes in Sodium silicate synthesis.

Characterization techniques

X-ray Powder diffraction

X-ray powder diffraction is one of the most versatile method in material analysis. We can obtain material composition, particle size, phase composition, lattice parameters and atomic level parameters e.g. miller indices.[14] X-rays are generated when collimated monochromatic 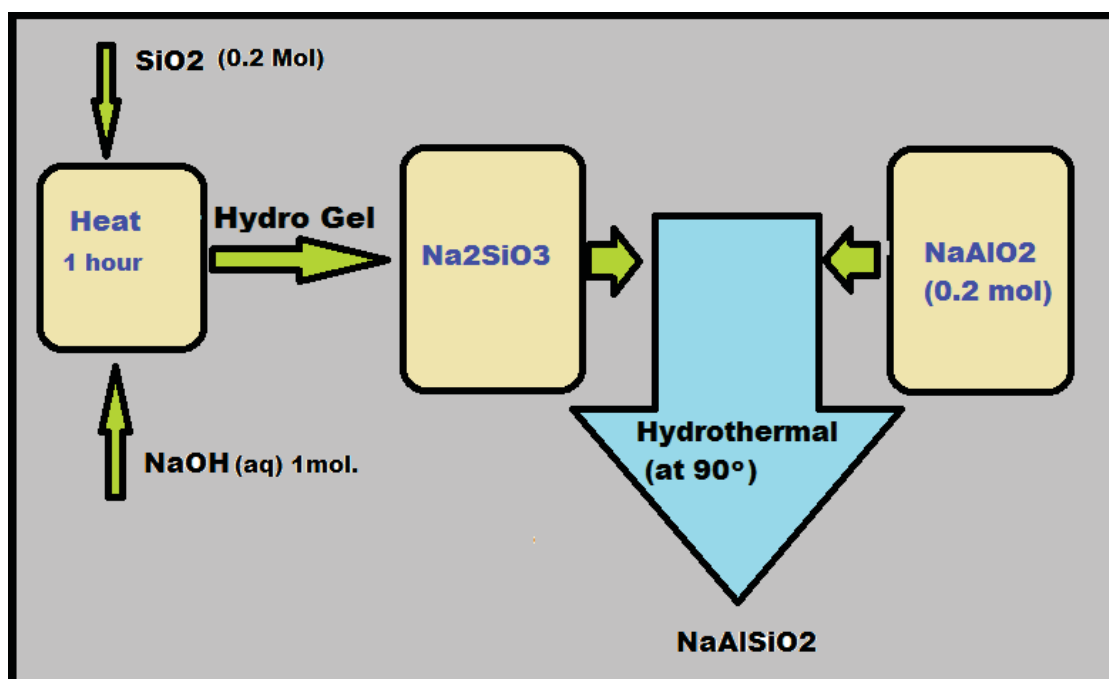high energy electron beam is diffracted after being reflected from a sample, constructive and destructive interferences occurs creating peak and troughs of intensities that are recorded by an electronic counter. The process takes place when the primary (incident) X-ray beam penetrates the nanomaterial sample, colliding with the atoms, this interaction emits high energy photons that get scattered in an array that leads to

the constructive and destructive interference, this is diffraction.

The interferences in the waves are responsible for producing fringes of bright and dark lines that are counted by an electronic detector. The fringes are recorded against the glancing angle between the incident beam and the reflected beam. The glancing angle is found to be 28, the angle 8 is called the Bragg angle [15]. When diffraction takes place a phase shift in the reflected beam is a multiple of 2n, A mathematical expression that refers to this relationship is called the Bragg's law and is written as [16].

$$nJ = 2d\sin8 \tag{3.1}$$

where n is an integer, d is the planar spacing in the lattice, J is the wavelength of the beam, and 0 is the glancing angle of the incident X-ray, see figure 3.3.

Reading of a X-ray diffraction data are recorded by a detector that outputs its record into a computer that is loaded with diffraction analysis software [17]. The computer build up a graph of X-ray intensity against the angular position 20 and the resulting graph is called a diffractogram. Each peak in a diffractogram is unique to a particular atom in the nanomat.erial. Figure 3.4 show the actual X-ray machine, the sample table is kept stationary, while the X-ray gun and the detector may be rotated at an angle 180 degrees vertically. The sample table can be rotated in 360 degrees horizontally, making it possible to X-ray the sample from all possible angles.
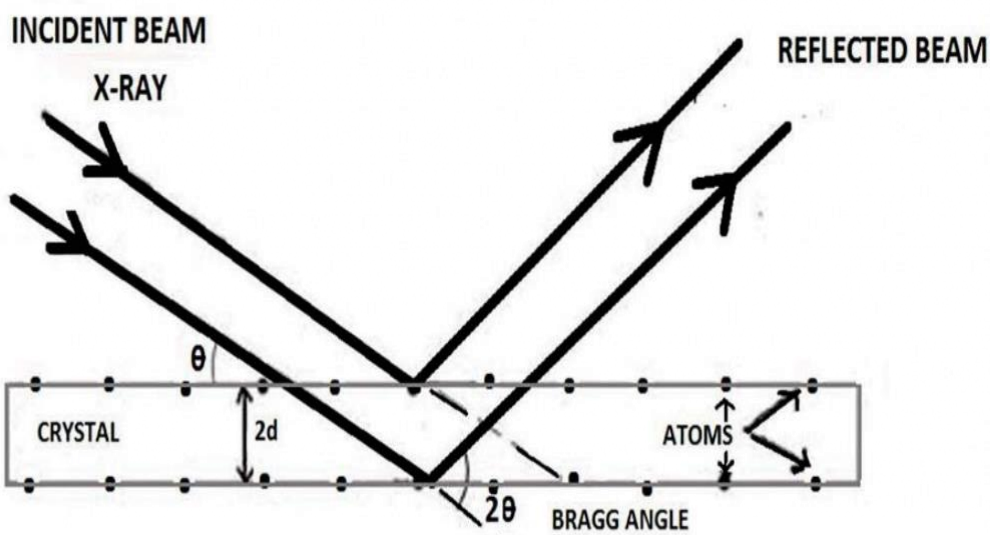
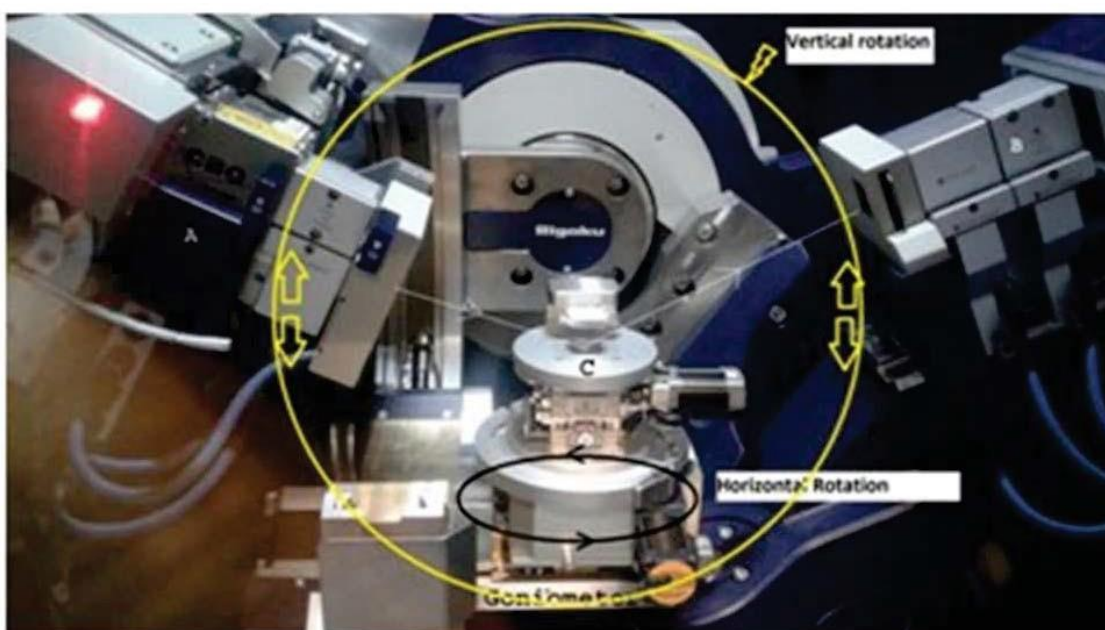**Figure 3.3** X-ray beam being reflected by atoms in a crystalline sample.

Figure 3.4 The X-ray Source, the X-ray tube labeled A, the electronic X-ray Detector B, the sample table labeled C and both horizontal and vertical rotation axis. (the Model Smart Lab Rigaku RU 300 X-ray Diffractometer).

High Resolution Scanning Electron Microscope-(HR-SEM)

High-Resolution Scanning Electron Microscope (HR-SEM) is an analytical research tool that probes materials surface via high-resolution imaging-based on rays of collimated electrons in a vacuum chamber. Contrarily, a light microscope uses visible light for imaging.

In principle, in an HR-SEM an electron detector within the chamber records and reconstructs reflected signals to a visual image of the sample under examination. The evident main advantage of HR-SEM over light microscopes is its much higher magnification ($> 100,000$ times) and relatively higher depth of field that can reach an order of up to 100 times that of a conventional light microscope. see their comparison in figure 3.5 .

Qualitative and quantitative chemical analysis information is also obtained using an energy dispersive X-ray spectrometer (EDS) attached to the HR-SEM. The well-established working principle of HR-SEM consists of the generation of a beam of incident electrons in an electron column above the sample chamber. Moreover, electrons are produced by a thermal emission source which can be either a heated tungsten filament or by a field emission cathode. Besides, the energy of the generated incident electrons can be as low as 100 eV or as high as 30 keV depending on the evaluation objectives. More importantly, the electrons are focused into a small beam by a series of electromagnetic lenses in the HR- SEM column [13]. It is worth mentioning that the HR-SEM column and sample chamber are kept at moderate vacuum typically from 10^{-5} to 10^{-7} Torr to ease electrons to travel smoothly from the electron beam source to the sample target and further to the detectors. Finally, an HR-SEM image is formed during incident electron beam scanning in a raster pattern across the sample's surface.

In the present study, HR-SEM images of NaAlSiO$_2$ crystals were collected using the JEOL JSM-7800F field-emission scanning electron microscope (FE-SEM) equipped with Energy Dispersive X-ray spectrometer (EDX) from the Physics Department (UNISA Science Campus.)
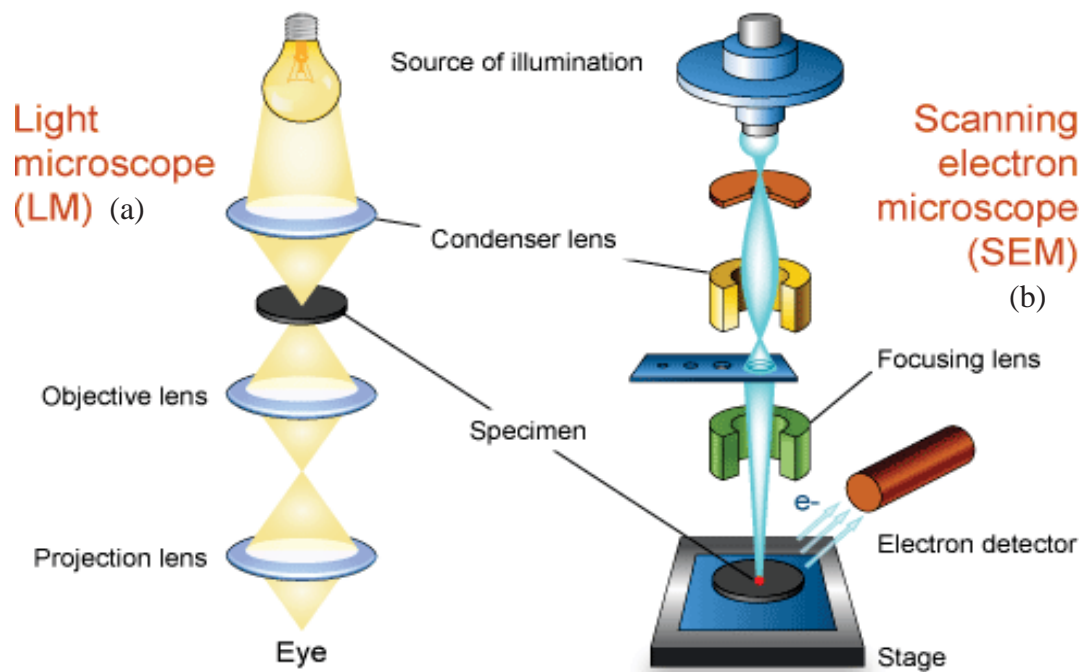
Figure 3.5 Showing a comparison of the SEM column(b) and the light microscope(a), it should be noted in SEM electrons are the probing means[20].

Near Infra-Red Fourier- Transform Spectroscopy (FTIR)

The vibration modes in the samples were identified using Fourier Transform Infrared (FTIR) spectroscopy which is a qualitative analytical technique for material analysis. The FTIR is also known as vibration spectroscopy.

In the working principle of FTIR shown in figure 3.6, an interferogram is generated as a result of the radiation interference between two beams. The interferogram is a signal which is a function of the change of path length between the beams. It is important to note that the two domains of distance and frequency are interconvertible by the Fourier-Transform. The key component in the FTIR spectrometer is an interferometer via which the generated radiation passes through before reaching the sample and further the detector. During signal amplification in which undesired high-frequency components are removed by a filter, the radiation information is converted to numerical form using an analog-to-digital converter for final transmission to the computer software for Fourier-transformation [26].

The FTIR can identify an unknown nanomaterial, determine the quality of a sample, and determine the quantity of a compound. The FTIR spectrum gives the intensity against the frequency or the wave number *1/J*. Each and every sample produces a spectrum that is unique to itself and thus a fingerprint to its chemical and physical characteristics [21].In the present study, the spectra were collected at room temperature in the transmittance mode using a Perkin-Elmer NIR + S P10 STD spectrometer (UNISA Science Campus).
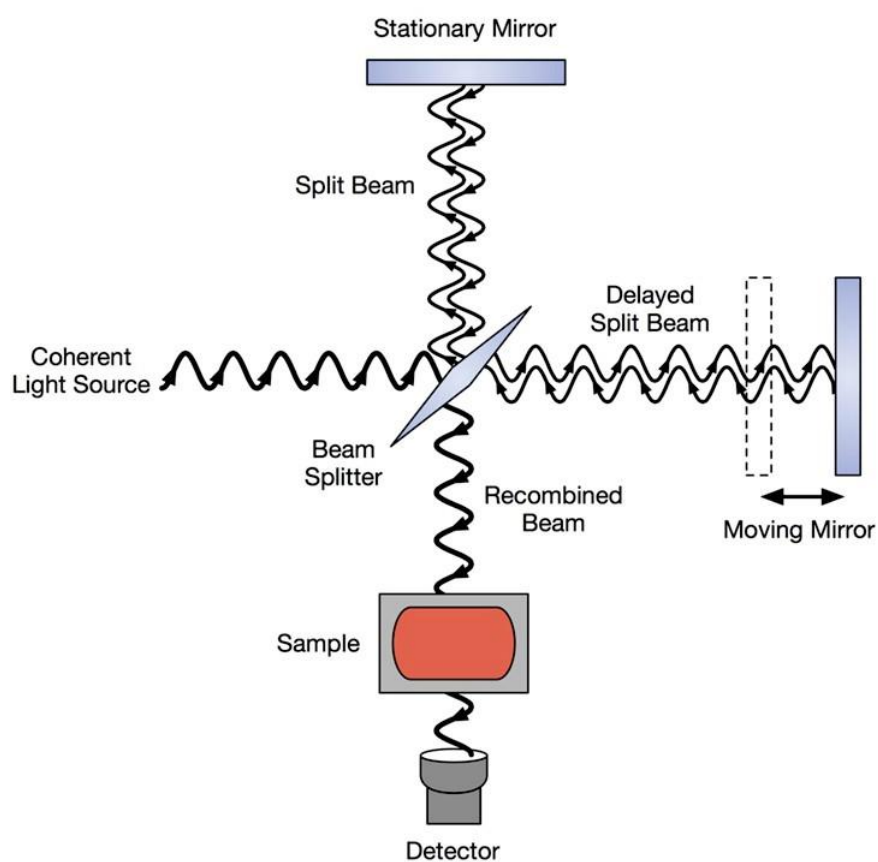
Figure 3.6 FTIR interferometer internal workings.

Ultra violet visible to Near-Infra-red spectroscopy

In the present study, we used UV-ViS-NiR Spectroscopy, a modern analytical technique available in our laboratory. The UV-ViS-NiR technique was used to study light intensity passing through a solvent containing a sample specimen in the ultraviolet and visible ranges in terms of wavelengths expressed in nanometers. Generally, it is used for quantitative analysis which consists of the estimation of compound amount known to be present in the specific sample diluted specimen [10] seen in figure 3.7.

Fundamentally the processes involved in absorption spectrometry are absorption and transmission which are governed by Lambert's Law. According to Lambert's Law, each layer of equal thickness of an absorbing medium absorbs an equal fraction of the radiant energy that travels through it [10].

Considering the intensity of the incident radiation as I_o and that of the transmitted light as I, hence the fraction transmitted is expressed as:

$$I/I_o = T$$

and the percentage transmission is

$$\%T = I/I_o \times 100$$

while the absorbance:

$$A = \log_{10}(I_o/I)$$
$$= \log_{10}(100/T)$$
$$= cL \qquad\qquad (3.2)$$

where the length of the radiation path through the sample specimen L is expressed in m, the concentration of absorbing molecules in that path c is expressed in $molar^{-1}$, and the molar extinction coefficient is expressed in $mol^{-1}m^2$.

In the present study the Lambda 1050 UV-VIS-NIR spectrophotometer, located in the Physics Department (UNISA Science campus) was used to investigate the absorption properties of the samples.
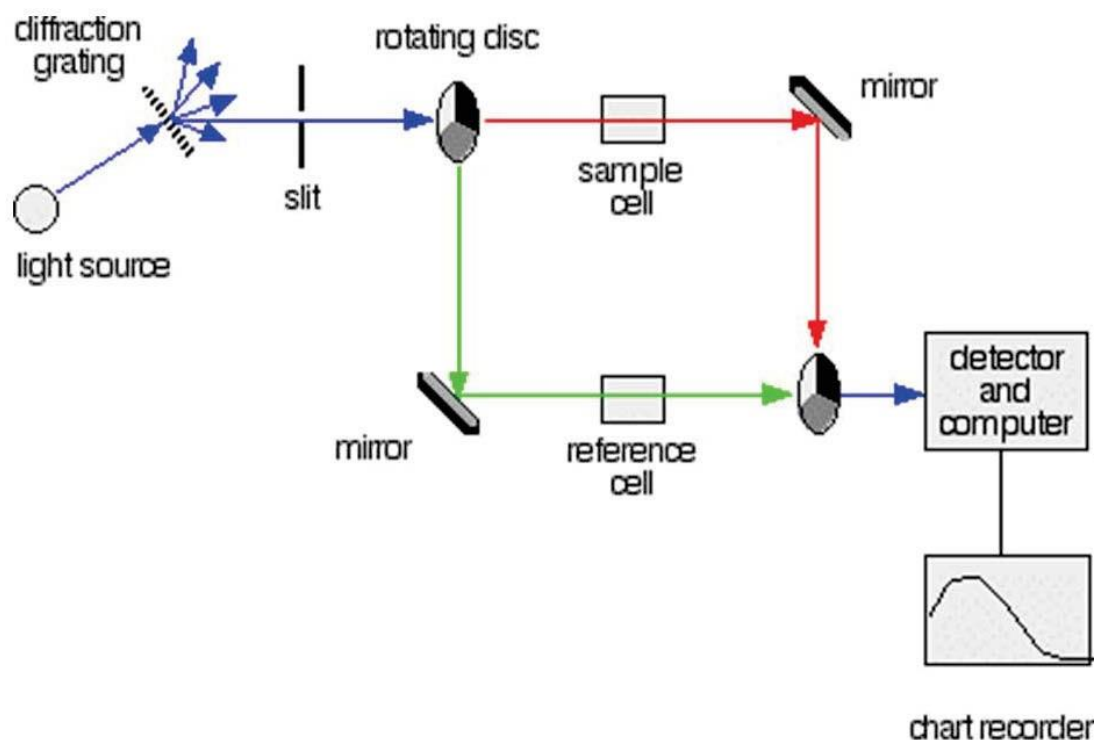
Figure 3.7 The schematic diagram of a double-beam UV-ViS-NiR is spectrophotometry platform [31].

Photoluminescence spectroscopy

Photoluminescence is an analytical, non-destructive and contactless technique. It is used to probe a material's luminescence properties. Basically, a photon beam directed at a sample is absorbed and imparts excess energy into the material through photo excitation. Moreover, the excess energy may be emitted out of the sample as light or luminescence. When photo excitation occurs, we denote it as photoluminescence.

Furthermore, photo excitation is responsible for electron migration from ground state and upper states into permissible excited states within a material. The excited electrons return to equilibrium (ground state) releasing the excess energy in a radiative process (light) or non-radiative process. In addition, emitted light (photoluminescence) energy relates to the difference in energy levels between the two electron states involved in the transition between an excited state and an equilibrium state. More importantly, the quantity of emitted light is related to the relative contribution of the radiative process [14]. In this present experimental study, the PL measurements were performed using a F LS980 spectroscope by Edinburgh, located at the Physics Department (University of the Free State) seee figure 3.8 and picture in figure 3.9 .

41
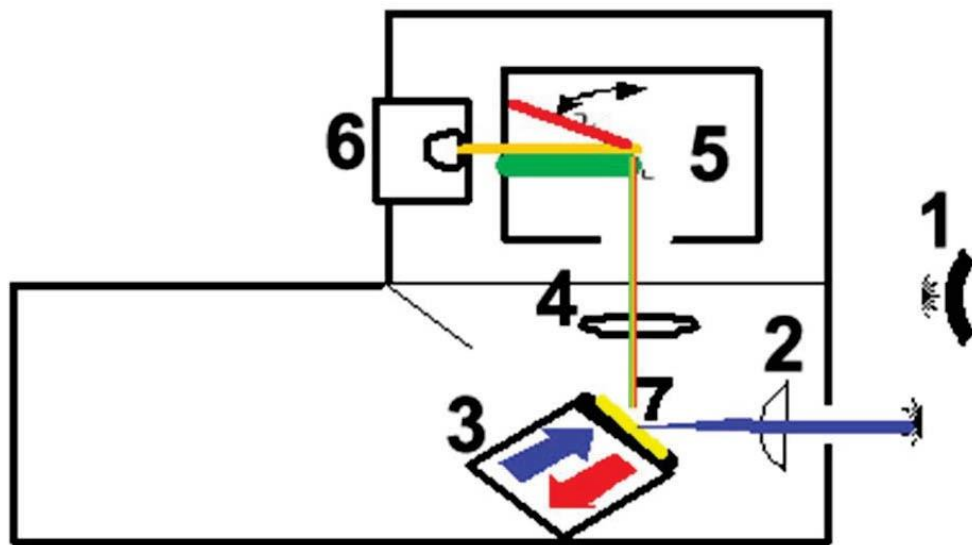
Figure 3.8 Schematic diagram for the FLS980 spectroscopy by Edinburgh Instruments [27].[Accessed 2019 12 15]

Figure 3.9 A picture of the FLS980 photoluminescence spectrometer; Laser lab 1

University of the Free State (UFS).

Temperature Measurements

A modified photo-luminescence measuring unit capable of measuring emission fluorescence of an excited doped rare earth phosphor at room temperature was modified for our study [28], seen in figure 3.10. In the present work, temperature measurements of the doped rare earth $NaAlSiO_2$ material under investigation was performed using a temperature controller unit, coupled with an XYZ stage, sample heater as well as sample holder. Moreover, the heating and excitation of the investigated material was successfully achieved using a copper (Cu) sample holder, to which a home made sample holder was installed inside a heating element [29].

Basically, the used sample holder consists of a Cu cylinder with a 2 mm hole in the centre, in which the sample to be investigated was loaded. In addition, it also contains a 1 mm hole off centre, in which a thermocouple junction was inserted to gauge the temperature of the sample [29]. Interestingly, the modification included a custom build in heater that is software controlled through a Manson switching mode power supply. 1-30 VDC, 15 A, model HCS-3302. This maintained a steady temperature as desired.

The temperature was measured by a thermocouple (K-type) unit that also displayed the temperature. The two units, the temperature reader and the power supply were connected to a digital-to-analogue and analogue-to-digital converter (VDAQ lite micro DAQ data acquisition, serial D1000014395) then connected to a personal computer. More importantly, a proportional input derivative (PID) controller is in cooperated in the temperature control program and thus controls the samples temperature.

The doped $NaAlSiO_2$ was excited at 980 nm (2W) pulse laser and the intensity spectra recorded as the temperature was varied downward from 450 ^{o}C to 50 ^{o}C (steps of 1 ^{o}C). The temperature measurements set up used in the current work is located at the Electronics and Instrumentation Divisions at the University of the Free State.

Calculation of colour coordinates using the commission international de L E'clairage (CEI) software (GoCIE) to ascertain colour tuning characteristics of the emission beam was applied [30].

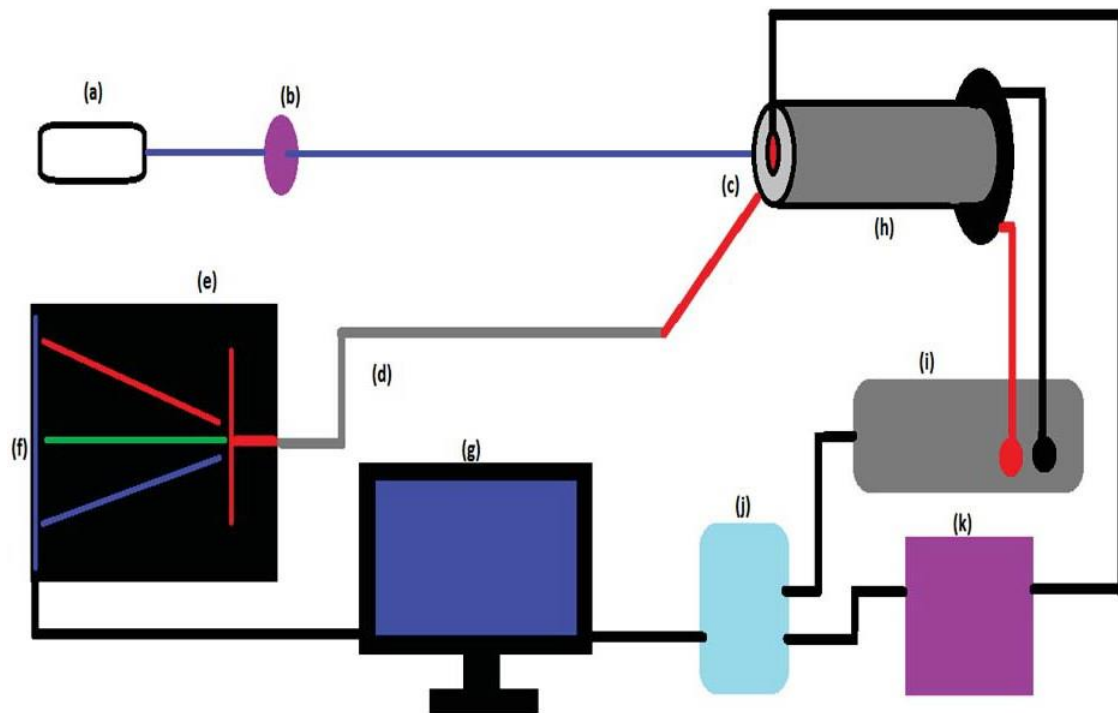**Figure 3.10** Experimental setup for analyzing temperature dependent fluorescence intensity, (a) 980 *nm* diode laser, (b) filter, (c) NaAlSiO$_2$ doped phosphor material, (d) fibre optic cable, (e) diffraction grating, (f) CCD camera, (g) computer, (h) heating element, (i) power supply, (j) thermocouple, (k) temperature display unit and (l) digital-to-analog and analog-to-digital converter [28].

References

[1]   Blatter F and E. Schumacher. 'The preparation of pure zeolite (NaY) and its conversion to high silica Faujisite'. *Journal of chemical education* 67.6, (1990). pp. 519-521.

[2]   Kosanovic C. 'Study of micro structure of amorphous alumino-silicate gel before and after its hydrothermal treatment'. *Micropor. mesorpor. Mater.*110.2-3, (2007). pp. 177-185.

[3]   Georgiev D., BogdanovB., MarkovskaI., and Y.Hristovet. 'A study on the synthesis and structure of zeolite NAX'. *J. Chem. Tech. and Meta.* 48.2, (2013). pp. 168-173.

[4]   Manuel M. 'Direct Synthesis of functional Zeolitic materials'. *Matt. Sc.*, (2012). p. 24.

[5]   Hums E. 'Synthesis of Phase-Pure Zeolite Sodalite from Clear Solution

Extracted from Coal Fly Ash'. *J Thermodyn Catal* 8.2, (2017). pp. 1-11.

[6]   Townsend, J.E., Poole, S.B. and Payne, D.N.'Solution doping techniques forfabrication of rare earth doped for optical fibres'. *Electronic letters* 23.7, (2017). pp. 329- 331.

[7]   Khattak, AK; Afzal, M; Saleem, M; Yasmeen, G;and Ahmad, R. 'Surface modification of aluminium by metal doping'.*Colloids and surfaces* 162(2000)., pp. 99-106.

[8]   BalkusKJ., and Kieu T. Ly.The preparation and characterization of NaX-type zeolite'.*Protocole* 901 68.10 (1991), pp. 875-877.

[9]   Molimer M., and Nasaar E.J. 'Direct synthesis of functional zeolite material's.*MaterialScience*789525, (2012). pp. 1-24.

[10]   Bren U. 'Preparation of Sodium silicate'. *Microporous and mesoporousd Matt*. 40, (2000). pp. 43-52.

[11]   Valentin P., LubomiraTosheva, , and Krassimir N. Bozhilov. 'Synthesis of zeolites nanocrystals at room temperature'. *Langmuir* 21, (2005). pp. 10724-10729.

[12]   Pinkas J. 'Chemistry of silicates and aluminosilicates'. *Ceramics* 49.4, (2005). pp. 287-298.

[13]   Altmore A., Capittel F.,   Nicola Corriero, and   CorradoCuocci

 'The rietveld refinement in the EXPO software: a powerful tool at the end of the elaborate crystal structure solution pathway. *Crystal*8, (2018) . pp. 20312-20327.

[14]   Hideo Toraya. 'Introduction to X-ray analysis using the diffraction method'. *Rigaku Journal* (2016). pp. 32-86

[15]   Bunaciu A. 'X-ray diffraction: Instrumentation and Applications'.

analytical chemistry 45, (2015). pp. 289-299.

[16]   Sharma R., Bisen D. P., Usha Shuklaand B.G. Sharma. 'X-ray diffraction: a powerful method of characterizing Nano materials'. *Reser. Sc. and Tech* 4.8, (2012). pp. 77-79.

[17]   Brandenburg GR .*Software match3, Phase Identification from Powder*

Diffraction, https://www.crystalimpact.de. 2019.[Accessed:2019-03-10]

[18] Joel Datumn. *A guide to scanning electron microscope observation*, http://www.geology.wisc.edu. (1996). [Accessed:2019-07-05]

[19]   Nanyang   Technological   university   Singapole.   *SEM   bridging   course*. https://research.ntu.edu.sg. (2018). pp 156-174

[20]   Thermonicolet. *Introduction to Fourier Transform Infrared spectroscopy*. https:

//www.chem.uci.edu/~dmitryf/manuals/Fundamentals/FTIR\%20principles.   Pdf (2019)[Accessed:2019-12-25].

[21]   PerkinElmer.   FTIR   model   NIR   SP10   std.   ht tps://www.perkinelmer.com/ [Accessed:2019-08-16]

 [22]   Sigmaaldrich. *Infra-red spectrum table*. https: / / www .sigmaaldrich .com /

technical-documents/articles/biology/ir-spectrum-table.html [Accessed20191225].

[23]   Salzburg university. *Basic uv-vis theory, concepts and applications*. http:

/ / www . uni - salzburg . a t / fileadmin / oracle _ file_ imports / 359201 . PDF[Accessed:2019-09-10].

[24]   PerkinElmer. *perkinelmer 1050 uvvis spectroscopy.* https://www.perkinelmer. Com[Accessed:2019-12-12].

[25]   Mokoena Priscila Puseletso. *Up-conversion of infrared to visible light in rare- earths doped phosphate phosphors for photodynamic therapy application.* https://scholar.ufs.ac.za/mokoenapp.pdf. MA thesis. University of free state. (2017).

[26]   Edinburg   Instrument.   *FLS980   Spectrometer.*   https://www.edist.com/wp content/uploads/2015/04/FLS980-spectrometer.pdf [Accessed20191230].

[27]   Juestel RG. *Optical spectroscopy analytical equipment*. https://www.fh-muenster.de/ciw/do wSpectroscopy-Analytic-Equipment-RG-Juestel-2019-10.pdf [Accessed 2019 12 15]. 2019.

[28]   Erasmus LJB *Measuring the optical thermometry properties of*

La2O2S:Eu phosphor material. SAIP proceeding 2015 (2015).

[29]   Erasmus LJB *Development of an optical thermometry system for phosphor materials, MSc dissertation*. MA thesis. Physics, University of the Free State. (2017).

[30]   Bhushan P. Kore, Ashwini Kumar, Lucas Erasmus,Robin E. Kroon, Jacobus J. Terblans, Sanjay J. Dhoble, and Hendrik C. Swart. 'Energy Transfer Mechanisms and Optical Thermometry of BaMgF4:Yb3+,Er3+ Phosphor'. *Inorg. Chem.* 57, (2018). pp. 288-299.

[31]   Kabongo G. L. "*Luminescence investigation of zinc oxide nanoparticles doped with rare earth ions*". MSc thesis. University of South Africa, Physics Department. (2013).

Chapter 4

Synthesis, structure, morphology and chemical composition of sodium aluminium silicate (NaAlSiO$_2$)

Introduction

During the past decades, Zeolites crystals investigation have been the center topic of tremendous interest due to its puzzling anti-Stokes fluoresence properties among others [1-3]. Its application in laser cooling relies on absorption of low-entropy and coherent light with Planck's photon energy hv followed by optimal radiation high-entropic spontanous emission with a mean energy relatively higher compared to that of the initial absorbed coherent light. Fundamentally, the energy difference in fluorescence which leads to cooling is obviously extracted from the internal energy of the system [4].

Figure 4.1 shows sodium aluminium silicate (NaAlSiO$_2$) crystals in a two dimensional (2-D) orientation structure and are members of the group Zeolites. Moreover, Zeolites have small pores and channels of molecular dimensions, these enhance shape selectivity and increase the surface area of contact with the doping ions [5, 6]. This make them suitable for application in doping.

SOD (6MR)
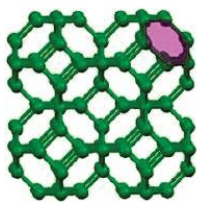
Figure 4.1 Sodolite's topology with 6 member-ed ring pores of 2.8 A [7].

Interestingly, Zeolites have high thermal stability making them suitable for up-converting high-temperature applications. But also making it possible to be synthesized at high temperatures from liquid precursors [7, 8]. Finally, $NaAlSiO_2$ has active ions composed of the bonds of $[AlO]^4$ and $[SiO]^4$, it is these bonds that attract the doping ions into the 2- dimensional channels [9]. Sodium aluminium silicate is known to be a good ion exchange andhas high porosity, this makes it suitable for doping up-conversion application [10, 11, 12, 13,14].

Isolated clusters (nanoparticles)

Ion-exchanged cations / covalently bonded metal (oxide) centers

Single atoms incorporated in the framework

Figure 4.2 Ions exchange process in the host's matrix [6].

Figure 4.2 shows the ion exchange process during doping, the symbol M represents the

49

positively charged doping ion. These zeolites may find application in phosphor screens, infra-red detectors, micro-electronic laser application, and in bio-medicals [15].

Experimental

Crystals of $NaAlSiO_2$ were synthesized as outlined in section 3.2, from pure reactants of sodium aluminate (99% purity), anhydrous sodium hydroxide (98% purity), silicon dioxide (99% purity), and de-ionized water, all were obtained and were used as purchased from Sigma Aldrich.

Several synthesis methods were investigated and the best reaction process (hydrothermal synthesis) was adopted.

Synthesis of pure $NaAlSiO_2$ crystals

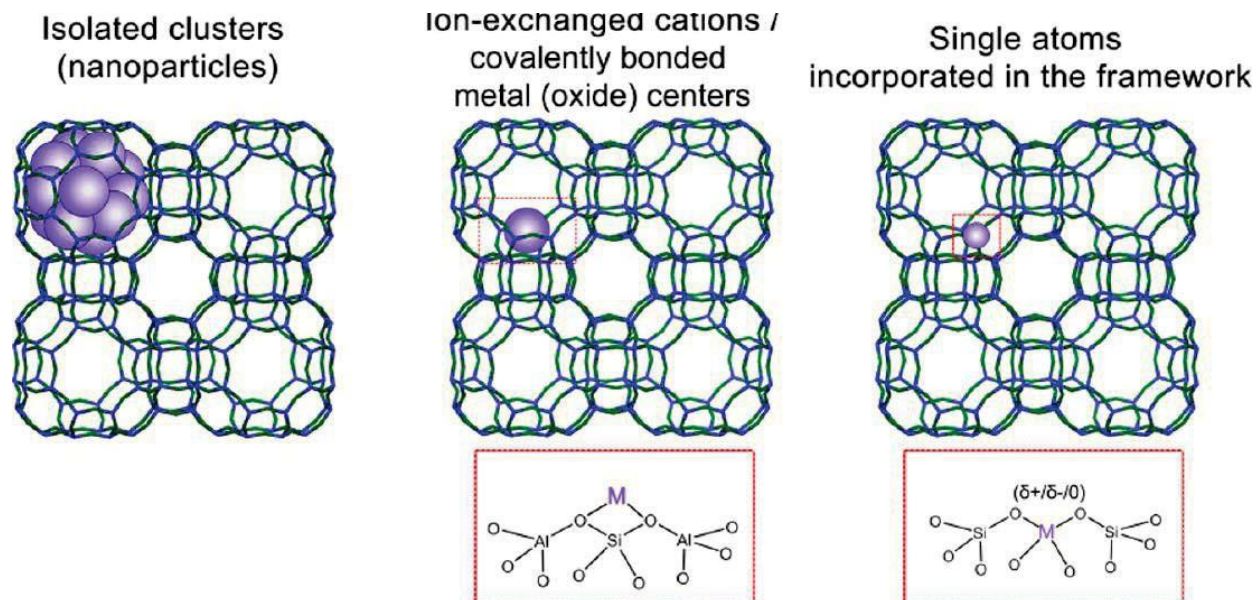In a Teflon container, pure Na_2SiO_3 was prepared by heating an aqueous solution of $NaOH$ and silica gel SiO_2 to boiling point until water glass was formed, this process took one hour. The water glass Na_2SiO_3 was cooled to room temperature and then suction filtration was performed to separate the silicate from the solution [16]. The filtered solid was dried in an oven at 90 $^\circ$ C, followed by a hydrothermal process that starts with the dissolution of the $NaAlO_2$ into de-ionized water and reacted with an aqueous solution of Al_2SiO_5 inside an oven kept at a constant temperature of 90 $^\circ$C.Hence, the reaction forms a white gelatinous substance that is washed with de-ionized water in a centrifuge separation system to lower the pH from 14 to between 7 and 8. Once pH 7-8 is achieved the white precipitate is dried in an oven at 105 $^\circ$C for 2 hours and then stored in an airtight container for structural studies and doping.

Incipient wetness impregnation doping method follows. Where a wetness process is applied for 24 hours as the doping ions are mixed in solution form with the host and left to undergo inter-ion exchange under an ultrasonic vibration system. Finally, analysis by the following techniques XRD, SEM, EDS, and FTIR was carried out. X-ray diffraction work was performed using the Model Smart Lab Rigaku RU 300.X-ray Diffractometer equipped with CuKa radiation of $J= 1:5406$ A X-ray source. A pure silicon sample was used to standardize the Smart lab Rigaku RU 300 X-ray before any measurements were done. The crystalline size

was obtained from measured peak broadening and using the Scherer equation calculations [17].

Moreover, phase matching, determination of crystalline sizes, unit cell parameters, crystalline morphology, and porosity of zeolite compounds were carried out. On the other hand, morphological and chemical analysis studies were performed using the field emission X-ray scanning electron microscope (HRSEM) [18] equipped with electron dispersion x-ray spectroscopy (EDS). Specifically, surface grain and their interaction with the dopant grains were studied. Electron dispersion x-ray scan (EDS) was conducted to establish thegrain distribution in the matrix in a mapping analysis and elemental composition.

A complete structure of exact match to JCPDS code 11-1401 was obtained and chemical analysis, phase matching, calculations of crystalline sizes, crystalline morphology, and porosity of the $NaAlSiO_2$ crystals was carried out [19, 20].

Results and discussion

Structural analysis
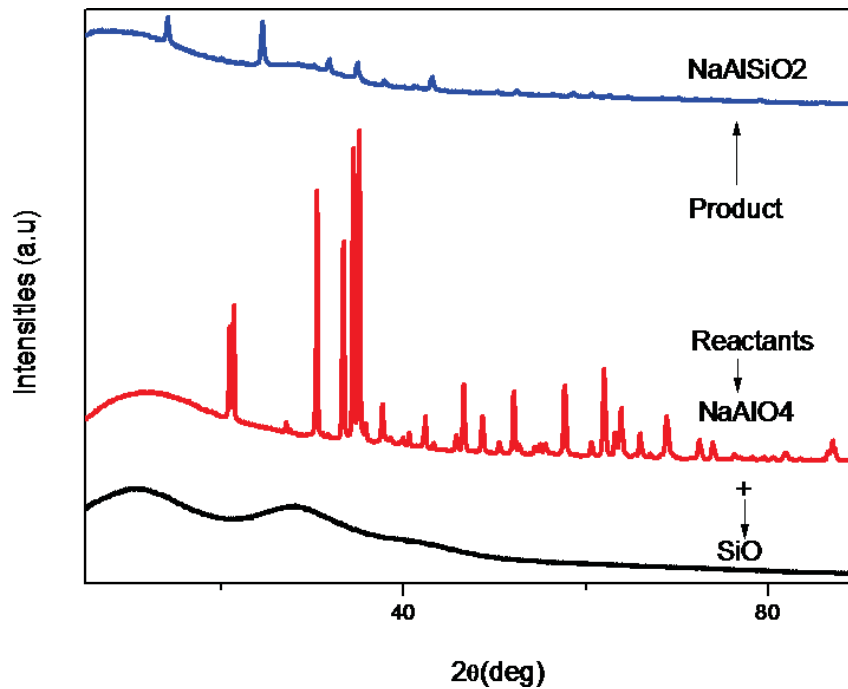
Figure 4.3 Comparison of XRD patterns of the precursors (SiO_2 and $NaAlO_4$) and the

synthesized $NaAlSiO_2$.

Figure 4.3 shows the XRD spectra of sodium aluminium silicate ($NaAlSiO_2$) as well as the precursors. The XRD spectra of the ($NaAlSiO_2$) are different from the two main reactants i.e. silicon dioxide (SiO_2) and sodium aluminate ($NaAlO_4$).

The results show a new product in the name of $NaAlSiO_2$ was formed as confirmed by the peak matching of the standard JCPDS no. 11-1401, see Figure 4.4. There is a matched shift of peak position by 2 degree on all the peaks to the left of the standard (JCPDS No 11- 1401), this is attributed to the possible increase in lattice parameters, mainly due to difference in ionic radii between the host and the dopants [16].
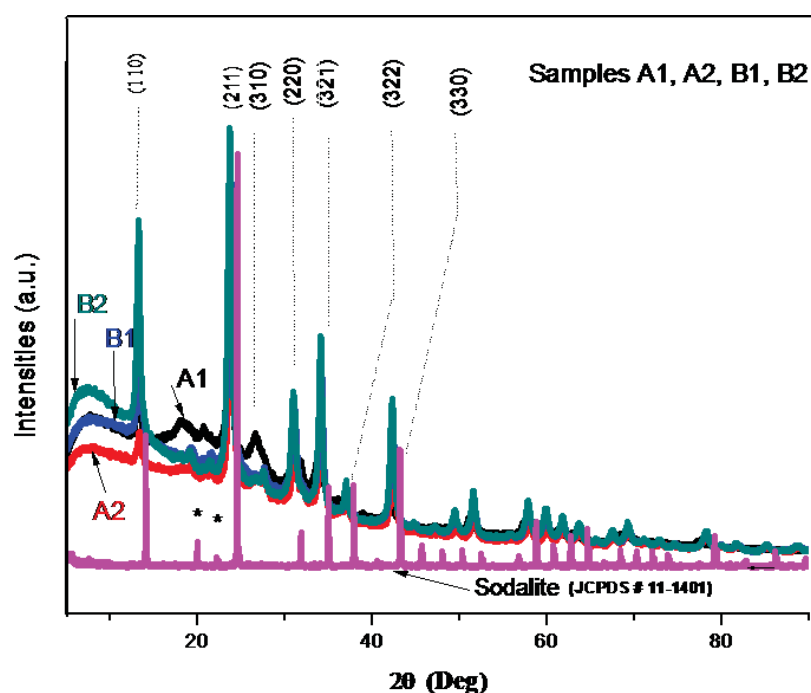
Figure 4.4 XRD Patterns of samples A1, A2, B1, and B2 synthesized at 2 hrs,4 hrs, 24 hrs and 336 hr s respectively, compared to that of sodalite (JCPDS#11-1401) [8].

The XRD spectra of samples A1, A2, B1, and B2 (prepared at different reaction times) are presented in figure 4.5. The figure shows the miller indices, peak positions for the four different samples as extracted from the chamber at different times. It is clear that the synthesis time affects the crystalline formation, the longer the time it takes the higher the diffraction peak intensities. It is the width of the peak that determines crystallinity , the narrower the better the crystals. The miller indices are shown for the first calculated seven peaks, with three principle diffraction points shown as (110, 220, and 330).

Miller indices are determined by us ing a process called diffraction pattern indexing [21], which utilizes Bragg's law and angle 2θ of diffraction to calculate the values (hkl).The peaks at 20 and 21 degrees diffraction miller indices points (marked with an asterisk) did not match any known miller indices and thus were thought to belong to a minor impurity within the crystal.

The Scherer equation fundamental to crystalline size calculation can be written as;

$$FWHM(2\vartheta) = \frac{\lambda A}{D \cos \vartheta} \qquad (4.1)$$

Such that

$$D = \frac{\lambda A}{FWHM(\vartheta)} \qquad (4.2)$$

where *FWHM* is the full-width-at-half-maximum length of the peak, *2θ* is the angle of scattering in radians, *λ* is the X-ray wavelength, */λ* is a dimensionless constant equals 0.94 in our case, and *D* is the dimension of the assumed cubic crystallites.

Scherer equation (4.2) was used to calculate the crystalline size from the XRD diffraction peaks [22]. Crystalline sizes calculated were 20.4 nm, 14.5 nm, 37.4 nm, and 23.3 nm for samples A1, A2, B1 and B2 respectively. The highest diffraction peak was recorded at 23.5 ± 0.4(*2θ*) for each sample, the peaks were at the same position and thus we concluded that they all had the same elemental composition [24]. The inter planer separation or lattice separation d was calculated at 3.75 ± 0.05 *nm*, using Eq. 4.2 . The FWHM was found to vary from 1.8600 for our smallest crystals to 0.6400 for the largest crystal, thus peaks broaden as the crystal size decreases or in other words the longer the synthesis time the higher the 'crystallinity'.
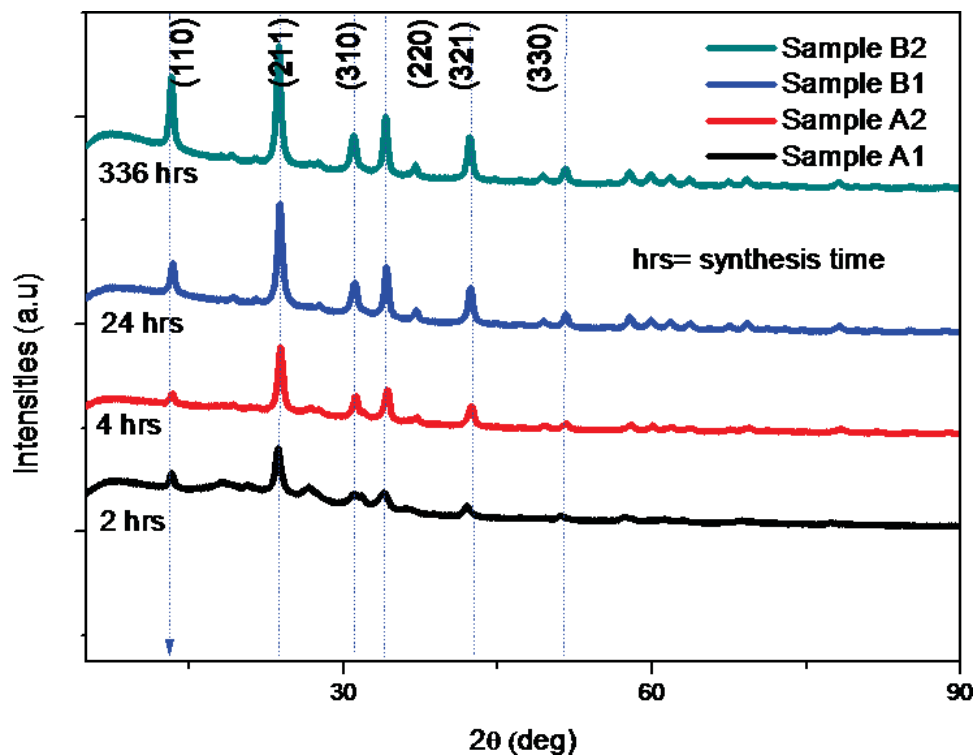
Figure 4.5: XRD spectra of the prepared samples A1, A2, B1, and B2 sodium

aluminium silicate showing indexed peaks and synthesis time in hours.

There is a matched shift of peak position by 2 degrees on all the peaks to the left of the standard JCPDS No 1. 1-1401. This is attributed to the increase of lattice parameters, mainly due to difference in ionic radii between the host and the dopants [27].

Microstructure

Figure 4.6 shows the four SEM micrograph obtained from samples A1, A2, B1 and B2, with (a) showing unique cubic structures with well-defined edges of the sodium aluminium silicate, (b) shows the structure with aggregates that are ideally s pherical balls with spaghetti-like threads intertwined within the group. (c) Shows structures of flowery nature with even distribution, and (d) shows very regular tetrahedral structure uniform within the group. It is clear that the synthesis product underwent four different phases as time increasedin 2 hours, 4 hours, 24 hours, and 336 hours respectively.
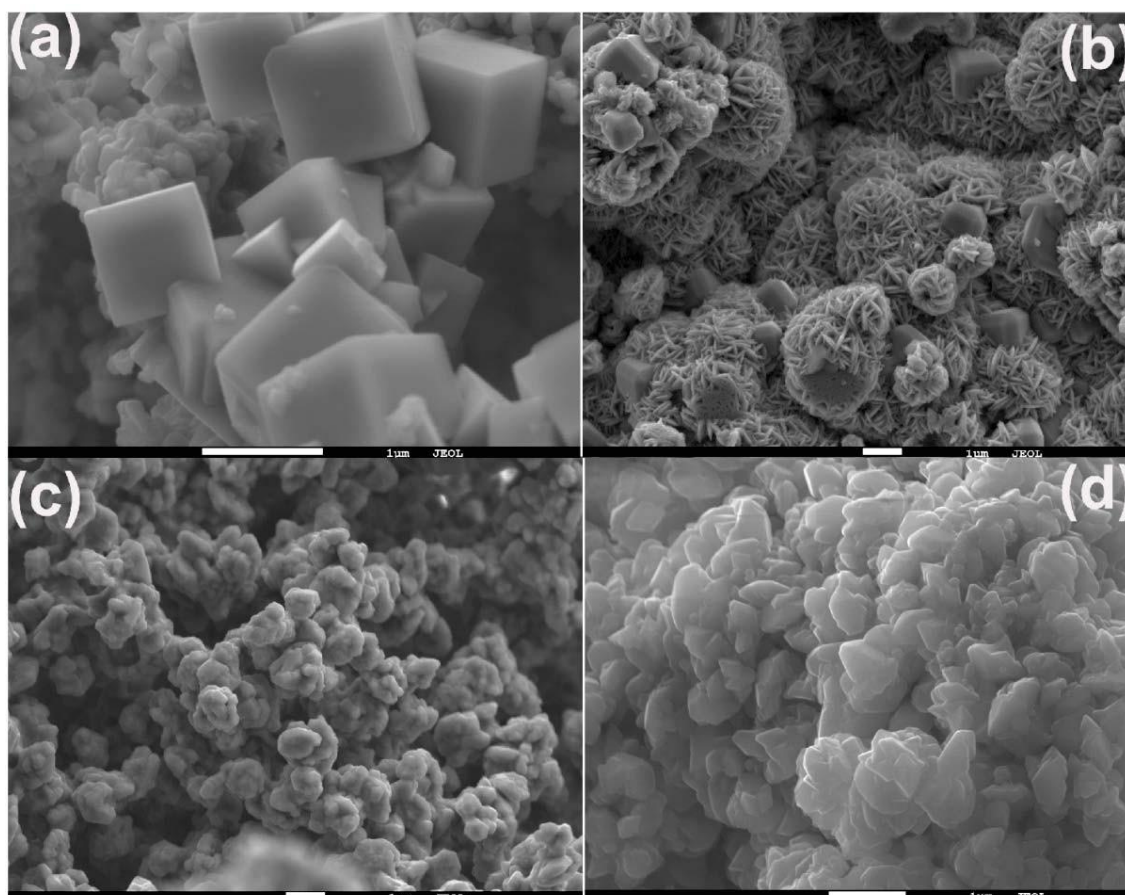
Figure 4.6   Sample A1 labeled~(a), A2~(b), B1~(c), B2~(d) extracted after 2 hrs, 4 hours, 24 hours, and 336 hours respectively

(a)

Full scale counts: 31706   NaAlSiO4-ErYb-02(1)

(b)
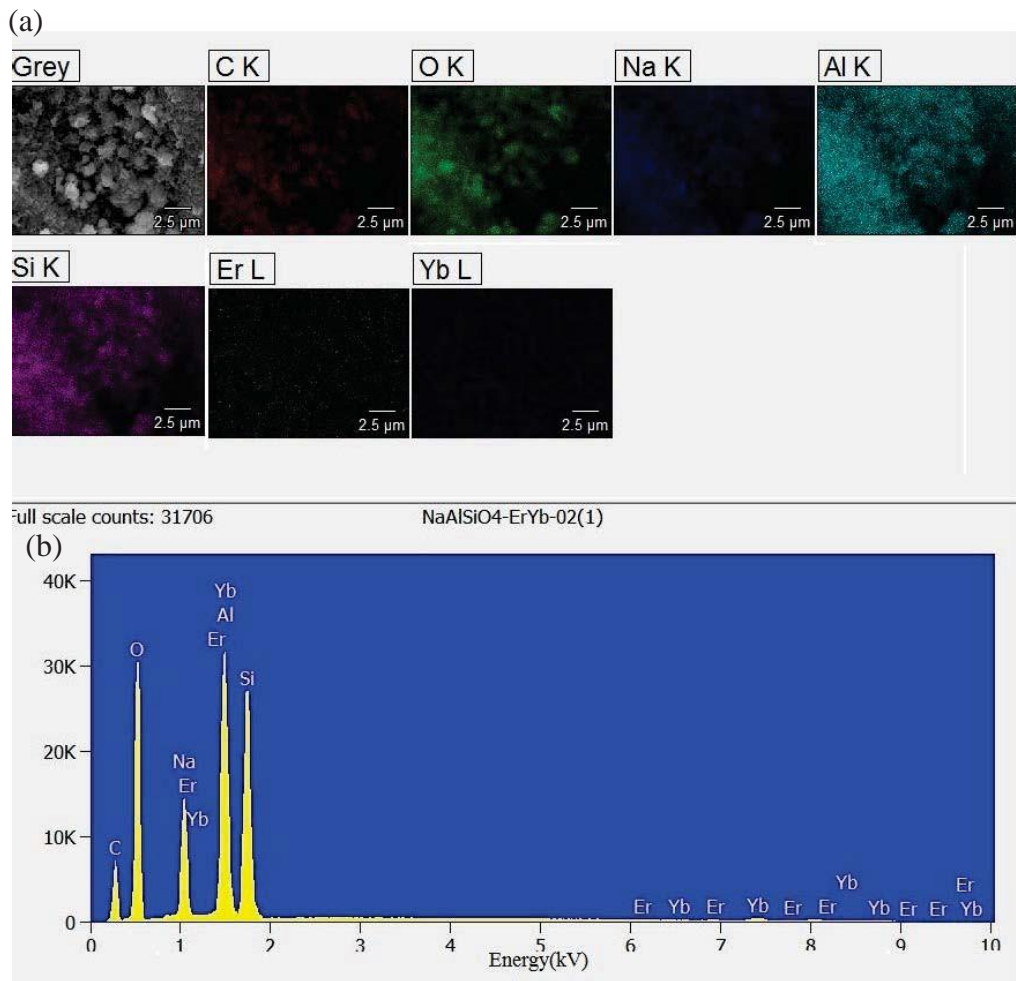
Figure 4.7(a and b) Sample A1 co-doped with 2 % Er [3+] and 20 % Yb [3+] electron dispersion X-ray spectroscopy showing the elemental mapping and a graphical representation of element composition against excitation energy in keV.

The grain size is in the range from 0.3---1.0 *nm*, figure 4.6. The surface of the sample has dopant ions Er^{3+} and Yb^{3+} embedded into the matrix, this decreases its porosity [26].The mapping images in figure 4.7 (a) show there is a uniform distribution of all ions within the group. From EDS, in figure 4.7 (b), elemental composition values from EDS calculated the compound of the sample A1 as the amorphous Sodium aluminium Silicate; $Na_4Al_2Si_2O_{46}$ [27].

The silicon/aluminium (Si/Al)ratio was found to vary from 0.95 to1.02 very close to 1 as desired.

Fourier transform infrared spectroscopy(FTIR)

The FTIR spectroscopy was done to establish what covalent bonds exist within the synthesized $NaAlSiO_2$.
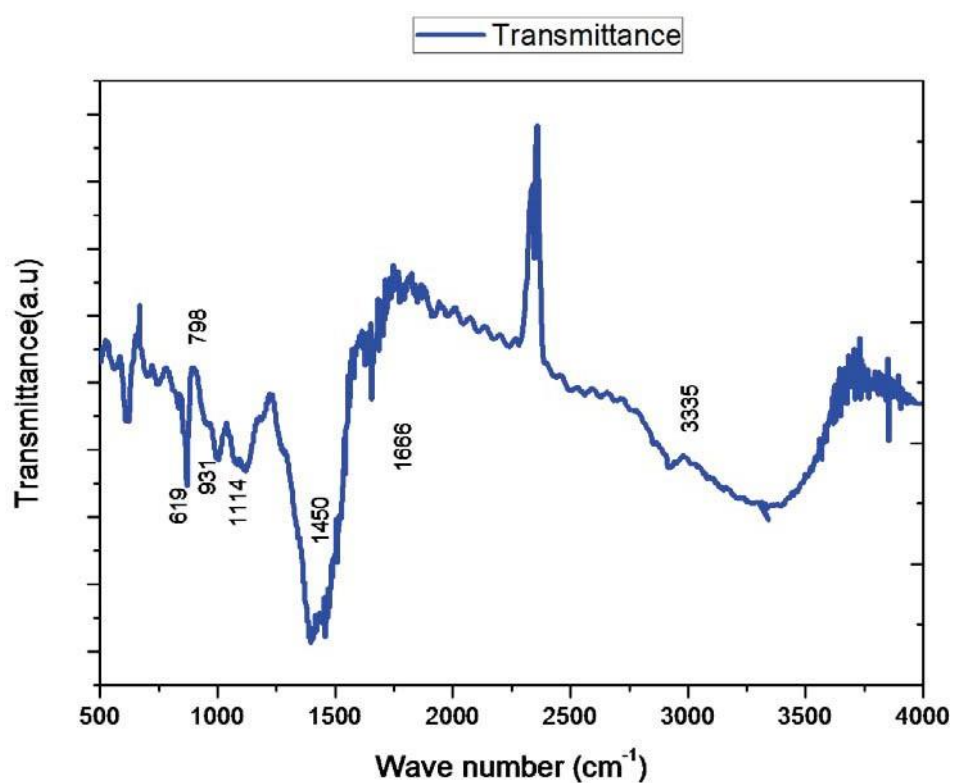
Figure 4.8: Fourier transform the transmittance curve for sample A1.

From figure 4.8 the FTIR transmittance vibration bonds at 3335 and 1666 cm^{-1} are due to the -OH stretching and -OH bending vibration respectively [28]. The p eaks at 1104, 931, and 619cm^{-1}

are associated with the Al-O-Al, Al-O vibrations, and the NO^2 respectively; the NO^2 could be as a result of the un-reacted do-pants precursor. Peaks observed at 1450, 1114, and 798 cm^{-1} are associated with the contribution of the stretching modes of Si-O, Si-O-Si, and the O-Si-O vibrations respectively. The peaks at 1104 c m^{-1} are likely due to of Si-O-Al vibration. The stretch from 1200-1000 cm^{-1} is related to Si-O-Si and Al-O-Si bonds that create a weakened silicon-oxygen bond at 931 cm^{-1} [29].

We see that we have a hydrated sample with high -OH vibration bonds present in the group that can induce quenched non-radiative relaxation [30]. Thus we must extract the -OH from the host sample before we perform any up-conversion experiments.

Conclusion

$NaAlSiO_2$ pure crystals were successfully synthesized in a hydrothermal process and doped with Er^{3+} ions and co-doped at various concentrations with Er^{3+}/Yb^{3+} ions before being annealed at 400° C. Our samples were estimated by X RD as sodalite or (anhydrous $NaAlSiO_2$) with an average crystal size between 14 nm and 37 nm. SEM and EDS verified the presence of the dopant ions whose dimensions were of nanoscale sizes. No impurities were present in the EDS spectra.

Morphological structures showed the presence of cubic face-centered, hexagonal phase, several striking bowls made of inter-locking stick shapes, and finally, the diamond-shaped regular shapes. FTIR suggested the presence of -OH vibration bond a nd un-reacted parent dopant nitrate, which called for additional annealing at the optimum temperature to enhance up-conversion in the doped $NaAlSiO_2$.

References

[1] SaeidRostami, alexander Albrecht, azzurravolpi, and Mansoor sheik-bahae. 'Observation of optical refrigeration in a holmium-doped crystal', *Photonics Research* 7(4), (2019). pp. 445-451.

[2] PringsheimP. 'Zweibemerkungeni.ber den unterschied von lumineszenz- und temperaturstrahlung,'*Z. Phys.* 57, (1929).pp.739-746 .

[3] S heik-BahaeM. and Epstein R. I. Optical refrigeration,'*Nat. Photonics* 1, (2007).'pp. 693-699.

[4] Smith B. and Maesen TLM. 'Towards a Molecular Understanding of Shape Selectivity' .*Nature* 451 , (2008). pp. 671-678.

[5] Csicsery S. M. 'Shape-Selective Catalysis in Zeolites'.*Zeolites*4, (1984). pp. 202-213.

[6] Nikolay Kosinov, Chong Liu and Emiel J.M. Hensen. Engineering of Transition Metal Catalysts Confined in Zeolites.' *Chem. Matter.* 30, (2018).pp. 3177-3198.

[7] CrucianiG.'Zeolites upon Heating: Factors Governing Their Thermal Stability and Structural Changes.'*J. Phys. Chem. Solids* 67, (2006). pp. 1973-1994.

[8] Blakeman P. G. 'The Role of Pore Size on the thermal stability of

Zeolite Supported Cu SCR Catalysts.' *Catal. today* 231, (2014). pp.56-63.

[9] BrennaU. , H. Ernst b , D. Freude b , R. Herrmann. 'Preparation of Sodium silicate'. *Microporous and mesoporousdMatt. 40*, (2000). pp. 43-52.

[10] Lili Xing, Xiaohong Wu, Rui Wang, Wei Xu, and Yannan Qian. 'Upconversionwhite-light emission in $Ho^{3+}/Yb^{3+}/Tm^{3+}$ tridoped $LiNbO_3$ single crysta', *Optics Letters,*Vol. 37, Issue 17, (2012). pp. 3537-3539

[11] Volker Bachmann, Cees Ronda and Andries Meijerink. 'Temperature quenching of yellow Ce^{3+} luminescence inYAG:Ce'.*Chem. mater.* 21.10,(2009). pp. 2077-2084.

[12]   Hai Guo, Ning Dong, Min Yin, Weiping Zhang, Liren Lou, and ShangdaXi..'Visible up-conversion in rare earth ion-dopedGd$_2$O$_3$nano crystals'. *J.Phys.Chem.* B 108.50, (2004). pp. 19205-19209.

[13]   Bryan M. van der Ende, Linda Aartsa and AndriesMeijerink.'Lanthanide ions as spectral converters for solar cells'. *Phys.Chem.*11.47 , (2009).pp. 11081-11095.

[14]   Rivera, V. A. G., Ferri, F. A., Nunes, L. A. O., and M arega, E. 'White light up-conversion of nano crystalline Er/Tm/YbdopedtetragonalGd4'. *Opt. Mater* 33.4, (2011). pp. 643-646.

[15]   Gallis K. W., J. T. Araujo , K. J. Duff, J. G. Moore and Landry C. C. 'The Use of Mesoporous Silica in Liquid Chromatography.'*Adv. Mater.* 11,(1999). pp. 1452-1455.

[16]   Bini Marcella. peak shift in X-Ray Diffraction.'url: https : / / www . researchgate .net / post / What are all possible reasons for thepeakshiftinX-ray+Diffraction/5545069df079ed5a298b4620 .[Accessed 15-09-2018] (2015).

[17]   Victor A. Drits, Jan Srodon, and D.D. Eberl.'XRD measurement of mean crystalline thickness of little and illite/snoctile; reappraisal of the Kubler index and the scherrer equation.' *Clays and clay materials* 45.1, (1997). pp. 461-475.

[18]   Joel Datumn.'A guide to scanning electron microscope observation', http://www.geology.wisc.edu(1996).

[19]   ChristianBaerlocher.'Database   of   Zeolite   Structures', http://doi.org/10.17616/R3HS6N. switzerland. (2018).

[20]   Soorya Kabekkodu. 'Diffraction data base(ICDD)' ,http://www.icdd.com/. http://www.icdd.comNewtown Square, PA, USA. (2018).

[21]   Ullah Z, AtiqS.,and Naseem S. 'Indexing the Diffraction Patterns and Investigating the CrystalStructure of Pb-doped Strontium Ferrites'. *J. Sci. Res*. 5.2 (2013), pp. 235-244.

[22]   Julian R. H. Ross. 'Catalyst characterization'. *contemporary catalysis*

(fundamentals and current application)..doi: ht tps : / / doi . or g / 10 .1016/ B978-0-444- 63474-0.00016-3. (2019).

[23]   Li Han, and Jiafeng Yao. 'Hollow zeolite structure formed by crystallization in cross linked polyacrylamite hydrogels'. *J. Mater. Chem*. 18, (2008). pp. 3337-3341.

[24]   Chauhan A.and Chauhan P. 'Powder X-ray Techniques and its Application in Science and Technology'. *J. annalbioannal Tech* 5.5, (2014). p. 1000212.

[25]   Takeuchi I, Long CJ, Famodu OO, *and* Murakam M. 'Data management and visualization of x-ray diffraction spectra from thin film ternary composition spreads'.*Review of Scientific Instruments*. 76, (2005). p. 062223.

[26]   Sales A, Sousas DG, and Rodrigues HO. 'Power dependent up-conversion in Er^{3+}/Yb^{3+} co-dopedBiNbO$_4$phosphors'. *Ceramics International*142,(2016)pp. 6899-6905.

[27]   Manuel M. Tosheva,, Valentin P. Valtchev,& Boriana Mihailov. 'Direct Synthesis of functional Zeolitic materials'. *Matt. Sc*. (2012). p. 24.

[28]   Tingjie Chen,MinNiu, and Xiaodong Wang. 'Synthesis and characterisation of poly-aluminium silicate sulphate (PASS) for ultra-low density fibre brands (ULDF)' *RSV adv*. 68, (2015). pp. 193187-93193.

[29]   FiorenzoVetrone, John-Christopher Boye,and John A. Capobianco. 'Significance of Yb^{3+}concentration on the up c onversion mechanism in co doped Y_2O_3 : $Er^{3+}/$ Yb^{3+} nanocrystal.' *J. appl. Phy*. (2004).96, pp. 661-667.

[30]   Riikka Arppe, Iko Hyppanen, Niina Perala, and Riikka Peltomaa. 'Quenching of the up-conversion luminescence of NaYF$_4$:Yb^{3+},$Er^{3+}$and NaYF$_4$:Yb^{3+},Tm^{3+} nanophosphors by water'. *Nanoscale* 7, (2015). pp. 11746-11757.

[31]   Kabongo G. L. '*Luminescence investigation of zinc oxide nanoparticles doped with rare earth ion's'*. MSc thesis. University of South Africa, Physics Department. (2013).

Chapter 5

Up-conversion luminescence properties of Er^{3+}; $Yb3^+$ co-doped $NaAlSiO_2$

Introduction

Over the past decades, material scientists have unveiled the unique luminescence characteristics of light emitting materials that revolutionized the technology development of photonic devices. Among the most prominent innovations, up-conversion of co-doped rare earth phosphors has attracted a lot of research interest to understand their characteristics and possible application in solid-state laser, medical diagnostics, white light-emitting diodes (LEDs), bio-imaging, and laser optical cooling(optical refrigeration) [1, 2, 3, 4, 5].Amongst others, a direct beneficiary of up-conversion is the possible cooling of solids by laser light pumping in a process of thermalization called laser optical cooling, an area that has shown a lot of interest to physicists and material scientists in the last two decades [6, 7, 8, 9]. Moreover, the demand for up-converting materials has seen special interest directed at the investigation of rare-earth-doped phosphors that are pumped with low energy laser at the near infra-red region. These pumped phosphors emit photons in the visible region as a result of up-conversion taking place [10, 11, and 12].

Rare-earth doped materials with low phonon energies are known to favor up-conversion emission in the visible region, these come about as a result of multiple relaxations accompanied by non-radiative decay [13]. Moreover, trivalent rare-earth ions of Er^{3+}; Yb^{3+}; Tm^{3+} and Ho^{3+} demonstrate efficient up-conversion processes when doped into suitable hosts [14, 15, 16]. Specifically, Er^{3+} ions do generate efficient up-conversion emission in the visible region and are utilized in this particular application [17, 18]. In addition, the Er^{3+} is used as an activator and co-doped with a sensitizer Yb^{3+} for enhancement of high emissions after pumping at 980 nm [19, 20, 21, 22, and 23].

Recently, sodium aluminium silicate has been studied extensively as a n absorbent material and a molecular sieve in the industrial separation of effluents [24, 25]. However, little to no research exists of its photonic behavior in up-conversion laser pumping at 980 nm. Interestingly, rare-earth doped sodium aluminium silicate crystals show low phonon energy and are thus suitable for laser cooling [26]. In this work, Er^{3+}/Yb^{3+} co-doped sodium aluminium silicate up-conversion luminescent samples were synthesized andcharacterized. Pure crystals of sodium aluminium silicate were synthesized and the cubic phase of the silicate was investigated. Finally, the photonic properties of the doped and co-doped sodium aluminium silicate were characterized in ultra violet-visible-near infra- red spectroscopy (UV-ViS-NiR), photoluminescence (PL), and photo-thermometry spectroscopy.

Experimental

An incipient wetness doping technique was used in doping and co-doping [27].Samples of un-doped and Er^{3+} doped sodium aluminium silicate crystals were synthesized and dopedwith different concentrations of Er^{3+} from 0 mol % , 1 mol%, 2 mol%, and 3 mol%. These samples were examined for their emissions spectra in the region of 400 nm to 1000 nm using a UV/ViS/NiR spectro photometer. The second set of experiments was done using the host $NaAlSiO_2$ doped at 1mol % of Er^{3+},1 mol% Yb^{3+}, and 1 mol% of co-doped Er^{3+}/Yb^{3+}.A third set of the samples were doped at 1mol % Er^{3+},2mol % Er^{3+}, 3mol % Er^{3+}.

Photoluminescence analysis was conducted in the visible spectrum to the near-infrared region (400 nm to 800 nm). The concentration of Yb^{3+} was kept at a constant value as recommended [6, 28, 29]. These samples were annealed at 400ºC in an electric oven for one hour, and then analyzed for up-conversion emission characteristics after cooling. This was done with a pumping laser of 980 nm with 2 watts continuous beam.

A fourth set of samples were doped at 1mol%Er^{3+}; 2mol%Er^{3+}; 3mol%Er^{3+} and 4mol%Er^{3+} then co-doped with 20 mol%Yb^{3+}. The samples were sintered at 1100º C as the optimum temperature for annealing recommended (5 % of the melting point of the Host)[30], then characterized for up-conversion emission under 980 nm laser pumping.

Photonic characterization

Up-conversion luminescence data were collected after pumping with continuous infrared beam laser at 980 nm . Furthermore, up-conversion power dependence of the samples was characterized with a rectangular pulsed low energy laser of 500 Hz at 20 K Cps and 2ms. In addition, temperature dependence measurements were carried out in a modified photoluminescence spectroscopy coupled with a PMT detector making a thermo- spectrometer.

The visible region transmittance spectra were recorded using a PerkinElmer Lambda 1050 UV-ViS-NiR spectrometer at a resolution of 0.5 nm. Then photoluminescence emission and up-conversion experiments were carried out in normal laboratory ambient conditions using an Edinburgh Instruments FLS980 spectrometer. Power dependence measurements were carried out in the photoluminescence spectrometer and the power was varied from 0.0 to 1.5 watts in steps of 0.2 and luminescence emission intensities were recorded over the range of 500 to 720 nm. Temperature measurements were performed using the same PL spectrometer fitted with a PMT detector. The samples were heated to 450 ^oC and let to cool slowly to ambient temperature as emission intensities are recorded.

Results and discussion

UV-ViS-NiR

Figure 5.1 show UV-ViS-NiR spectra of un-doped, single doped Er^{3+} and co-doped Er^{3+}/Yb^{3+} NaAlSiO$_2$ held at an equal concentration of 1mol % for both dopants.
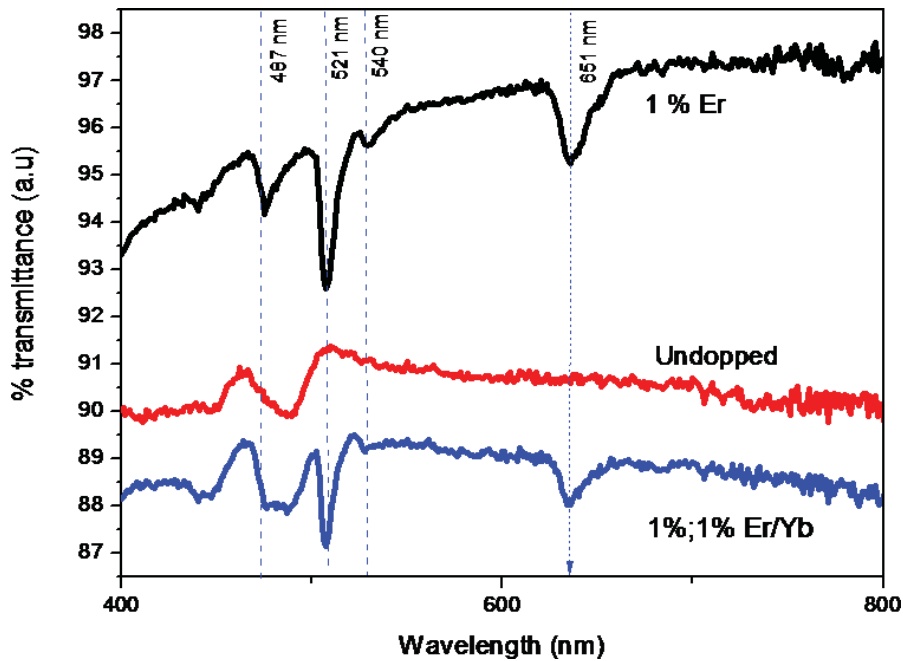
Figure 5.1 UV/ViS/NiR transmittance spectra of NaAlSiO$_2$ host singly doped and doubly doped with 1 mol % Er^{3+}, and 1 mol % $Er^{3+}/$ 1 mol % Yb^{3+}.

Comparison of the un-doped NaAlSiO$_2$ spectrum with that of the 1mol % Er^{3+} shows the 1 mol% Er^{3+} doped sample to have several absorption centers in the visible and the NiR region [31,]. Moreover, it was observed that the co-doped 1mol %$Er^{3+}/$1 mol%Yb^{3+} spectrum has a broader absorption band at around 521 nm as compared to the single doped 1 mol%Er^{3+} pointing to an enhancement of absorption due to the Yb^{3+} co-dopant [32]. Interestingly, there are up-conversion absorption centers in the visible region from the Er^{3+} ions due to their

complimentary f-f energy level composition [33]. For evaluation purposes, the 1 % mol Er^{3+} doped and 1 % mol both Er^{3+}/Yb^{3+} are compared to the un-doped host. Consecutively, the absorption bands observed at 521nm (green) were assigned to $^2H_{11/2}$---$^4I_{15/2}$ transitions, while the 540 *nm* (emerald green) band was due to $^4S_{3/2}$---$^4I_{15/2}$ transition and finally the 651 *nm* (red) corresponded to $^4F_{7/2}$---$^4I_{15/2}$ transition of Er^{3+} [35].

Furthermore, the host in this experiment was kept in the same phase which influences the presence of absorption centers in hosts doped with rare earth phosphors [34].

In figure 5.1, N aAlSiO$_2$ co-doped 1mol%Er^{3+}/1 mol%Yb^{3+} show a higher percentage transmittance than the singly doped Er^{3+} in the visible to near IR regions.

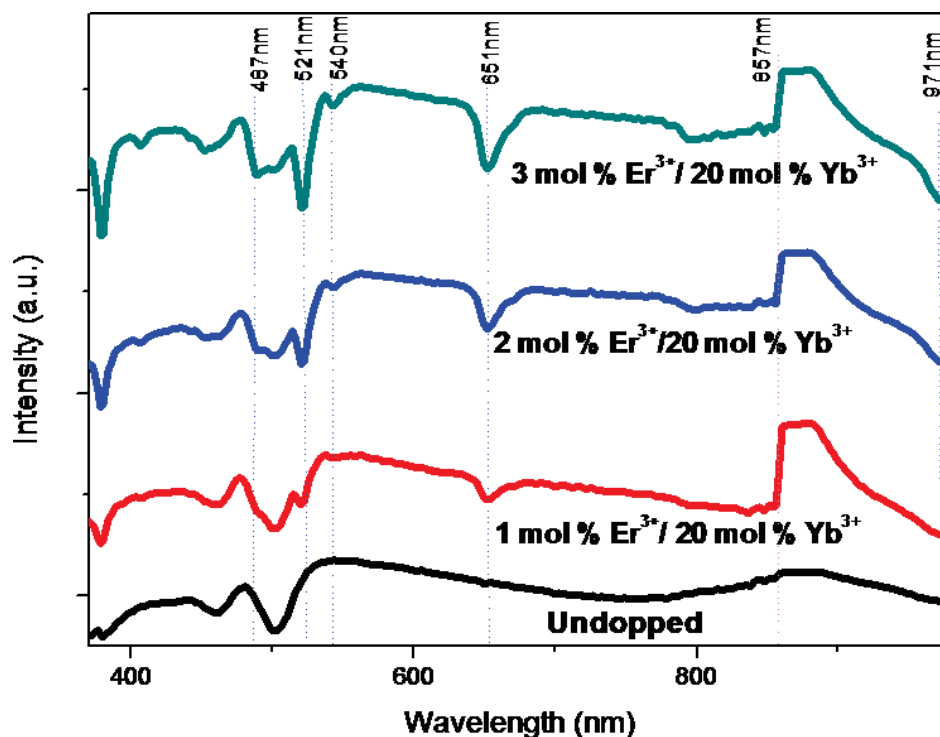**Figure 5.2:** UV/ViS/NiR transmittance spectra of NaAlSiO$_2$ host, successively doped with 1 mol % Er^{3+}, 2 mol % Er^{3+}; 3 mol% Er^{3+} all co-doped at 20 mol % of Yb^{3+}.

These absorption centers suggest a possible up-conversion emission with IR pumping at 980 nm resulting in excitations, the absorption band emission is shown more vividly in the PL experimentation section 5.3.2.

Figure 5.2 show UV/VIS/NIR transmittance spectra of un-doped $NaAlSiO_2$ and samples doped with 1 mol% Er^{3+}; 2 mol% Er^{3+}; 3 mol% Er^{3+} with a fixed sensitizer concentration of 20 % Yb^{3+}, both showing absorption centers. Precisely, five absorption luminescence centers are detected in the spectra region from 400 nm to 1000 nm (visible to NIR), these peaks are located at 971 nm, 651 nm, 540 nm, 521 nm, and 487 nm, respectively. It is worth mentioning that the un-doped (black pattern) pattern did not show any absorption bands in the visible-NIR excitation region, as there are no excitable ions in an un-doped material: It is worth mentioning that the absorption efficiency (intensity) increased with the increase in the concentration of Er^{3+}.

For detailed investigations, the $NaAlSiO_2$ samples were co-doped with Er^{3+} and Yb^{3+} based on the 2 mol % Er^{3+} doped $NaAlSiO_2$ samples which exhibited the highest emission intensity. Moreover, the concentration of 20 mol % of the sensitizer Yb^{3+} was maintained constant as recommended in the literature [6, 28, and 29]. Observations revealed that in the region of 400 nm - 1100 nm, five absorption bands appeared at 971 nm, 651 nm, 540 nm, 521 nm, and 487 nm. It is important to note that doping with Er^{3+} shows emission peaks while co-doping with Er^{3+}/Yb^{3+} resulted in a remarkable emission enhancement effect on the peaks intensities.

The knot on the detector curves at around 857 nm shows the change of the laser sensing detector from InGaAs to PbS detector as the transition from near infra-red to far infra-red regions starts.

Photoluminescence of Er^{3+}; Yb^{3+} co-doped $NaAlSiO_2$

Figure 5.3 displays up-conversion luminescence spectra of $NaAlSiO_2$ sample with Er^{3+} at different concentrations of 1, 2, 3, and 4 mol % while $Yb^{3+}$was kept at 20 mol% and annealed at 400 ºC.
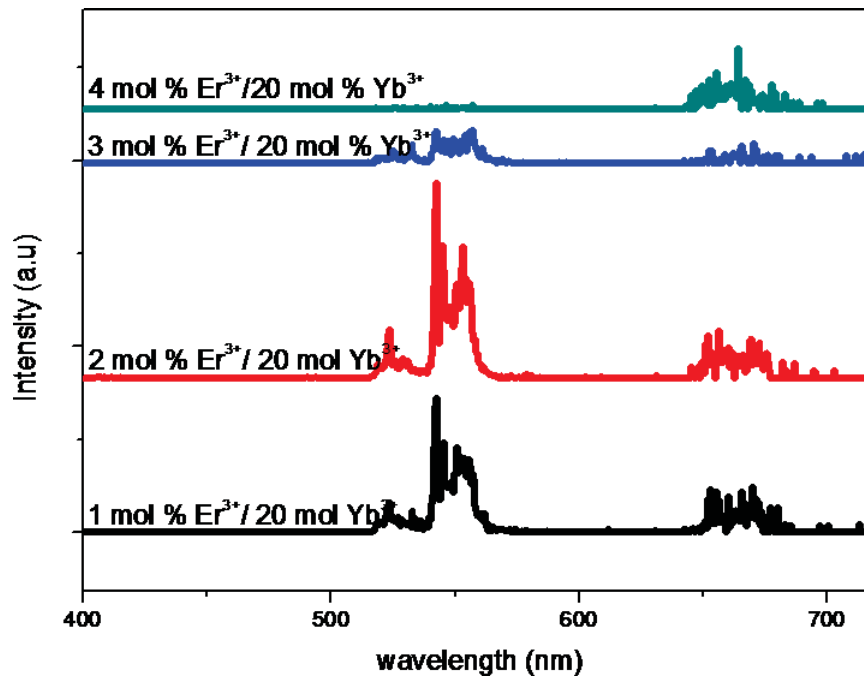
Figure 5.3   Up-conversion luminescence spectra of $NaAlSiO_2$ samples co-doped with Er^{3+} at 1 mol %, 2 mol %, 3 mol %, and 4 mol % all co-doped with Yb^{3+} 20 mol % and annealed at 400 ºC.

The up-conversion low intensities observed in figure 5.3 are due to impurity quenchin and the presence of absorbed molecular OH group that cause non-radiative relaxation leading to severe quenching of up-conversion emission [36]. Moreover, OH group presenceis a weakness of the incipient wetness doping method used. Also, luminescence intensity quenching could be due to the result of several factors, including absorbed impurities, intermolecular interactions, and energy transfer inefficiency as well [37].

The spectra revealed that four prominent up-conversion absorption centers are active, with up-conversion emission intensities increasing from 1 mol % Er^{3+} to 2 mol % Er^{3+}, before decreasing at 3 mol% Er^{3+}, resulting from concentration quenching. A further decrease in the intensity was observed at the 4 mol% Er^{3+} sample, thus the highest emission intensity was observed at 2 mol% Er^{3+} concentrations. It is worth to remindthat, all the emission peaks recorded were lower than expected. It was observed that all four samples have three absorption bands of excitation, two in the green region and one in the red region, the intensity in the green region at about 540 nm increased to a maximum in the 2 mol %Er^{3+}/20 mol %Yb^{3+} co-doped sample and drops considerably in the 3 mol % Er^{3+} and 4 mol % Er^{3+} samples, respectively.

The green (521 nm) and red (651 nm) emissions originate from the states$^4S_{3/2}$ ---$^4 I_{15/2}$ and $^4F_{9/2}$---$^4 I_{15/2}$transitions respectively. At low IR excitation, the green region benefits from ETU entirely, while the red region has two excitation modes, the multi-phonon relaxation (MPR) and ETU from upper $^4S_{3/2}$ and lower intermediate$^4I_{13/2}$ states respectively [38, 39].

The emission intensities in the red region are much lower compared to the emissions in the green region. Also, the intensities in this region were observed to increase up to the maximum of 2 mol% Er^{3+} and then doped at 3 mol% Er^{3+}. However, the emission intensity begins to increase again at 4 mol% Er^{3+}. It is interesting to note that as the red emission peak increases, the green emission diminishes in intensity at these concentrations. This observation suggests that non-radiative relaxation process from$^4S_{3/2}$to $^4F_{9/2}$ is more favorable at higher concentrations of Er^{3+} (see figure 5.6).Finally, the Er^{3+}/Yb^{3+}energy transfer at 651 nm involves two back to back transfer methods, cross-relaxation energy transfer (CR) from the Er^{3+} in the $^4S_{3/2}$ excited state$^4S_{3/2}$ --- $^4 I_{13/2}$ into Yb^{3+} in the ground state $^2F_{5/2}$ — $^2 F_{7/2}$ [40, 41].
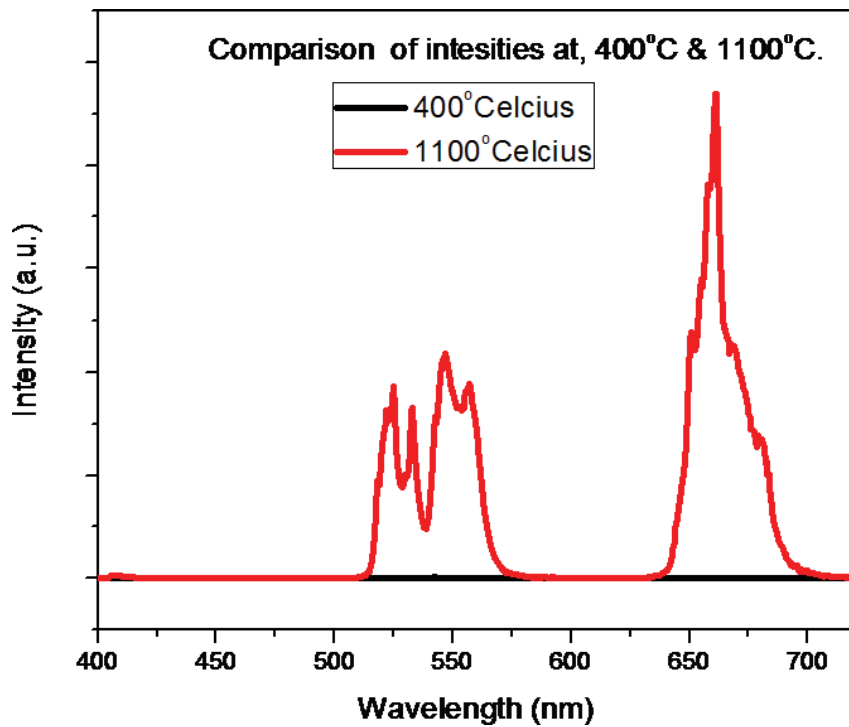
Figure 5.4   Effect of annealing temperature on up-conversion intensities of NaAlSiO$_2$ co-doped with 20 mol% Yb^{3+}/ 2 m ol% Er^{3+} at 400 $^o C$ and 1100 ^{o} C (sample A1) compared at the same scale.

Figure 5.4 show the up-conversion measurement revealing that the sample annealed at 1100 $^o C$ showed considerably higher up-conversion emission intensity, about 1000 times as compared to the sample annealed at 400 $^o C$.

The question of what annealing temperature to use arose after several measurements of up-conversion showed very weak to no e mission at all. Also, we found out that un-annealed samples showed zero up-conversion emissions and thus we consulted the following work by Rychlik et al. [32], where it was shown that the optimal annealing temperature should be about 5% below the melting point of the composition of the primer. Consequently, knowing that NaAlSiO$_2$ crystals have a m elting temperature between 1200° and 1400 ^{o} C, a 5% lower than melting point would be 1100 ^{o} C., thus 1100 $^o C$ was chosen as our annealing temperature [42].

As discussed earlier, the low intensity emissions at annealing temperature of $400\,^oC$ were highly enhanced by a nnealing at the optimal temperature $(1100\,^o\,C)$ as recommended, thus annealing at the 5 % below melting proved to be critical in enhancing high up-conversion emission [43].

Figure 5.5 presents the up-conversion emission intensity spectra of co-doped with Yb^{3+}/Er^{3+} at the concentration of 20 mol $%Yb^{3+}$ co-doped with 1 mol $%Er^{3+}$, 2 mol $%Er^{3+}$, 3 mol $%Er^3$, 4 mol $%Er^{3+}$ and annealed at 1100 °C.
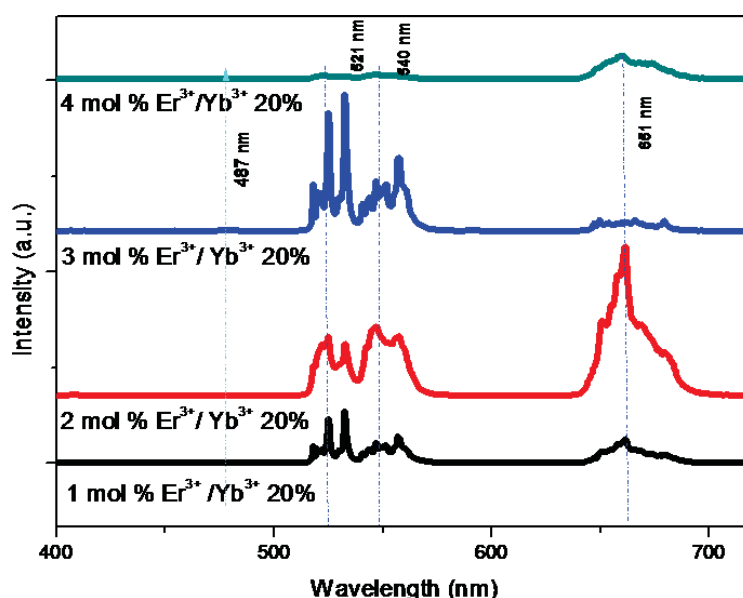
Figure 5.5 Up-conversion emission spectra of NaAlSiO$_2$ co-dope at

20 mol% Yb^{3+} and 1 mol%, 2 mol%, 3 mol% and 4 mol% of Er^{3+}

annealed at 1100 °C.

Figure 5.6 shows Up-conversion intensities against increasing percentage concentration of Er^{3+} at a co -doped constant concentration of 20 mol % Yb^{3+}, with each spectra represented by its frequency's colour. The spectra show three distinct emission bands visible with a fourth very weak band at 487 nm. Moreover, the three distinctive bands appear on the green, emerald green region centred at 521 nm and 540 nm and the last band at the red region at 651 nm.

72

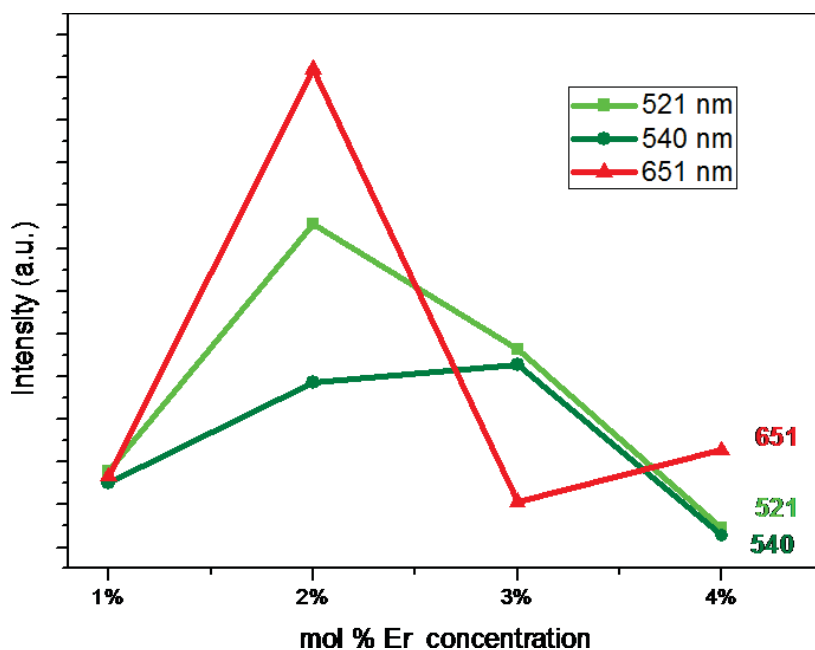**Figure 5.6** Up-conversion intensities against increasing percentage concentration (at 1 %, 2 %, 3 %, and 4 %) of Er^{3+}at a co-doped constant concentration of 20 mol % Yb^{3+}, with each spectra represented by its frequency's colour.

Figure 5.6 shows the green region and red region (all depicted by individual colours of their frequencies) intensities as concentration of the Er^{3+} is increased from 1% to 4%, The graph shows that the intensity increases as concentration increases from 1 % Er^{3+} to 3 mol % Er^{3+} and is then suddenly decrease at 4 mol % Er^{3+} in the green region 521 nm and emerald green 540 nm due to concentration quenching. Moreover, the red region at 651 nm presents a different picture with an intensity increase from 1 mol % Er^{3+} to a maximum value at 2 mol % Er^{3+} then a total quenching at 3 mol % Er^{3+} followed by a slight increase in 4 mol % Er^{3+}.

Figure 5.7 shows energy levels diagram of Er^{3+} and Yb^{3+} in sodium aluminium silicate and its up-conversion mechanism.

The Er^{3+}/Yb^{3+}, figure 5.7 excitation diagram shows a two-photon mechanism is involved in the up-conversion process, thus there are two possible excitation routes in the two-photon scheme [17, 51, 52].

The first route involves the absorption of a photon by the Yb^{3+}ion, which excites it from the ground level $^2F_{7/2}$to $^2F_{5/2}$. A transition follows as energy is transferred into an Er^{3+} ion at a level $^4I_{11/2}$ through an Energy transfer process (ETU), then a second photon excites the Er^{3+} to the $^4F_{7/2}$ where a non-radiative decay occurs with the release of green/blue light at 487 nm.

The second route of up-conversion involves the first photon being absorbed by the Er^{3+} thus exciting it from ground state $^4I_{15/2}$ to $^4I_{11/2}$, then it is populated by a second photon from the Yb^{3+} ion at $^2F_{5/2}$ level to excite it into level $^4I_{15/2}$, a non-radiative decay occurs releasing green light as the state relaxes to the ground state. The same process takes place at the different excitation bands in the 521 nm, 540 nm, and 651 nm releasing green, emerald green, and red light respectively.
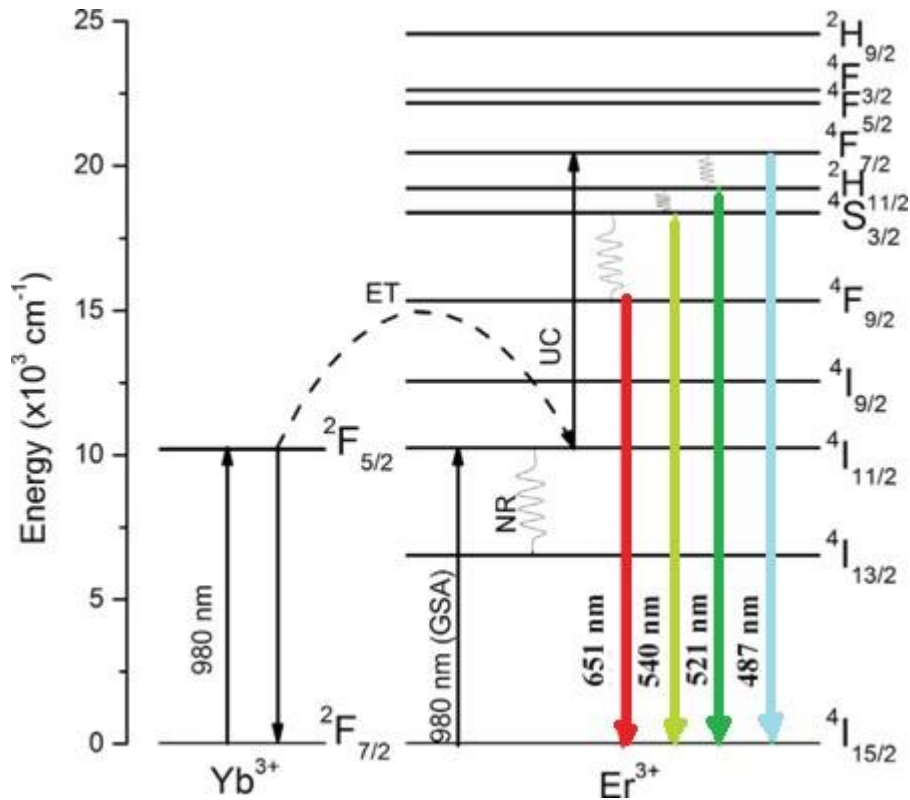
Figure 5.7 Energy levels diagram of Er^{3+} and Yb^{3+} in $NaAlSiO_2$ and its up-conversion mechanism [46].

These distinct excitation peaks are attributed to the 4f-4f electronic transitions of Er^{3+} ions and are assigned to $(^4F_{7/2} \text{---} ^4I_{15/2}),(^2H_{11/2} \text{---} ^4I_{15/2}), (^4S_{3/2} \text{---} ^4I_{15/2}), (^4F_{9/2} \text{---} ^4I_{15/2}),$ and $(^4I_{11/2} \text{---} ^4I_{15/2})$ transitions [44, 45].More importantly, the weaker 487 nm emission peak is two insignificant compared to the other peaks and appears as a speck in the patterns spectra [46].

It is worth noting that the emission intensities of rare earth doped silicates are determined by the excitation and absorption bands in the 4f-4ftransition levels, however by manipulating doping concentration and the matrix of the host colour tuning of the up-conversion luminescence can be achieved [47].

On pumping the doped sample with IR beam at 980 nm, electrons are excited through a

GSA process to the level $^2F_{5/2}$, a multi-phonon process of excitation takes place transferring(ET) the electrons to higher level $^4F_{7/2}$ then farther raised to occupy upper levels through UC process in a non-radiative process. These exited state levels are $^2H_{11/2}$, $^4 S_{3/2}$ and $^4F_{7/2}$.

A radiative decay process follows where all decays to ground state $^4I_{15/2}$, emitting green, emerald green and a r ed whose CIE colour coordinates are 521nm (x = 0.0820, y = 0.8340 green), 540 nm(x = 0.2296, y = 0.7543 emerald green) and 651 nm (x = 0.7264, y = 0.2735 Red), shown in figure 5.8 m arked squares in a CIE visualization diagram[55].

Figure 5.8 a CIE 1931 colour chromaticity diagram that gives visual image of
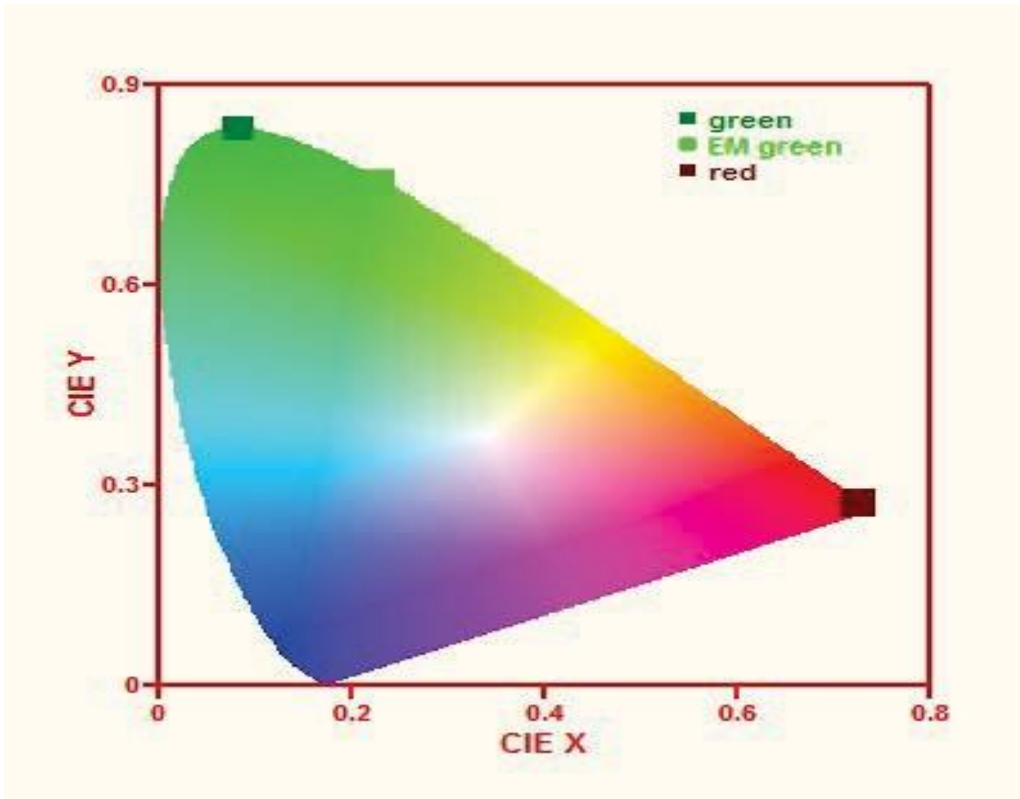
colour tunability in 2 mol %Er^{3+} / 20 mol % Yb^{3+} doped $NaAlSiO_2$ at 521 nm, 540 nm, and 651 nm shown in coloured square symbols.

As the Er^{3+} concentration is increased a quenching process takes place resulting in decreased emission intensities. This process is called concentration quenching and is a result of Er^{3+}dipole to dipole energy transfer interaction within neighboring ions. The interaction depends on the distance R across interacting ions and by resonance energy theory it follows 1/R6 dependence[48].As the concentration of the Er^{3+} is increased the

gap between the neighboring ions decreases so much that energy transfer occurs among the Er^{3+} ions creating quenching centers, thus up-conversion emission intensity is decreased. The host, $NaAlSiO_2$ is an oxide of the silicate group whose intermediate low phonon energy of about 1200 cm^{1} makes it suitable for investigation for up-conversion [49]. Er^{3+} doped oxides have been studied extensively to understand the up-converting mechanism.

In his work, Robert Anderson [50], suggested a new up-conversion mechanism that accounted for the unexpected pattern in the red region. He suggested that the emissions were due to a t hree-photon process in the co-doped Er^{3+}/Yb^{3+} system. The Er^{3+}/Yb^{3+} up-conversion system with three-photon emission presents a dynamic model that is difficult to predict as it has many levels of transition, we however may explain the two-photon emission model.

In their work, A.J.M. Sales and colleagues [46], found out that changing the concentration of the Yb^{3+} in an Er^{3+}/Yb^{3+} system from 1 % to12 % co-doped with a fixed concentration of Er^{3+} did not change the up-conversion emission intensities but stayed stable for the emission bands, thus to a greater extent it's the concentration of the Er^{3+} that controls the intensity of emission in the Er^{3+}/Yb^{3+} co-doped system. Also, A.J.M Sales et al, reported that the Er^{3+}/Yb^{3+} is a v ery efficient energy transfer up-converting pair because the Yb^{3+} ions have a larger absorption cross-section than the Er^{3+} ions in the NIR region[46].

Lifetime measurements of Er^{3+}; Yb^{3+} co-doped $NaAlSiO_2$

Lifetime measurements were performed to establish the average decay time (average decay time dependence is worked out at wavelengths of 521 nm, 540 nm, and 651 nm). The effective lifetime is as a result of the whole system in the up- conversion process including photon absorption, ion/electron excitation, cross-relaxation, and eventual photon emission as the excited ion/electron drops down to the ground state [43], what we have referred to as thermalization process.

Lower spectral response is as a result of an on-infinite effective lifetime of the

system's decay time. If radiative recombination was the only active factor, then the lifetime would be in the range of 10 *ms* and cannot be the only limiting factor for the up-conversion emission process [53]. Hence, the decay lifetime was estimated from decay fitting equations that were generated from the actual decay data.

Figure 5.9 shows the decay curves of our best emission up-converting samples A1, A2, and B2 (sample 1, 2, 3) respectively.
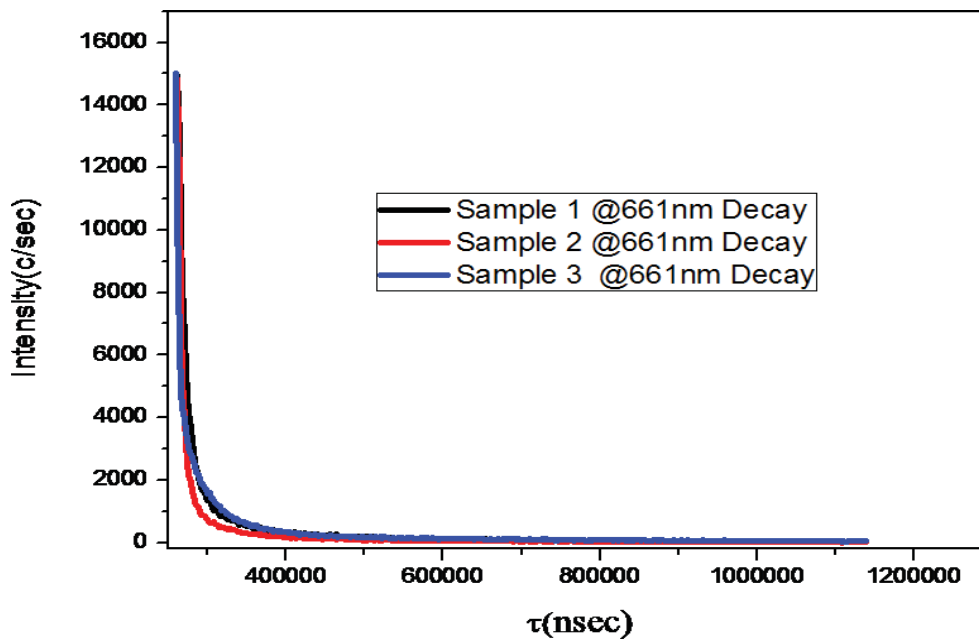
Figure 5.9 Decay curves of samples A1, A2 and B2, labeled sample 1, 2, and 3 respectively.

The excitation power density of the pumping source was a pulse excitation function of a rectangular nature of 500 *Hz* at 20 *kcps* and 2 *ms* whose maximum power was 1.5 watts [54]. Also, it is noted that our first three samples show different decay curve characteristics at the same wavelength (651 nm) and, that is attributed to the difference in the overall matrix of the up-converting ions/electrons, chemical composition, and dopants distribution within the host.

To do a proper fitting for the decay curves, the double exponential equation was chosen as it has an *R*-value of 0.99906 much better than the single exponential equation.

The double exponential equation is given as

$$y = A1e^{(-x/T\ 1)} + A2\ e^{(-x/T\ 2)} + y0 \tag{5.1}$$

The value T_1 is the decay lifetime of the up-conversion process, while the value T_2 is the rise time influenced by the emission state and the ETU rate overlaps exactly with the fitting curve (black spectra figure 5.9)[55].

Nine decay curves were generated and all their lifetime worked out, this was at three different wavelengths 521 nm , 540 nm, and 651 nm. The equation for calculating the T is given by for the double exponential decay curve;

$$= \frac{A1\ (\ 1)^2 + A2\ (\ 2)^2}{A1\ \ 1 + A2\ \ 2} \tag{5.2}$$

The worked out values for the decay lifetimes T are shown in the table 5.1

Table 5.1 Samples A1, A2, and B2 lifetime decay constant *r*.

Sample name	Wavelength (nm)	Lifetime (*r*) (*ns*)
A1	521	25059.73
A1	540	25130.58
A1	651	36433.37
A2	521	15369.41
A2	540	11539.31
A2	651	8153.65
B2	521	10250.73
B2	540	12163.15
B2	651	8849.9

The lifetime decay constants calculated can be classed as follows, sample A2 and B2 were synthesized in 4 and 24 hours and their decay constant is similarly ranging from 10250 *ns* to 15000 *ns* (10.25 *μs* to 15.00 *μs*) for the green region (521-540 nm) and 8153-8850 *ns* (8.15*μs* to 8.85 *μs*) for the red region.

Sample A1 was synthesized for 2 hours, it has very long lifetimes (comparatively) above 25000 *ns* to 36433.37 *ns* (25.00 *μs* to 36.43 *μs*) in both the green and the red region.

It was observed that different lifetimes were obtained for each of the samples of doped $NaAlSiO_2$ irrespective of the concentration of the doping agents and thus the emission intensities depended weakly on the doping ions present but more on the host's matrix [56].The values for the decay lifetimes calculated ranged from 8 microseconds to 36 microseconds within the expected time frame of microsecs to milliseconds [57].

Power dependence of Er^{3+}; Yb^{3+} co-doped $NaAlSiO_2$

In order to accurately elucidate the mechanism associated with the observed up-conversion luminescence, we conducted laser pump power dependence study. This contributes in the identification of the number of incident photons essential to excite doping ions in $NaAlSiO_2$ crystals. To successfully achieve this, the laser excitation pump power was gently increased and applied to the as-synthesized $NaAlSiO_2$ nanophosphors. As a result, the up-conversion luminescence intensities of $NaAlSiO_2$ nanophosphors increased with the laser power pump increased from 0.096 *W* to 1.5 *W*. This phenomenon implies that the emitted up-conversion intensity is directly proportional to the power of the exciting pump, where the power of the pump is intimately related to the number of incident photons needed to stimulate the doping ions into their excited state.

Figure 5.10a and 5.10b shows sample A1's 2-D power dependence curves with an incremental intensity of luminescence being seen as p ower factor that is increased from 0.96 *W* to 1.5 *W*. The increase in luminescence intensity is associated with change in population at differnt levels as pumping power is increased.

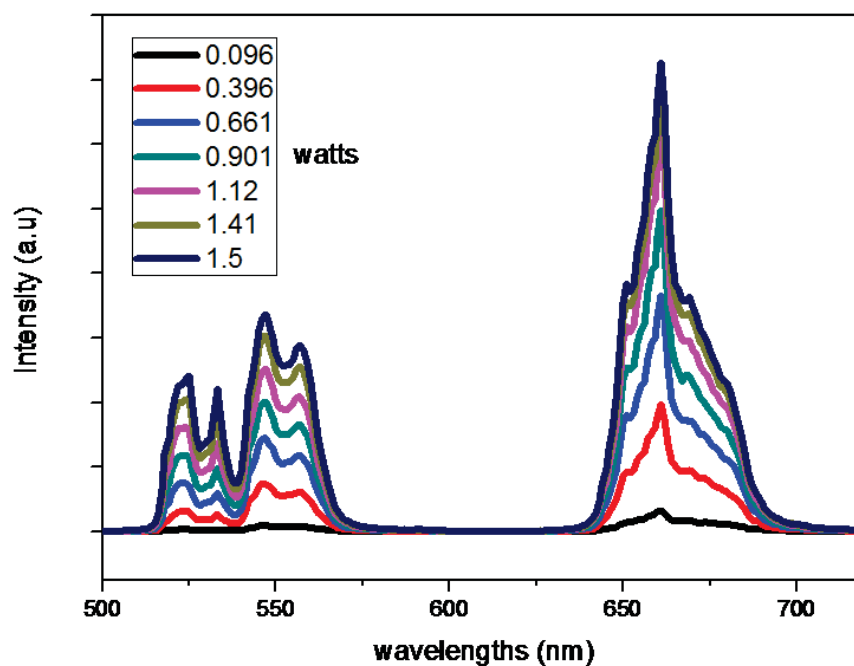**Figure 5.10a:** Sample A1 power dependence increment against wavelength.
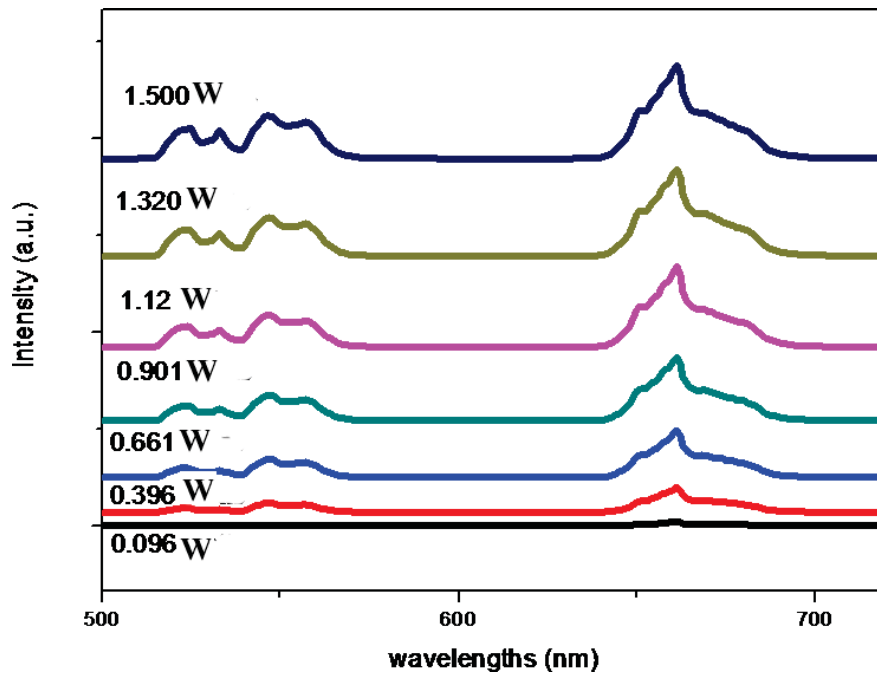
Figure 5.10b Sample A1 stacked incremental power patterns.

Figure 5.10c is a 3-D representation of the power dependence bars, showing the relationship between the pumping power, intensity, and wavelength. It is observed that the rate of intensity increment is not directly proportional to the increase in pumping power for all wavelengths.

Figure 5.10c Sample A1 power dependence 3D graphs for sample comparing the increase in pump power against luminescence in the visible region.

Figure 5.11 Sample A1 log of intensity against the log of power gradient curves.

Figure 5.11 shows the linear relationship between the logs of the intensities against the log of the pumping power. Three linear re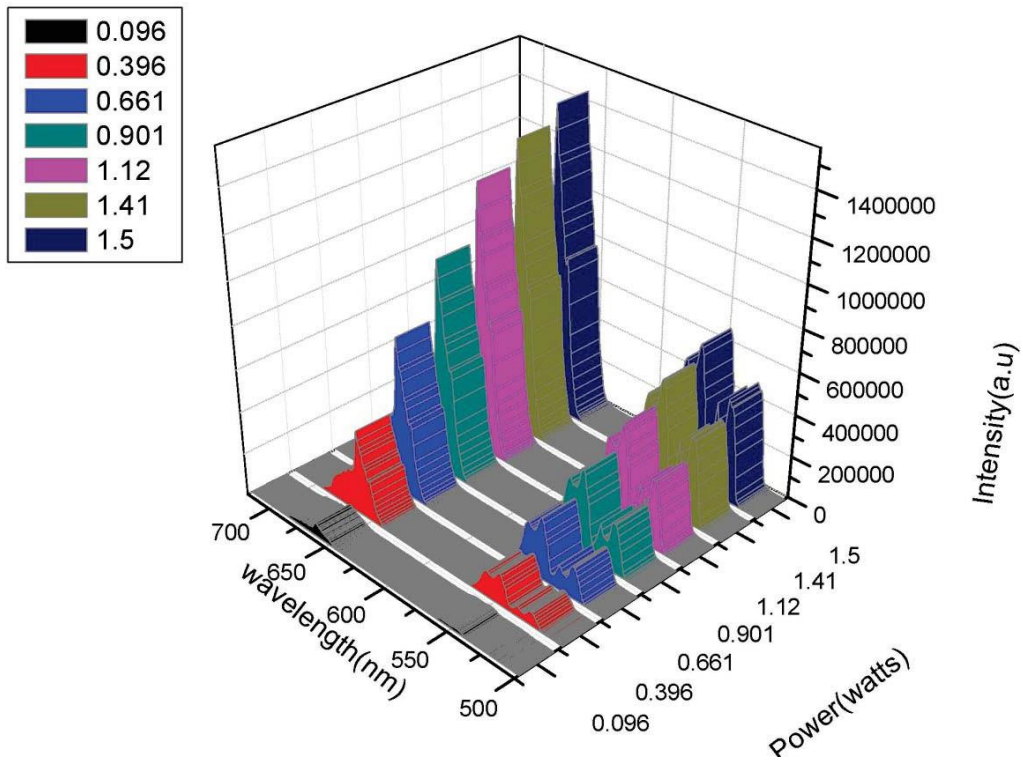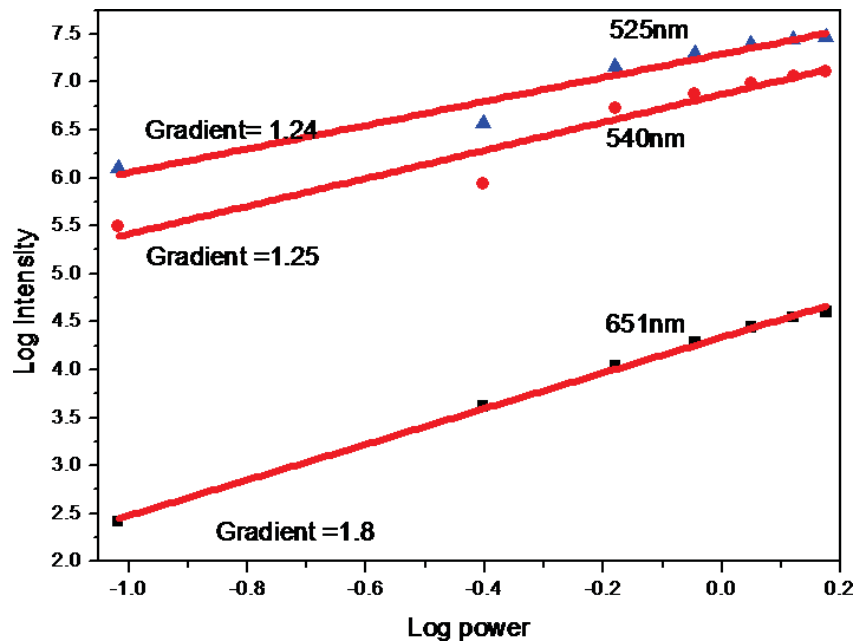lationships are observed at three luminescence absorption centers, gradients of the log intensity/log power are shown as 1.86, 1.25, and 1.24 for the 521 nm , 540 nm, and 651 nm respectively. These values correspond to the number of infrared phonon per visible photons emitted during the up-conversion process [58]. For the two-photon emission process (the green and the red emissions) an average or near two should be the gradient of the log I/ log power. The lower gradient values of 1.24 and 1.25 are attributed to the loss in linear decay and the up-conversion process depletion in the intermediate excited states. The gradient value of 1.85 (;: 2:0) suggests the up-conversion process in Yb^{3+}/Er^{3+} is a two-photon excitation process.

The maximum peak power for the power dependence increases with the exponential growth of a power function of type $y = X^p$, a possible characteristic of the equipment and the crystal under investigation [59].
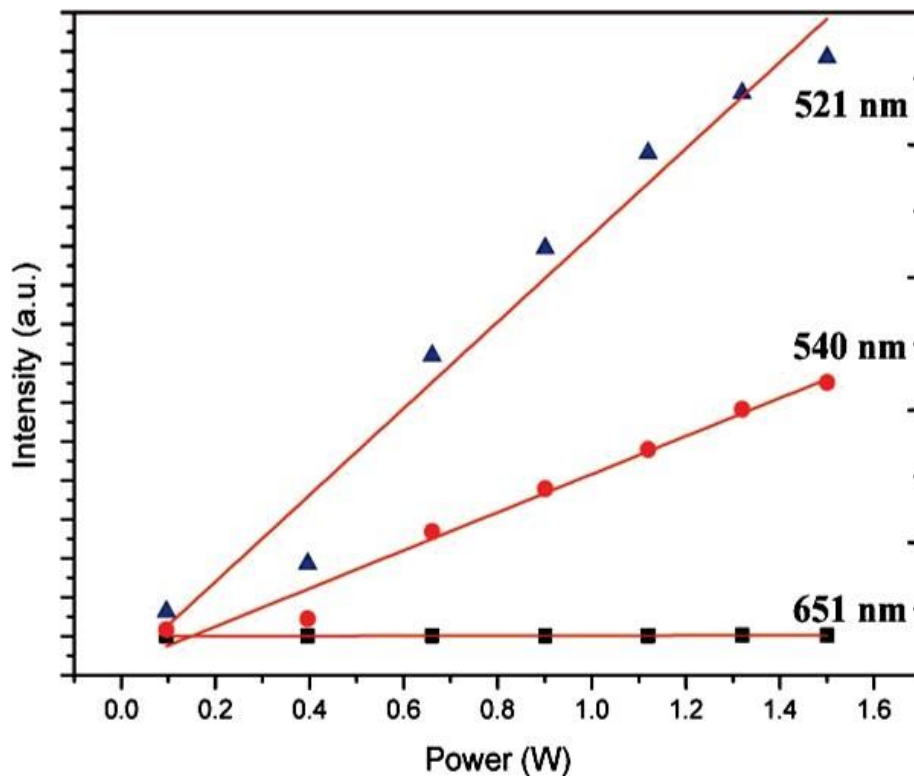
Figure 5.12: Sample A1 intensity versus power curve for peak max at 521 nm, 540 nm and 651nm.

Figure 5.12 shows intensity versus the power at peak values of 521 nm , 540 nm, and 651 nm as generated from experimental data. There is a direct proportionality of increase in emission intensity as the power is increased at 521 nm, 540 nm, and at 651 nm, as the wavelength increases the gradient of the rate of increase of intensity with power decreases to almost zero as we increase wavelength from 521 nm , through 540 nm to 651 nm. The best curves were fitted to obtain a power function curve whose equation was established as

$$y = A2 + \frac{A1 - A2}{1 + (x/x_o)^p} \qquad (5.3)$$

where A1, A2, and X_o are the constants of the curve. A power function has a character of approaching a maximum intensity value irrespective of the pumping power, this is obviously an intrinsic character of the emitting system or the excitation mechanism in the up-conversion process [60].

Temperature dependence of Er^{3+}; Yb^{3+} co-doped NaAlSiO₂

Figure 5.13 a shows emission spectra of intensity versus wavelength that was generated with each spectra overlapping over almost each other as the temperature and intensity were recorded at steps of 0.0001 nm of the wavelength for the range 400 nm to 750 nm. region). Intensity against wavelength at different temperatures from 50 ° − 400 °C. step 1 °C, it is interesting to observe that for all temperatures, the emission lines for different transitions are obvious. However, it is observed that the intensity of UCL decreases gradually with the increase of temperature for both emissions, which can be assigned to significant thermal quenching of UCL as a result of its worse crystallinity and surface absorption [59]. The sample's temperature was varied from 50 °C to 400 °C in reverse order, (i.e. the samples were heated to 400 °C and allowed to cool to ambient) as measurements of emission intensity against temperature were recorded.   .
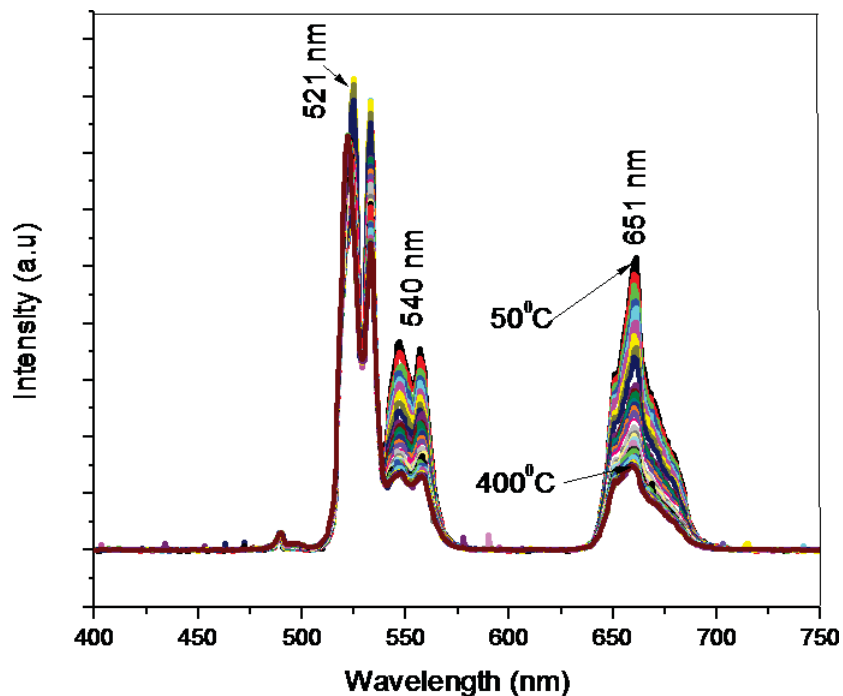
Figure 5.13a Sample A1 intensity against wavelength at different temperatures from 50 ° - 400 ° C. step 1 °C.

Figure 5.13b shows temperature against absorption intensity decay spectra as the temperature was increased from $40\,^{o}C$ to $400\,^{o}C$. They showed an exponential decay as the temperature was increased, suggesting a log relationship.
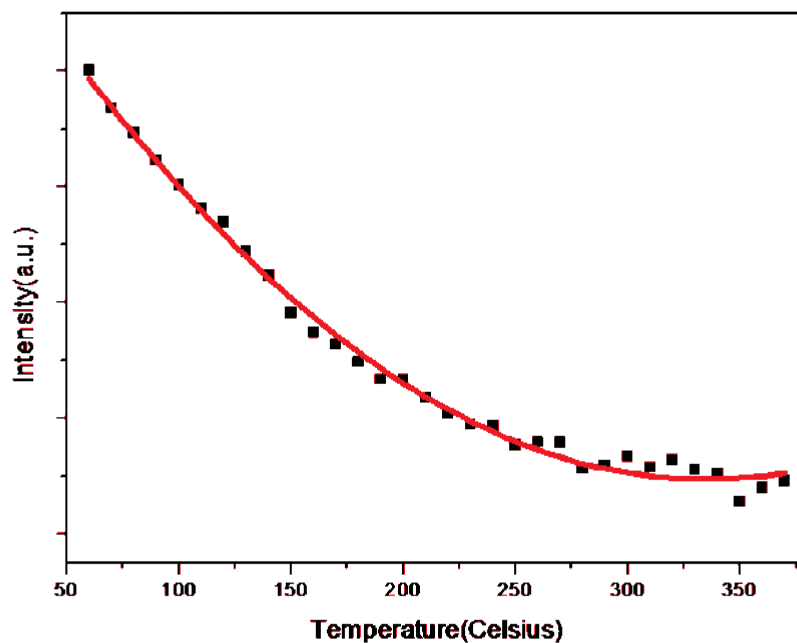
Figure 5.13b: sample A1 temperature intensity decay curve, showing intensity against. temperature.

An exponential decay curve of intensity with increasing temperature was observed, suggesting a logarithmic relationship between the two.
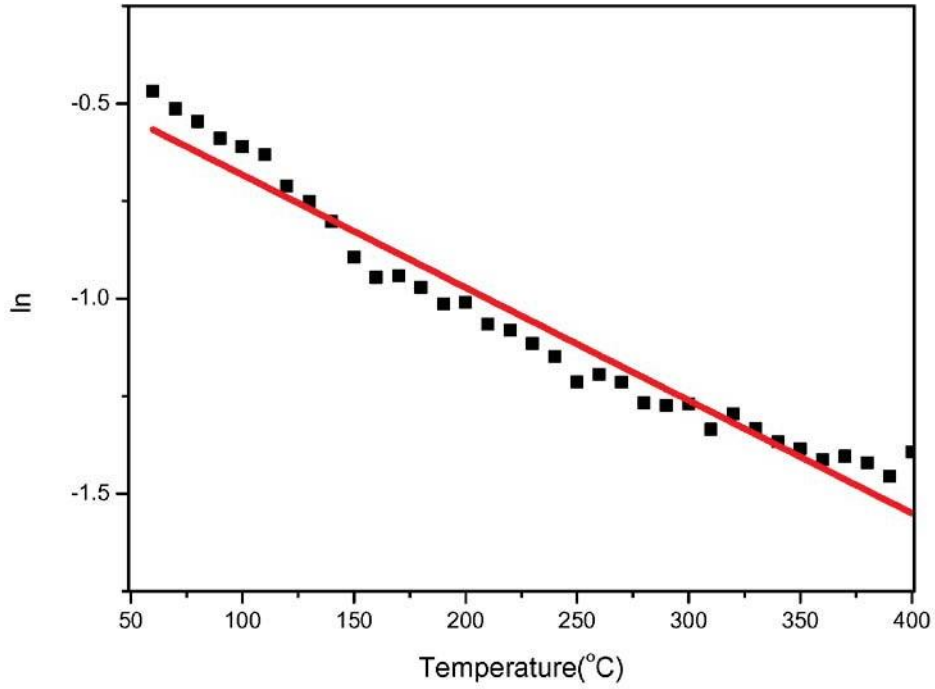
Figure 5.14: sample A1 log intensity against temperature at 661 nm absorption.

Figure 5.14 shows a log of intensity against temperature dependence spectra, although the temperature-dependent data was not corrected, the changes in the log of absorption intensities as a function of temperature are a ccurate and showed straight-line decay with uniform negative gradient and thus the potential of the sample for temperature sensing applications was established [59].

Conclusion

Er^{3+} and Er^{3+}/Yb^{3+} co-doped $NaAlSiO_2$ crystals were successfully synthesized. Hydro-gel, hydrothermal, and incipient wetness doping processes were used. The synthesized samples were characterized using various analytical techniques. Besides conducting XRD, SEM, EDS, and FTIR analysis, the FTIR showed the presence of absorbed OH group that led us to perform an optimized annealing process, to eliminate quenching of up-conversion emission.

The up-conversion luminescence absorption intensities were highly enhanced when doping was optimized to 2 % mol Er^{3+}/ 20 % mol Yb^{3+} More importantly, three up-conversion absorption centers were recorded in the visible region at 521 nm, 540 nm, and 651 nm, corresponding to (in the emerald green, green, and red region of the visible spectrum) colours, respectively.

Lifetime measurements showed decay times in the range of 10421 *ns* to 28874 *ns* that suggested an increased ion excitation that lead to long after glow fluorescence.

Further investigation of power dependence measurements showed the presence of the two-photon excitation mechanism as the main process of up-conversion. Consecutively, temperature dependence showed a linear relationship between the log of the intensity against the temperature with a negative gradient as the temperature rose, thus qualifying the co-doped $NaAlSiO_2$ for possible temperature sensing application in the range 50 ^{o} C to400 ^{o} C.

References

[1]   Renuka Bokolia, Kondepudy Sreenivas, O. Thakur, and Vineet Rai, 'Electrical properties and light up-conversion effects in $Bi_{3.79}Er_{0.03}Yb_{0.18}Ti_{3-x}W_xO_2$ ferroelectric ceramics', *Ceramics Int*er., 42.5(2015) pp. 60431-43.

[2]   LojpurV., Nikolic G., and DramicaninM. D, 'Luminescence thermometry below room temperature via up- conversion emission of $Y_2O_3{:}Yb^{3+}Er^{3+}$ nanophosphors', *J. Appl. phys.*, 115 (2014)pp. 203106.

[3]   Auzel F, 'Up-conversion anti stoke process with f and d ion in solids', *Chem. Rev.* 104 (2004) pp. 139-143.

[4]   Guanying Chen, HailongQiu, Paras N. Prasad , and Xiaoyuan Chen, 'Up-conversion nano partials design, nano chemistry and application in theranostics'. *Chem. Rev.,* 114(2014) pp. 5161-5214.

[5]   Epstein R.I., Buchwald M.I., Edwards B.C., Gosnell T.R, and MunganC.E,'Observation of laser-induced fluorescent   c ooling of a solid'. *Nature,*377(1995) pp. 500- 503.

[6]   Bowman H and Morgan C, 'New materials for Optical cooling', *Appl.Phys.,* 71.B (2000) pp. 807-811.

[7]   Elton Soares de Lima Filho, Galina Nemova, Sebastien Loranger, and Raman Kashyap, 'Laser induced cooling of a Yb:YAG crystal in air at atmospheric pressure', *Opt. Express,* 21.21 (2013) pp. 24711-719.

[8]   Denis V. Seletskiy, Seth D. Melgaard, Alberto Di Lieto, Mauro Tonelli, and Mansoor Sheik-Bahae,'Laser cooling of a semiconductor load to 165K',*Opt.Express,* 18.17 (2010) pp. 18061-18066.

[9]   Sheik-Bahae M., and Epstein R.I,'Andet al. 'Laser cooling of solids demonstration of 115K all solid- state cryocooler', *IEEE,* 978.1 (2013) pp. 4577-1507.

[10]   Tyagi Neetu, Reddy, A. Amarnath, and NagarajanR, 'KlaF4:Er an efficient up-conversion phosphor',*J. Opt.Matter*, 33.1(2010) pp. 42-47.

[11]   Dosev D., and Kennedy I.M. 9, 'Fluorescence up c onversion in SM doped Gd_2O_3'.*Appl.Phy. lett.,* 88.1 (2006) pp. 011906.

[12]   Hai Lin, Gerald Meredith, Shibin Jiang, Xiang Peng, and Tao Luo, 'Transition and visible up-conversion in Er^{3+}doped niobic tellurite glass', *Appl. Phys.,* 93.1(2003) pp. 186- 191.

[13]   Yannick Ledemi, Mohammed El Amraoui, Jefferson L. Ferrari , Pier-Luc Fortin , Sidney J.L. Ribeiro, and Younes Messaddeq, 'Infrared to visible up-conversion luminescence in Er^{3+}/Yb^{3+} doped titanate glass prepared by containerless processing', *J.Lumin.*, 132.4(2012) pp. 1025-1029.

[14]   Vijay Singh, Vineet Kumar Rai, Katharina Al-Shamery, JorgNordmann, and Markus Haase, 'NIR to visible up-conversion in Er^{3+}/Yb^{3+} co-doped $CaYAl_3O_7$ phosphor obtained by solution combustion process'*, J. Lumin.,*131.12(2011) pp. 2679-2682.

[15]   Ying Yua, YngdongZhenga , F eng Qina , L ixinLiua , C hangbinZhenga , G uanying Chena , ZhiguoZhanga, and WenwuCaoa, 'Influence of Yb^{3+} concentration on up-conversion luminescence of Ho^{3+}',*Opt. Commun.*, 284.4 (2011) pp. 1053-1056.

[16]   Markus Haase, and Helmut Schafer, 'Up-converting nanoparticles', Chem.*Int. Ed.,* 50.26(2011) pp. 5808-5829.

[17]   Chen G., Somesfalean G, ZhangZ G, Sun G, and Wang F.P, 'Ultraviolet up- conversion fluorescence in rare-earth-ion- doped Y_2O_3 induced by i nfrared diode laser excitation', *Opt. Lett.,* 32.1(2007) pp. 87-89.

[18]   Yannick Ledemi, Mohammed El Amraoui , Jefferson L. Ferrari , Pier-Luc Fortin,

Sidney J.L. Ribeiro, and YounesMessaddeq, 'Infra-red to visible up-conversion luminescence in Er^{3+}:Y_2O_3 transparent ceramics'. *J. Lumin.,* 122.0(2007) pp. 8-10.

[19]   Guofeng Wang, Qing Peng, and YadongLi, 'Synthesis and up-conversionluminescence of BaY_2F_8:Yb^{3+}/Er^{3+}nanobelts',*Chem. Commun.*, 46.40 (2010) pp. 7528-7529.

[20]   Xiaorui Hou, Shengming Zhou, Wenjie Li, Yukun Li, Hui Lin, Hao Teng, and TingtingJia, 'Investigation of up-conversion luminescence in Er^{3+}/Yb^{3+}co-doped yttria transparent ceramic'*, J.Am.Ceram.Soc.,*93.9(2010) pp. 2779-2782.

[21]   Singh Vijay, Kwak Ho-Young, Rai Vineet Kumar, Watanabe S, Gundu Rao T K, and Ledoux-RakIsabelle, 'Infrared emission and defect centres in Er and Yb co- dopeY$_3$Al$_5$O$_{12}$ phosphors', *J.Appl.Phys.*, A100.4(2010) pp. 1123-1130.

[22]   Suresh Kumar Jakka, K. Pavani, M.P.F. Grai;a, and Manuel Jorge Soares, 'Enhanced green up-conversion by controlled ceramization of Er^{3+}-Yb^{3+} co-doped sodium niobium tellurite glass-ceramics for low temperature sensors', *J. Alloy. Compd.*, 617(2014) pp. 108- 114.

[23]   Pavani K.,Grai;a M. P. F., Soares M. J., and Valent M.A, 'Enhancement of infrared emission in Er^{3+}, Yb^{3+} co-doped sodiumniobium tellurite nano-glass-ceramics', *Phys.Status Solid B:BasicRes.*,250.4(2013) pp. 837-842.

[24]   SimovicS., and Kraljevic Sandra. 'Critical review on zeolite clinoptilolite safety and medical application in vivo'. *Frontier in pharmacology*. (2018), 9, p1350.

[25]   Wilfred L.F. Armarego, 'Common Physical Techniques Used in Purification'.

Purification of Laboratory Chemicals',Sciencedirect,Elsevierinc. 2017.

[26]   Setsuhisa T. And Tehichi H, 'Local structure and 1.5 p m quantum efficiency oferbium doped glasses for optical amplifiers'. *J. Non-Crystalline Solids,* 196 (1996) pp. 101- 105.

[27]   Binh M. Q., 'Influence of various support Y-Al$_2$O$_3$, and SBA-15 on H DO performance of NiMO Catalyst', *Catal. Lett.,* 145.2 (2014) pp. 1-6.

[28]   Xi-xian Luo, and Wang-he Cao, 'Up-conversion luminescence of holmium and ytterbium co-doped yttrium oxysulfide phosphor', *Mat. lett.,* 61.17(2007) pp. 3696-3700. doi: https://doi.org/10.1016/j.matlet.2006.12.021.

[29]   Dwivedi Y., 'Advances in rare earth spectroscopy and application', *J.nanosci and Nano technol.,* 14.2 (2014) pp. 1578-96.

[30]   Rychlik W., Spencer W.J., and RhoadsRychlikR. E, 'Optimization of the annealing temperature for DNA amplification in vitro', *Nucleic Acids Res.,* 18.21 (1990) pp. 6409- 6412.

[31]   Haizhou Lu, Yu Peng , Huanqing Ye , Xianjin Cui, Jianxu Hu, Hang Gu, and Lu H, 'Sensitization, energy transfer and infra-red emission decay modulation in Yb^{3+}-doped $NaYF_4$nano particles with vi sible light through a perfluoro anthra quinone chromophore', *Sci Rep.,* 7 (2017) pp. 5066-5076.

[32]   Xingtao Gao, and Israel E. Wachs, 'Investigation of Surface Structures of Supported Vanadium Oxide Catalysts by U V-vis-NIR Diffuse Reflectance Spectroscopy', *J. Phys. Chem*., 104(2000) pp. 1261-1268.

[33]   Talane T. E., *Study of Structural and Optical Properties of Undoped and RareEarth Doped TiO_2 Nanostructures*. MA thesis. University of South Africa, Physics Department (2018).

[34]   Bahtat A., Bahtatc C., Garapona B Jacquiera J., and Mugniera, 'Up-conversion fluorescence spectroscopy in Erbium TiOPlanar', *J. Non-crystalline solids.,* 202 (1996) pp. 16-22.

[35]   Singh V., 'Optical characterization, absorption and up-conversion luminescence in Er^{3+} and Er^{3+}/Yb^{3+}doped In 203 phosphor', *J. Non- crystalline solids,* 176 (2016) pp. 347- 355.

[36]   RiikkaArppe-Tabbara, IkoHyppanen, NiinaPerala, and RiikkaPeltomaa, 'Quenching of the up-conversion luminescence of $NaYF_4$:Yb^{3+},$Er^{3+}$and NaYF4:Yb^{3+},Tm^{3+}nanophosphors by water', *Nanoscale,* 7(2015) pp. 11746-11757.

[37]   Zheming Wang, John M. Zachara, Gassman Paul and OdetaQafoku, 'Fluorescence spectroscopy of U(VI)-silicates and U(VI)-contaminatedHanford sediment',*Geochimica et Cosmochimica Acta,* 69.6 (2005) pp. 1391-1403.

[38]   Van UitertL.G., H.J.Levinstein, and W.H.Grodkiewicz,'Infrared stimulable rare earth oxy-halide phosphors: their synthesis, properties and application',*Mater Res Bull.,* 4 (1969) pp. 381-389.

[39]   Wittke J.P., YocomP. N., WittkeJ. P., and I. Ladany, 'Y_2O_3:Yb:Er-new red-emitting infrared-excited phosphor', *JAppl Phys.,*43(1972) pp. 595-600.

[40]   Ostermayer F.W., GeusicJ. E., MarcosH. M., Van UitertL. G., and van der ZielJ. P., 'Preparation and properties of infrared-to-visible con- version phosphors', *Metall. Trans.,* 2(1971) pp. 747-755.

[41]   Zhang J., 'Observation of efficient population of the red-emitting state from the green state by non-multi phonon relaxation in the Er^{3+}-Yb^{3+}system',*J. Light, Sc. and Apll.,* 4 (2015) pp. 239-245.

[42]   National Center for Biotechnology Information (USA), *Sodium aluminosilicate*, CID=19758701. PubChem Database. https://pubchem.ncbi.nlm.nih.gov/compound/Sodium-aluminosilicate, (2018)(accessed on Jan. 6, 2020).

[43]   Strumpel C., *Application of Erbium doped up c onverters to silica solar cells*. PhD Thesis. Germany: University of Konstanz (2007).

[44]   Johannsen S. R., *Up-conversion of near infra-red light through Er doped TiO_2 and the effect of plasmonics and co-doping with ytterbium*, PhD Thesis. University of Aarhus , Denmark (2015).

[45]   Naresh V. and Buddhudu. S., 'Analysis of visible-NIR emission and photoluminescence quenching in Er^{3+}:Bi_2O_3-AlF_3-TeO_2-B_2O_3glasses',*Eur. J. Glass Sci. Technol.* B, 56 (2015) pp. 255-262.

[46]   Sales AJM, 'Power dependent up-conversion in Er^{3+}/Yb^{3+} co- doped$BiNbO_4$phosphors'. *Ceramics International,* 142 (2016) pp. 6899-6905.

[47]   Haizhou Lu, William P Gillin, and Ignacio Hernandez, 'Concentration dependence of the up-and down-conversion emission colours of Er^{3+}-doped Y_2O_3: a time-resolved - spectroscopy analysis,*Phys Chem,* 16(2014) pp. 20957-20963.

[48]   Ding Y., 'Enhancement on concentration quenching and up conversion luminescence of Beta $NaYF_4$ Er^{3+} Yb^{3+}co doping with LI ions', *J. Alloy Comp*., 599 (2014) pp. 60-64.

[49]   Miller A., and Finlayson D.M. 1st ed. *Laser sources and applications.* CRC press 1996 ISBN 9780750304443.

[50]   Anderson Robert, Steve J. Smith P. Stanley May, and Mary T. Berry, 'Revisiting the NIR to visible up-conversion mechanism to B – $NaYF_4$: Yb^{3+}/$Er^{3+'}$, *J. Phys. Chem. lett.,* 5.1(2014) pp. 36-42.

[51]   Vetrone F and Boyer J. C., 'NIR to visible up-conversion in nano crystalline and bulkLu$_2$O$_3$:Er^{3+}',*J. Phys. Chem.,* B106.22 (2002) pp. 5622-5628.

[52]   Jourart JP, 'Evidence for Er3+ Tm3+ energy transfers in cadmium fluoride crystals'. *J. Lumin*., 21.2 (1980) pp. 153-164.

[53]   Liang Shen, Yanjun Fang, Yang Bai , Yehao Deng, Mengmeng Wang, Yongfeng Lu, and Jinsong Huang, 'A Self-Powered, Sub-nanosecond-Response Solution-Processed Hybrid Perovskite Photodetector for Time-Resolved Photoluminescence-Lifetime Detection,*Adv. Matter'*, 28.48(2016) pp. 10794-10800.

[54]   Bergstrand J., Qingyun Liu a, Bingru Huang q , a nd XingyunPengc.,'On the decay time up-conversion luminescence', *Nanoscale,* 11(2019) pp. 4959-4969.

[55]   Bhushan P. Kore, Ashwini Kumar, Lucas Erasmus, Robin E. Kroon, Jacobus J. Terblans, Sanjay J. Dhoble, and Hendrik C. Swart, 'Energy Transfer Mechanisms and Optical Thermometry ofBaMgF$_4$:Yb^{3+},Er^{3+} Phosphor', *Inorg. Chem*., 57 (2018) pp. 288-299.

[56]   Golding P. S., Golding S.D., Jackson T.A. King, and Markus Pollnau, 'Energy transfer processes in Er^{3+}-doped and Er^{3+},Pr^{3+}- co-doped ZBLAN glasses', *J. Phys. Rev*.B, 62(2000) pp. 856.

[57]   Tao Wei, Ying Tian, Fangze Chen, MuzhiCai,Junjie Zhang, Xufeng Jing, Fengchao Wang, Qinyuan Zhang and Shiqing Xu, 'Mid-infrared fluorescence, energy transfer process and rate equation analysis in Er^{3+} doped germanateglass', *Scientific Report,* 4(2014)pp. 6060.

[58]   PollnauM, GamelinD. R., Li.thiS. R., Gi.delH. U., and Hehlen M. P., 'Power dependence of up-conversion luminescence in lanthanide and transition-metal-ion systems', *Phys. Rev. B,*61(2000) pp. 3337-3346. doi: 10 . 11 03 /.url: ht tps : / / link . aps.org/doi/10.1103/PhysRevB.61.3337.

[59]   Bhushan P. Kore, Ashwini Kumar, Lucas Erasmus, Robin E. Kroon, Jacobus J. Terblans, Sanjay J. Dhoble, and Hendrik C. Swart, 'Energy Transfer Mechanisms and Optical Thermometry of BaMgF$_4$:Yb^{3+},Er^{3+}Phosphor,*Inorg. Chem*., 57(2018) pp. 288-299.

[60]   Jagannathan Thirumalai, *Luminescence: An Outlook on the Phenomena and t heir Applications*. Intech Rijeka Croatia (2016).

Chapter 6

Summary and recommendations

This dissertation reports on the hydro thermal syntheses of $NaAlSiO_2$ crystal doped with rare-earth ions (Er^{3+}, and Yb^{3+}). An exhaustive characterization of their structural, elemental, morphological, absorption and emission properties was conducted using several analytical techniques   such as X RD, SEM-EDS, UV-ViS-NiR, FTIR and PL, spectroscopy respectively.

Significantly the synthesized pure crystalline Sodalite $NaAlSiO_2$ showed crystals of sizes of 14 nm to 37 nm with highly up-converting luminescence when doped with rare earth ions. The XRD revealed a stable sodalite structure without phase transitions. The HR-SEM images confirmed the Zeolites porous morphology of the crystals, EDS elemental analysis revealed chemical composition of the samples whose mapping showed even distribution of the expected ions in the sample.

The photonic investigation was conducted successfully and discussed in detail. Furthermore, up-conversion properties of Er^{3+} and Yb^{3+} co-doped $NaAlSiO_2$ crystals through UV-ViS-NiR and PL spectroscopy were extensively studied, emission intensities from electronic transitions were found to be greatly enhanced with doping at 2 mol% Er^{3+}/ 20 mol% Yb^{3+}. Overall, three prominent up-conversion emission lines were recorded in the visible region at 521 nm, 540 nm, and 651 nm, which could be associated with emerald green, green and red regions in the visible spectrum, respectively.

Further photonic investigation in power and temperature dependence revealed a possible application of the Er^{3+}, and Yb^{3+} co-doped $NaAlSiO_2$ crystals as temperature sensor devise in the region of 50 ^oC to 400 ^oC. It is evident that the host material presents a possible application in sensing of temperatures in bodies, this may be used in biomedical cancer research or industrial sensing devises.

Future prospects

In this work, all synthesized samples showed highly enhanced up-conversion emission in the green to red region of the visible spectrum. This calls for an investigation on blue emission from doped $NaAlSiO_2$, if successful it w ould contribute to fabrication of a pure white light emitting material for LEDs. In addition, based on the ever-growing interest of up-converting porous materials in solar cells applications, the prepared $NaAlSiO_2$ crystals are promising materials for photovoltaic applications in order to improve devices efficiency.

Appendix A.

Publication and conference/workshops

South African Institute of Physics (SAIP) 2018 conference, Poster Presentation, 'Investigating laser optical cooling in doped $NaAlSiO_2$.' Bloemfontein, free state, University of Free State, South Africa.